

# HADRONIC AND NUCLEAR PHENOMENA IN QUANTUM CHROMODYNAMICS\*

STANLEY J. BRODSKY

*Stanford Linear Accelerator Center  
Stanford University, Stanford, California 94305*

## Abstract

Many of the key issues in understanding quantum chromodynamics involves processes at intermediate energies. We discuss a range of hadronic and nuclear phenomena—exclusive processes, color transparency, hidden color degrees of freedom in nuclei, reduced nuclear amplitudes, jet coalescence, formation zone effects, hadron helicity selection rules, spin correlations, higher twist effects, and nuclear diffraction—as tools for probing hadron structure and the propagation of quark and gluon jets in nuclei. Many of these processes can be studied in electroproduction, utilizing internal targets in storage rings. We also review several areas where there has been significant theoretical progress in determining the form of hadron and nuclear wavefunctions, including QCD sum rules, lattice gauge theory, and discretized light-cone quantization.

## 1. Introduction

One of the outstanding triumphs of theoretical physics has been the development of quantum chromodynamics. The QCD Lagrangian density,

$$\mathcal{L}_{QCD} = -\frac{1}{2} \text{Tr} [F^{\mu\nu} F_{\mu\nu}] + \bar{\psi}(i \not{D} - m)\psi$$

$$F^{\mu\nu} = \partial^\mu A^\nu - \partial^\nu A^\mu + ig[A^\mu, A^\nu]$$

$$D^\mu = \partial^\mu + ig A^\mu$$

describes a renormalizable theory of spin- $\frac{1}{2}$  quark field and spin-1 gluon fields with exact symmetry under SU(3)-color local gauge transformations. According to QCD, hadrons, nuclei, and their interactions can be described in terms of the quark and gluon degrees of freedom. This premise appears consistent with experiment, particularly in the enumeration of the hadron spectrum and in the whole range of high momentum transfer phenomena, where because of asymptotic freedom and factorization theorems for inclusive and exclusive phenomena, the theory

---

\* Work supported by the Department of Energy, contract DE-AC03-76SF00515.

has high predictability.<sup>1</sup> The general structure of QCD indeed meshes remarkably well with the facts of the hadronic world, especially quark-based spectroscopy, current algebra, the approximate point-like structure of large momentum transfer inclusive reactions, and the logarithmic violation of scale invariance in deep inelastic lepton-hadron reactions. QCD has been successful in predicting the features of electron-positron and photon-photon annihilation into hadrons, including the magnitude and scaling of the cross sections, the complete form of the photon structure function, the production of hadronic jets with patterns conforming to elementary quark and gluon subprocess, as well as phenomena associated with the production and decay of heavy hadrons. Recent Monte Carlo studies incorporating some features of coherence (angle-ordering) have been successful in reproducing the detailed features of the two-jet ( $q\bar{q}$ ) and three-jet ( $q\bar{q}g$ ) reactions. All of the experimental measurements appear to be consistent with the basic postulates of QCD, that the charge and weak currents within hadrons are carried by fractionally-charged quarks, and that the strength of the interactions between the quarks and gluons becomes weak at short distances, consistent with asymptotic freedom.

Nevertheless, despite the general acceptance of QCD as the fundamental theory of the strong and nuclear interactions, there are very few reliable quantitative QCD predictions for the properties of the hadrons and nuclei themselves, e.g.

- (a) The theory predicts hadronic states or resonances for virtually every color singlet combination of quarks and gluons. Unfortunately, the only quantitative tool for determining the QCD spectrum, lattice gauge theory, only provides a rough guide. Predictions for exotic color singlet states such as gluonium ( $gg, ggg$ ) or quark-gluon hybrids ( $gq\bar{q}, q\bar{q}q\bar{q}$ ) are very indefinite. Nuclear exotic states such as hidden color resonances and strange nuclei such as the di-lambda H also await definitive calculation.
- (b) There are no reliable calculations of even the simplest properties of hadrons, e.g. static properties such as the nucleon magnetic moments. This can be contrasted with QED predictions of ten significant figures for lepton gyromagnetic ratios.
- (c) At present there are no reliable calculations in QCD of scattering amplitudes or cross sections at low momentum transfer.
- (d) We have no detailed theory of the nuclear force.
- (e) The fundamental processes entailing quark and gluon jet hadronization can only be parametrized by elaborate Monte Carlo programs.

In principle, QCD could give just as accurate a description of hadronic phenomena as quantum electrodynamics provides for the interactions of leptons. However, because of its non-Abelian structure, calculations in QCD are much more complex. The central feature of the theory is, in fact, its non-perturbative nature which it is believed leads to the confinement of quarks and gluons in color-singlet bound

states. Because of the confinement of the colored quanta, observables always involve the dynamics of bound systems; hadron-hadron interactions are thus at least as complicated as the Van der Waals and covalent exchange forces of neutral atoms.

Unlike atomic physics, the constituents of hadrons are highly relativistic; because the forces are non-static, a hadron cannot be represented as a state of fixed number of quanta at a fixed time. The vacuum structure of the QCD Hamiltonian relative to the perturbative basis is also complex; virtually every local color-singlet operator constructed from the product of quark and gluon fields may have a non-zero vacuum condensate expectation value.

At large distances, the gluonic sector of QCD has been shown to be effectively equivalent to a non-linear sigma model of pseudoscalar mesons, at least for large number of colors.<sup>2</sup> The resulting topological solitons (Skyrmions) can be consistently identified as baryons. It remains to reconcile this representation of hadrons at long wavelength with the intuitive concept of the mesons and baryons as composites of quark fields at short distances.

Despite the complexity of the theory, QCD has several key properties which make calculations tractable and systematic, at least in the short-distance, high momentum-transfer domain. The critical feature is asymptotic freedom: the effective coupling constant  $\alpha_s(Q^2)$  which controls the interactions of quarks and gluons at momentum transfer  $Q^2$  vanishes logarithmically at high  $Q^2$ :

$$\alpha_s(Q^2) = \frac{4\pi}{\beta \log(Q^2/\Lambda_{\text{QCD}}^2)} \quad (Q^2 \gg \Lambda^2). \quad (1)$$

[Here  $\beta = 11 - \frac{2}{3}n_f$  is derived from the gluonic and quark loop corrections to the effective coupling constant;  $n_f$  is the number of quark contributions to the vacuum polarization with  $m_f^2 \lesssim Q^2$ .] The parameter  $\Lambda_{\text{QCD}}$  normalizes the value of  $\alpha_s(Q_0^2)$  at a given momentum transfer  $Q_0^2 \gg \Lambda^2$ , given a specific renormalization or cutoff scheme. The value of  $\alpha_s$  can be determined fairly unambiguously using the measured branching ratio for upsilon radiative decay  $\Upsilon(b\bar{b}) \rightarrow \gamma X$ :<sup>3</sup>

$$\alpha_s(0.157 M_\Upsilon) = \alpha_s(1.5 \text{ GeV}) = 0.23 \pm 0.03. \quad (2)$$

Taking the standard  $\overline{MS}$  dimensional regularization scheme, this gives  $\Lambda_{\overline{MS}} = 119_{-34}^{+52}$  MeV. A recent analysis of logarithmic scale-breaking of the isoscalar nucleon structure functions  $F_2(x, Q^2)$  and  $xF_3(x, Q^2)$  from deep inelastic neutrino and anti-neutrino interactions in neon by the BEBC WA59 collaboration<sup>4</sup> gives values for  $\Lambda_{\overline{MS}}$  in the neighborhood of 100 MeV. In more physical terms, the effective potential between infinitely heavy quarks has the form [ $C_F = 4/3$  for

$n_c = 3]$ ,<sup>5</sup>

$$V(Q^2) = -C_F \frac{4\pi\alpha_V(Q^2)}{Q^2}$$
$$\alpha_V(Q^2) = \frac{4\pi}{\beta \log(Q^2/\Lambda_V^2)} \quad (Q^2 \gg \Lambda_V^2) \quad (3)$$

where  $\Lambda_V = \Lambda_{\overline{MS}} e^{5/6} \simeq 270 \pm 100$  MeV. Thus the effective physical scale of QCD is  $\sim 1 f_m^{-1}$ . At momentum transfers beyond this scale,  $\alpha_s$  becomes small, QCD perturbation theory should begin to become applicable, and a microscopic description of short-distance hadronic and nuclear phenomena in terms of quark and gluon subprocesses is expected to become viable.

The above argument is the main basis for the reliability of perturbative calculations for processes in which all of the interacting particles are forced to exchange large momentum transfer (a few GeV). Complimentary to asymptotic freedom is the existence of factorization theorems for both exclusive and inclusive processes at large momentum transfer which are valid for all gauge theories. In the case of exclusive processes (in which the kinematics of all the final state hadrons are fixed), any hadronic scattering amplitude can be represented as the product of a hard-scattering amplitude for the constituent quarks, convoluted with a distribution amplitude for each in-going or out-going hadron. The distribution amplitude contains all of the bound-state dynamics and specifies the momentum distribution of the quarks in each hadron independent of the process. The hard scattering amplitude can be calculated perturbatively in powers of  $\alpha_s(Q^2)$ . The predictions can be applied to form factors, exclusive photon-photon reactions, photoproduction, fixed-angle scattering, etc.

In the case of high momentum transfer inclusive reactions (in which final state hadrons are summed over), the hadronic cross section can be computed from the product of a perturbatively-calculable hard-scattering subprocess cross section involving quarks and gluons convoluted with the appropriate quark and gluon structure functions which incorporate all of bound-state dynamics. Since the distribution amplitudes and structure functions only depend on the composition of the respective hadron, but not the nature of the high momentum transfer reaction, the complicated non-perturbative QCD dynamics is factorized out as universal quantities. Recently there has been encouraging progress in actually calculating these fundamental quantities, which we shall review in some detail here. Eventually these calculations can be compared in detail with the phenomenological parameterization extracted from inclusive and exclusive experiments.

The central unknown in the QCD predictions is the composition of the hadrons in terms of their quark and gluon quanta. Recently several important tools have been developed which allow specific predictions for the hadronic wave functions

directly from the theory. A primary tool is the use of light-cone quantization to construct a consistent relativistic Fock state basis for the hadrons in terms of quark and gluon quanta. The distribution amplitude and the structure functions are defined directly in terms of these light-cone wave functions. The form factor of a hadron can be computed exactly in terms of a convolution of initial and final light-cone Fock state wave functions. We will discuss light-cone quantization in detail in these lectures.

A second important tool is the use of QCD sum rules to provide constraints on the moments of the hadron distribution amplitudes.<sup>6</sup> This method, developed by Chernyak and Zhitnitskii, has yielded important information on the possible momentum space structure of hadrons. A particularly important advance is the construction of nucleon distribution amplitudes, which together with the QCD factorization formulae, predicts the correct sign and magnitude as well as scaling behavior of the proton and neutron form factors. A recent analysis by King and Sachrajda<sup>7</sup> has confirmed these results.

Another recent advance has been the development of a formalism to calculate the moments of the meson distribution amplitude using lattice gauge theory. The most recent analysis, by Martinelli and Sachrajda,<sup>8</sup> gives moments for the pion distribution amplitude in good agreement with the QCD sum rule calculation. The results from both the lattice calculations and QCD sum rules also demonstrate that the light quarks are highly relativistic in the bound state wave functions. This gives further indication that while potential models are useful for enumerating the spectrum of hadrons (because they express the relevant degrees of freedom), they are not reliable predicting wave function structure.

Since the intrinsic mass scales of QCD  $\Lambda_{\overline{MS}}$ ,  $\langle k_{\perp}^2 \rangle^{\frac{1}{2}}$ , and  $m_q (q = u, d, s)$  are less than a few hundred MeV, quark and gluon degrees of freedom should become evident at momentum transfers as low as a few GeV. The observation of Bjorken scaling at  $Q^2$  as low as 1 GeV<sup>2</sup> supports this argument. At larger momentum transfer, one studies logarithmic structure function evolution, the onset of new quark flavors, and multi-jet production. However, the dynamics of hadrons and nuclei in terms of their light quark and gluon degrees of freedom can be studied at moderate energies.

Several new experimental facilities are in fact being planned which will be able to probe QCD effects in the intermediate energy domain. These include

1. The CEBAF accelerator at Newport News, Virginia, which will provide a continuous high intensity source of electrons at energies of 4 GeV or higher.
2. Internal gas targets in PEP. Such a facility will allow a study of electroproduction at  $e^-$  or  $e^+$  energies up to  $\sim 15$  GeV. Polarized beams and polarized proton or nuclear targets are conceivable. The CEBAF and PEP internal

target facilities, because of their good duty factor, should allow for a complete study of the final states in electroproduction channel by channel in the energy range where Bjorken scaling and the quark degrees of freedom of the nucleon become manifest.

3.  $\bar{p}p$  facilities such as LEAR and the proposed AMPLE facility at Fermilab, which could allow studies of  $p\bar{p}$  annihilation at anti-proton laboratory energies up to 10 GeV.
4. Studies of  $\gamma\gamma$  annihilation at PEP and TRISTAN. The  $\gamma\gamma$  reactions (for real and virtual photons from tagged  $e^\pm$ ) provide some of the cleanest tests of QCD. One can test for the scaling laws of QCD in exclusive reactions with two large momentum scales, the virtual photon mass and the  $p_T$  of the reaction. An interesting feature of QCD is that at large  $p_T^2$ , the  $Q^2$  dependence of each exclusive virtual photoproduction amplitude becomes minimal for  $Q^2 \ll p_T^2$ . This can be contrasted with the vector meson dominance model which predicts a universal fall-off in  $Q^2$  at any  $p_T$ . This feature is due to the photon's point-like direct local coupling to the quark current in QCD.

One of the most important areas of investigation in electroproduction is the dependence on the nuclear target. The nucleus acts as a background field modifying the dynamics in interesting, though possibly subtle, ways. The observation of non-additivity of the nuclear structure functions as measured by the EMC and SLAC/American University collaborations have opened up a whole range of new physics questions:

1. What is the effect of simple potential model nuclear binding, as predicted, for example, by the shell model? What is the associated modification of meson distributions required by momentum sum rules?
2. Is there a physical change in the nucleon size, and hence the shape of quark momentum distributions?
3. Are there nuclear modifications of the nucleonic and mesonic degrees of freedom, such as induced mesonic currents, isobars, six-quark states, or even "hidden color" degrees of freedom?
4. Does the nuclear environment modify the starting momentum scale evolution scale for gluonic radiative corrections?
5. What are the effects of diffractive contributions to deep inelastic structure functions which leave the nucleon or nuclear target intact?
6. Are there shadowing and possibly anti-shadowing coherence effects influencing the propagation of virtual photons or redistributing the nuclear constituents? Do these appear at leading twist?
7. How important are interference effects between quark currents in different nucleons?<sup>9</sup>

It seems likely that all of these non-additive effects occur at some level in the nuclear environment. Clearly it will be difficult without further experimental clues to sort out all the physical effects. In particular it will be important to examine the  $A$ -dependence of each reaction channel by channel. We will discuss some predictions for the various mechanisms in these lectures.

The lectures are organized as follows: In sections 2-13 we present an introductory overview to QCD phenomenology, with special emphasis on electroproduction at intermediate energy scales. A number of novel effects are discussed such as color transparency, formation zone effects, and jet coalescence. Sections 14-16 provide a review of the theoretical basis for the predictions, with emphasis on light-cone Fock methods. A review of the discretized light-cone quantization method is given in section 16. A more detailed discussion of the application of QCD to exclusive amplitudes and the structure of hadron wave functions is then presented in sections 17-21. The important role of QCD helicity selection rules for exclusive charmonium decays is discussed in section 18. Special applications to exclusive nuclear amplitudes are presented in section 22.

## 2. Testing QCD in Electroproduction – An Overview to QCD Phenomenology

Deep inelastic lepton nucleon scattering has been one of the key testing grounds of QCD over the past two decades. Measurements of the nucleon and nuclear structure functions have not only tested the short-distance properties of the theory, (such as the scaling properties of structure functions and their logarithmic evolution with momentum transfer), but they have also illuminated the nonperturbative bound state structure of the nucleon and nuclei in terms of their quark and gluon degrees of freedom. For the most part, this information has been obtained from single-arm inclusive experiments where only the recoil lepton was detected.

One of the important potential advantages of an internal target facility in an electron storage ring is that the entire final state of electroproduction can be measured in coincidence with the scattered electron with close to  $4\pi$  acceptance. In the case of the PEP ring ( $E(e^\pm) \sim 15$  GeV), measurements can be performed well above the onset of Bjorken scaling. Both polarized and unpolarized hydrogen and nuclear targets may be feasible, and eventually even polarized electron beams may be available. High precision comparisons between electron and positron scattering would allow the study of higher order QED and electroweak interference effects. The asymmetry in the cross sections for  $e^\pm p \rightarrow e^\pm \gamma X$  can be sizeable,<sup>10</sup> providing a sum rule for the cube of the charges of the quarks in the target.

At the most basic level, Bjorken scaling of deep inelastic structure functions implies the production of a single quark jet, recoiling against the scattered lepton. The spectator system— the remnant of the target remaining after the scattered

quark is removed—is a colored  $\bar{3}$  system. (See fig. 1.) According to QCD factorization, the recoiling quark jet, together with the gluonic radiation produced in the scattering process, produces hadrons in a universal way, independent of the target or particular hard scattering reaction. This jet should be identical to the light quark jets produced in  $e^+e^-$  annihilation. In contrast, the hadronization of the spectator system depends in detail on the target properties. Unlike the quark jet, the leading particles of the target spectator system do not evolve and thus should not depend on the momentum transfer  $Q^2$  [at fixed  $W^2 = (q + p)^2$ ]. At present we do not have a basic understanding of the physics of hadronization, although phenomenological approaches, such as the Lund string model, have been successful in parameterizing many features of the data.

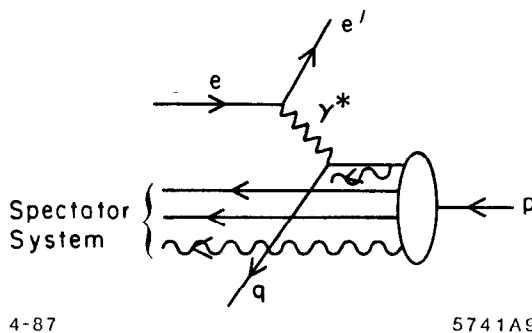


Fig. 1. Struck quark and spectator systems in electroproduction.

At a more detailed level, the features of the standard leading twist description are modified by coherent or non-perturbative effects. For example, higher twist—power-law suppressed contributions arise when two or more quarks recoil against the scattered lepton. At high energies, the quark jet does not change its state or hadronize over a distance scale proportional to its energy. Thus inelastic or absorptive processes cannot occur inside a nucleus—at least for the very fast hadronic fragments. We will discuss this target length condition<sup>11,12</sup> in more detail below. Nevertheless, a nuclear target can provide an essential tool for studying the detailed features of jet hadronization since the fast fragments are expected to scatter elastically in the nuclear medium, and the slow particles can interact inelastically and shower inside the nucleus. A review of the QCD predictions for jet hadronization can be found in ref. 13.

— Many of the novel features expected in QCD are also apparent in QED. It is thus often useful to keep a QED analog in mind, replacing the target by a neutral atom such as positronium. Even in QED where there is no confinement, one expects in certain kinematic regions significant corrections to the Bjorken scaling associated with positron or electron knockout, in addition to the logarithmic evolution of the QED structure functions associated with induced photon radiation.



For example, at low  $Q^2$ , the interference between amplitudes where different constituents are struck become important. Near threshold, where charged particles emerge at low relative velocities, there are strong Coulomb distortions, as summarized by the Sommerfeld<sup>14</sup> factor. In QCD these have their analog in a phenomena called “jet coalescence”<sup>15</sup> which we discuss below. The Coulomb distortion factor must be included if one wants to maintain duality between the inelastic continuum and a summation over exclusive channels in electroproduction.<sup>16</sup>

My main emphasis in the next sections, however, is in the study of exclusive channels in electroproduction. It is clearly interesting to study how the summation of such channels yields the total inelastic cross section. More important, each individual exclusive channel can provide detailed information on basic scattering mechanisms in QCD and how the scattered quarks and gluons recombine into hadrons. In certain cases such as Compton scattering and meson electroproduction, we can study new aspects of the light cone expansion for the product of two currents, thus extending the renormalization group analysis into a new domain.<sup>17</sup> The diffractive production of vector mesons at high  $Q^2$  can test the basic composition of the Pomeron in QCD. Further, as we discuss in section 4, measuring exclusive reactions inside a nuclear target allows the study of “color transparency”,<sup>18,19</sup> the “formation zone”,<sup>11</sup> and other novel aspects of QCD.

### 3. Exclusive Channels in Electroproduction

In high momentum transfer inclusive reactions, the underlying quark and gluon scattering processes lead directly to jet production in the final state. To leading order in  $1/Q^2$ , the cross sections and jet hadronization can be understood at the probabilistic level. In contrast, in *exclusive* electroproduction processes, one studies quark and gluon scattering and their reformation into hadrons at the *amplitude* level. Exclusive reactions thus depend in detail on the composition of the hadron wave functions themselves.

There is now an extensive literature, both experimental and theoretical, describing the features of large momentum transfer exclusive reactions. The QCD predictions are based on a factorization theorem<sup>20-23</sup> which separates the non-perturbative physics of the hadron bound states from the hard scattering amplitude which controls the scattering of the constituent quarks and gluons from the initial to final directions. This is illustrated for the proton form factor in fig. 2. Electroproduction of exclusive channels provides one of the most valuable testing grounds of this QCD formalism, since the incoming photon provides a probe of variable space-like mass directly coupling to the hard-scattering amplitude.

It has been known since 1970 that a theory with underlying scale-invariant quark-quark interactions leads to dimensional counting rules<sup>24</sup> for large momentum transfer exclusive processes; e.g.  $F(Q^2) \sim (Q^2)^{1-n}$  where  $n$  is the minimum

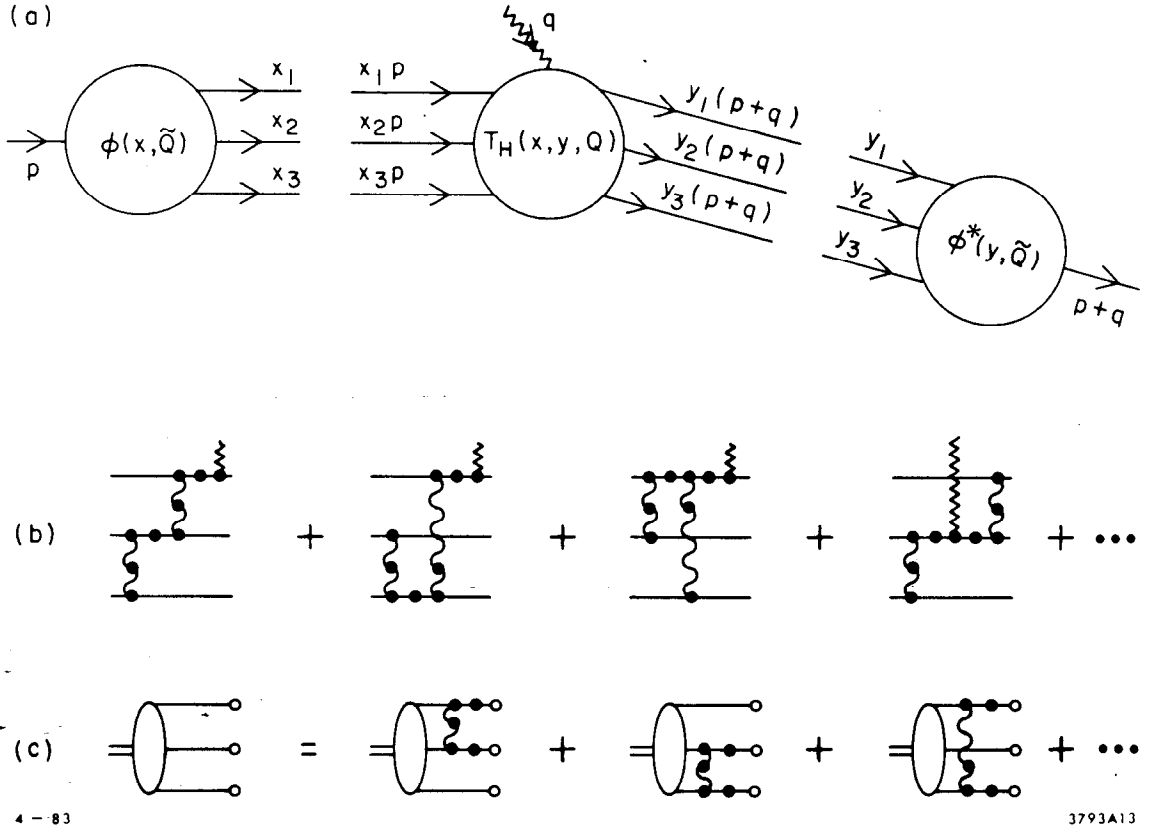


Fig. 2. (a) Factorization of the nucleon form factor at large  $Q^2$  in QCD. (b) The leading order diagrams for the hard scattering amplitude  $T_H$ . The dots indicate insertions which enter the renormalization of the coupling constant. (c) The leading order diagrams which determine the  $Q^2$  dependence of  $\phi_B(x, Q)$ .

number of quark fields in the hadron. QCD is such a theory; the factorization formula leads to nucleon form factors of the form:<sup>25</sup>

$$G_M(Q^2) = \left[ \frac{\alpha_s(Q^2)}{Q^2} \right]^2 \sum_{n,m} a_{nm} \left( \ln \frac{Q^2}{\Lambda^2} \right)^{-\gamma_n - \gamma_m} \times \left[ 1 + \mathcal{O}(\alpha_s(Q)) + \mathcal{O}\left(\frac{1}{Q}\right) \right].$$

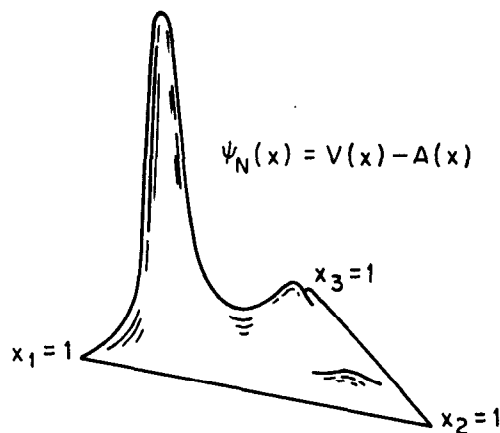
We review the derivation of this result in section 17. The first factor, in agreement with the quark counting rule, is due to the hard scattering of the three valence quarks from the initial to final nucleon direction. Higher Fock states lead to form factor contributions of successively higher order in  $1/Q^2$ . The logarithmic corrections derive from an evolution equation<sup>20,25</sup> for the nucleon distribution amplitude. The  $\gamma_n$  are the computed anomalous dimensions, reflecting the short

distance scaling of three-quark composite operators. The results hold for any baryon to baryon vector or axial vector transition amplitude that conserves the baryon helicity. Helicity non-conserving form factors should fall as an additional power of  $1/Q^2$ . Measurements of the transition form factor to the  $J = 3/2$   $N(1520)$  nucleon resonance are consistent with  $J_z = \pm 1/2$  dominance, as predicted by the helicity conservation rule.<sup>26</sup> A review of the data on spin effects in electron nucleon scattering in the resonance region is given in ref. 27.

It is very important to explicitly verify that  $F_2(Q^2)/F_1(Q^2)$  decreases at large  $Q^2$ . The angular distribution decay of the  $J/\Psi \rightarrow p\bar{p}$  is consistent with the QCD prediction  $\lambda_p + \lambda_{\bar{p}} = 0$ .

The normalization constants  $a_{nm}$  in the QCD prediction for  $G_M$  can be evaluated from moments of the nucleon's distribution amplitude  $\phi(x_i, Q)$ . There are extensive on-going theoretical efforts computing constraints on this nonperturbative input directly from QCD. The pioneering QCD sum rule analysis of Chernyak and Zhitnitskii<sup>6</sup> provides constraints on the first few moments of  $\phi(x, Q)$ . Using as a basis the polynomials which are eigenstates of the nucleon evolution equation, one gets a model representation of the nucleon distribution amplitude, as well as its evolution with the momentum transfer scale.

The QCD sum rule analysis predicts a surprising feature: strong flavor asymmetry in the nucleon's momentum distribution. The computed moments of the distribution amplitude imply that 65% of the proton's momentum in its 3-quark valence state is carried by the u-quark which has the same helicity as the parent hadron. (See fig. 3.) A recent comprehensive re-analysis by King and Sachrajda<sup>7</sup>



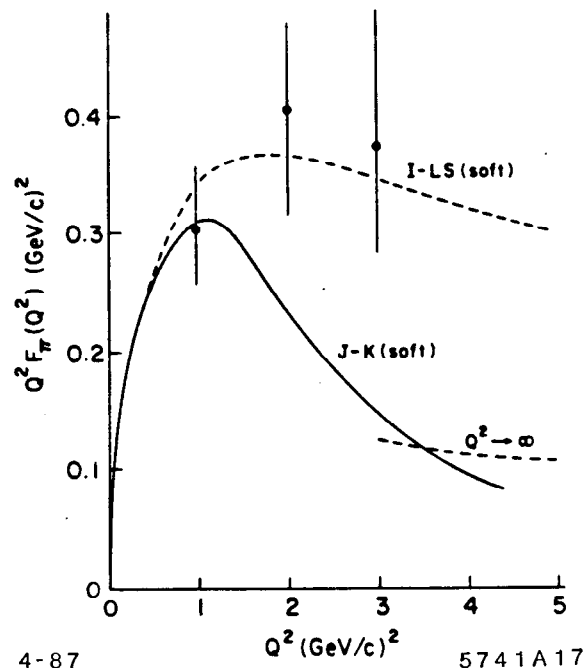
8-85

5207A7

Fig. 3. QCD sum rule prediction for the proton distribution amplitude.

has now confirmed the Chernyak and Zhitnitskii form in its essential details. In addition, Dziembowski and Mankiewicz<sup>28</sup> have recently shown that the asymmetric form of the CZ distribution amplitude can apparently be derived from a rotationally-invariant CM wave function transformed to the light cone using a Melosh-type boost of the quark spinors. The transverse size of the valence wave function is found to be significantly smaller than the mean radius of the proton—averaged over all Fock states. This was predicted in ref. 20. Dziembowski and Mankiewicz also show that the perturbative QCD contribution to the form factors dominates over the soft contribution (obtained by convoluting the non-perturbative wave functions) at a scale  $Q/N \approx 1$  GeV, where  $N$  is the number of valence constituents. Similar criteria were also derived in ref. 30. Results of the similar Jacob and Kisslinger<sup>31</sup> analysis of the pion form factor are shown in fig. 4. Claims<sup>32</sup> that a simple overlap of soft hadron wave functions could fit the form factor data were based on wave functions which violate rotational symmetry in the CM.

Fig. 4. Models for the “soft” contribution to the pion form factor. The Isgur-Llewellyn-Smith prediction<sup>32</sup> is based on a wave function with Gaussian fall-off in transverse momentum but power-law falloff at large  $x$ . The Jacob-Kisslinger prediction<sup>31</sup> is based on a rotationally symmetric form in the center of mass frame. The perturbative QCD contribution calculated with CZ<sup>6</sup> distribution amplitudes is consistent with the normalization and shape of the data for  $Q^2 > 1$  GeV<sup>2</sup>.



A detailed phenomenological analysis of the nucleon form factors for different shapes of the distribution amplitudes has been given by Ji, Sill, and Lombard-Nelsen.<sup>33</sup> Their results show that the CZ wave function is consistent with the sign and magnitude of the proton form factor at large  $Q^2$  as recently measured by the American University/SLAC collaboration.<sup>34</sup> (See fig. 5.) The fact that the correct normalization emerges is a non-trivial test of the distribution amplitude shape; for example, if the proton wave function has a non-relativistic shape

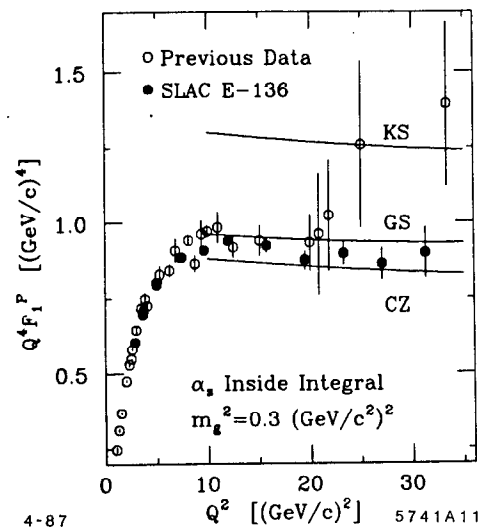
peaked at  $x_i \sim 1/3$  then one obtains the wrong sign for the nucleon form factor. Furthermore symmetrical distribution amplitudes predict a very small magnitude for  $Q^4 G_M^p(Q^2)$  at large  $Q^2$ . Gari and Stefanis<sup>35</sup> have developed a useful model for the nucleon form factors which incorporates the CZ distribution amplitude predictions at high  $Q^2$  together with VMD constraints at low  $Q^2$ . Their analysis predicts sizeable values for the neutron electric form factor at intermediate values of  $Q^2$ . (See fig. 6.)

Measurements of the two-photon exclusive processes  $\gamma\gamma \rightarrow \pi^+\pi^-$  and  $K^+K^-$  are in excellent agreement with the perturbative QCD predictions. The analysis is based on the factorization illustrated in fig. 7. The data<sup>36</sup> (see fig. 8) extend out to invariant mass squared  $10 \text{ GeV}^2$ , a region well beyond any significant contribution from soft contributions.

Nevertheless, one can question<sup>32</sup> the consistency of the perturbative QCD analysis, particularly for baryon reactions at moderate momentum transfer:

1. The perturbative analysis of the baryon form factor and large angle hadron-hadron scattering depends on the suppression of the endpoint regions  $x_i \sim 1$  and pinch singularity contributions. This suppression occurs automatically in QCD due to Sudakov form factors, as has been shown by Mueller<sup>21</sup> based on the all-orders analysis of the vertex function by Sen.<sup>39</sup> Since these analyses require an all-orders resummation of the vertex corrections, they cannot be derived by standard renormalization group analysis. In this sense the baryon and large angle scattering results are considered less rigorous than the results from analysis of the meson form factor and the  $\gamma\gamma$  production of meson pairs.<sup>37</sup>

Fig. 5. Comparison of perturbative QCD predictions and data for the proton form factor. The calculation, based on the CZ QCD sum rule distribution amplitude, is from ref. 33. The prediction depends on the use of the running coupling constant as a function of the exchanged gluon momentum. The data are from ref. 34.



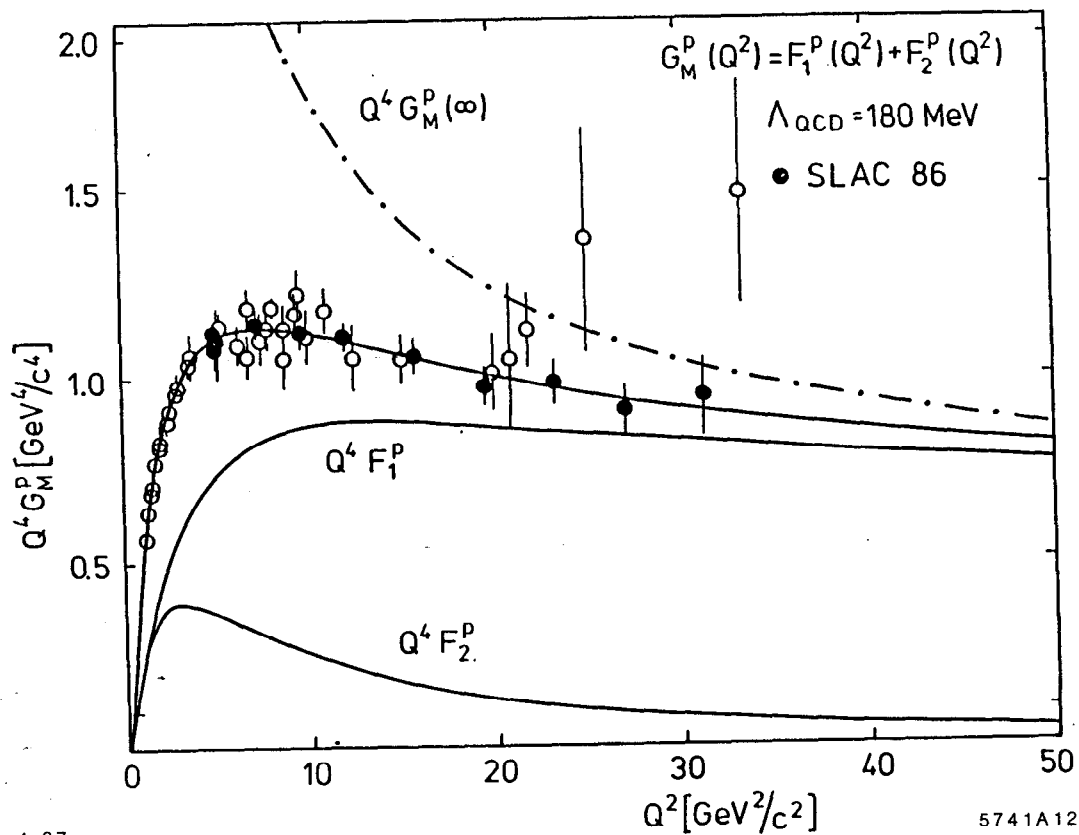


Fig. 6. Predictions for the nucleon form factors assuming VMD at low  $Q^2$  and perturbative QCD at high  $Q^2$ . From ref. 35.

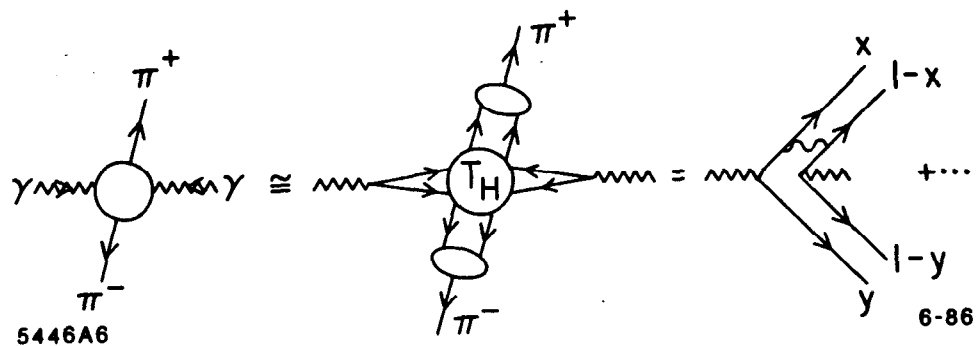


Fig. 7. Application of QCD to two photon production of meson pairs.

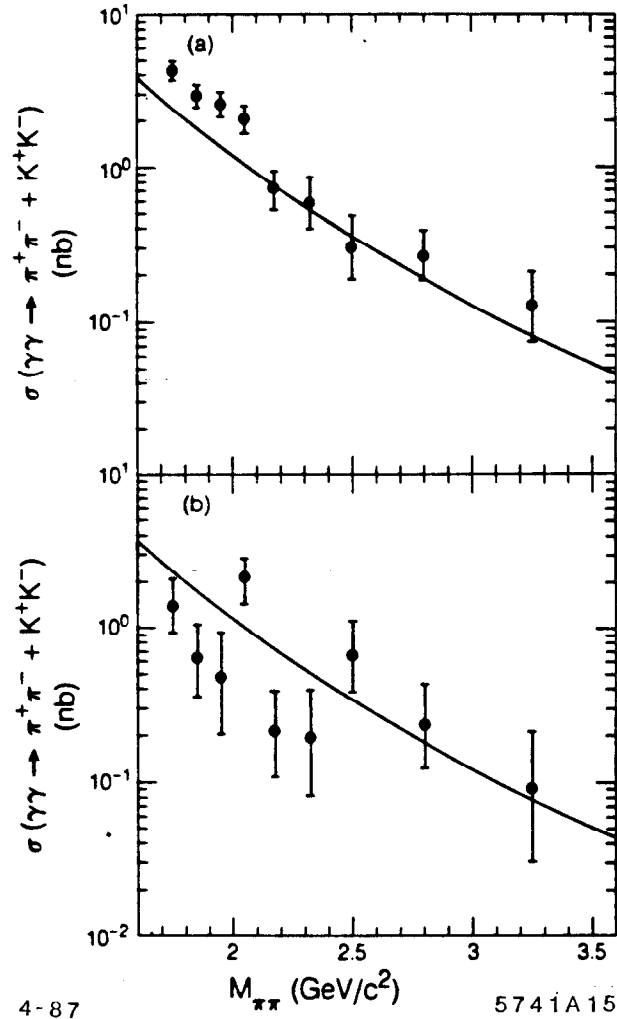


Fig. 8. Measurements<sup>36</sup> of exclusive two-photon reactions compared with the perturbative QCD predictions of ref. 37. The predictions are nearly independent of the shape of the meson distribution amplitudes.

2. The magnitude of the proton form factor is sensitive to the  $x \sim 1$  dependence of the proton distribution amplitude, where non-perturbative effects could be important. The CZ asymmetric distribution amplitude, in fact, emphasizes contributions from the large  $x$  region. Since non-leading corrections are expected when the quark propagator scale  $Q^2(1-x)$  is small, relatively large  $Q^2$  is required to clearly test the perturbative QCD predictions. A similar criterion occurs in the analysis of corrections to QCD evolution in deep inelastic lepton scattering. Dziembowski and Mankiewicz<sup>28</sup> claim that one can simultaneously fit low energy phenomena (the nucleon magnetic

moments), the measured high momentum transfer hadron form factors, and the CZ distribution amplitudes with a self-consistent ansatz for the quark wave functions.

A complete derivation of the nucleon form factors at all momentum transfers would require a calculation of the entire set of hadron Fock wave functions. (See fig. 9.) This is the goal of the “discretized light-cone quantization” approach<sup>40</sup> for finding the eigen-solutions of the QCD Hamiltonian quantized at equal light cone time  $\tau = t + z/c$ . using a discrete basis. We review this approach in section 15. Thus far results have been obtained for the spectrum and wave functions for QED and Yukawa field theories in one-space and one-time dimension. The structure function of the lowest mass bound state in QED [1+1] as a function of a scaled coupling constant is shown in fig. 10.

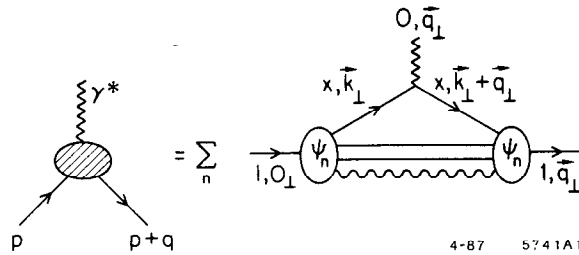


Fig. 9. Representation of electroweak hadron form factors in the light-cone formalism. The sum is over all charged quark lines and all Fock states  $\psi_n$ .

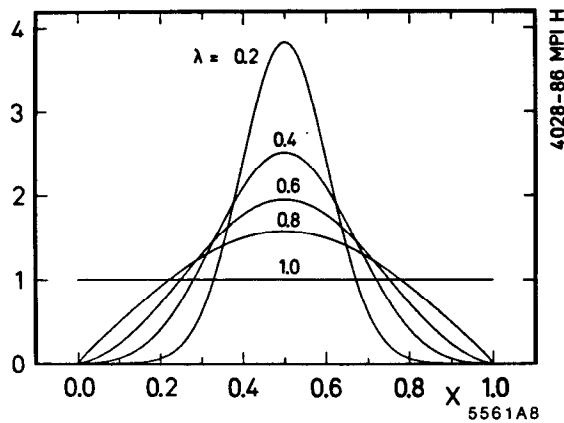


Fig. 10. The structure function of the lowest mass bound state for QED in 1+1 space-time dimensions, as calculated in the DLCQ formalism.<sup>38</sup>



## 4. Color Transparency

The QCD analysis of exclusive processes depends on the concept of a Fock state expansion of the nucleon wave function, projected onto the basis of free quark and gluon Fock states. The expansion is done at equal time on the light-cone and in the physical light-cone gauge. At large momentum transfer the lowest particle-number “valence” Fock component with all the quarks within an impact distance  $b_{\perp} \leq 1/Q$  controls the form factor at large  $Q^2$ . Such a Fock state component has a small color dipole moment and thus interacts only weakly with hadronic or nuclear matter.<sup>18,19</sup> Thus if elastic electron-scattering is measured as a quasi-elastic process inside a nucleus, one predicts negligible elastic and inelastic final state interactions in the target as  $Q$  becomes large. Integrating over Fermi-motion, one predicts<sup>30</sup> that the differential cross section is additive in the number of nucleons in the nucleus. The primary test of this idea is to study the attenuation of the recoil nucleon in quasi-elastic electron-nucleon scattering inside of a nuclear target. At large momentum transfers the final state nucleon should emerge from the target without suffering elastic or final state scattering. The shape of the transverse momentum distribution out of the scattering plane should be determined by the Fermi distribution alone.

A test of this novel effect, “color transparency”, has recently been carried out at Brookhaven for large momentum transfer elastic  $pp$  scattering in nuclear targets by a BNL-Columbia collaboration.<sup>41</sup> The initial results are suggestive of diminished absorptive cross sections at large momentum transfer. If these preliminary results are verified they could provide a striking confirmation of the perturbative QCD predictions.

The strong spin-asymmetries seen in elastic  $p$ - $p$  scattering<sup>42</sup> and the oscillations of the data modulating the predicted dimensional counting rule power-law fall-off<sup>43</sup> suggest possible resonant interference effects with the perturbative amplitude. [See also ref. 29.] These features evidentially cannot be explained in terms of the simplest QCD perturbative contributions.<sup>44</sup> (See fig. 11.) It is interesting to speculate whether one is observing an interference with pinch singularity contribution<sup>29</sup> or di-baryon resonances associated with the “hidden color” degrees of freedom of the six-quark state.<sup>45</sup> Since the resonant contributions are not coupled to small valence Fock states, one could expect significant final state corrections at energies where the resonances are important. Thus color transparency can be used to distinguish mechanisms for hadron scattering.

In the case of nucleon transition form factors measurable in inelastic electron nucleon scattering, the magnitude of the final state interactions should depend on the nature of the excited baryon. For example final state resonances which are higher orbital  $qqq$  states should have large color final state interactions.

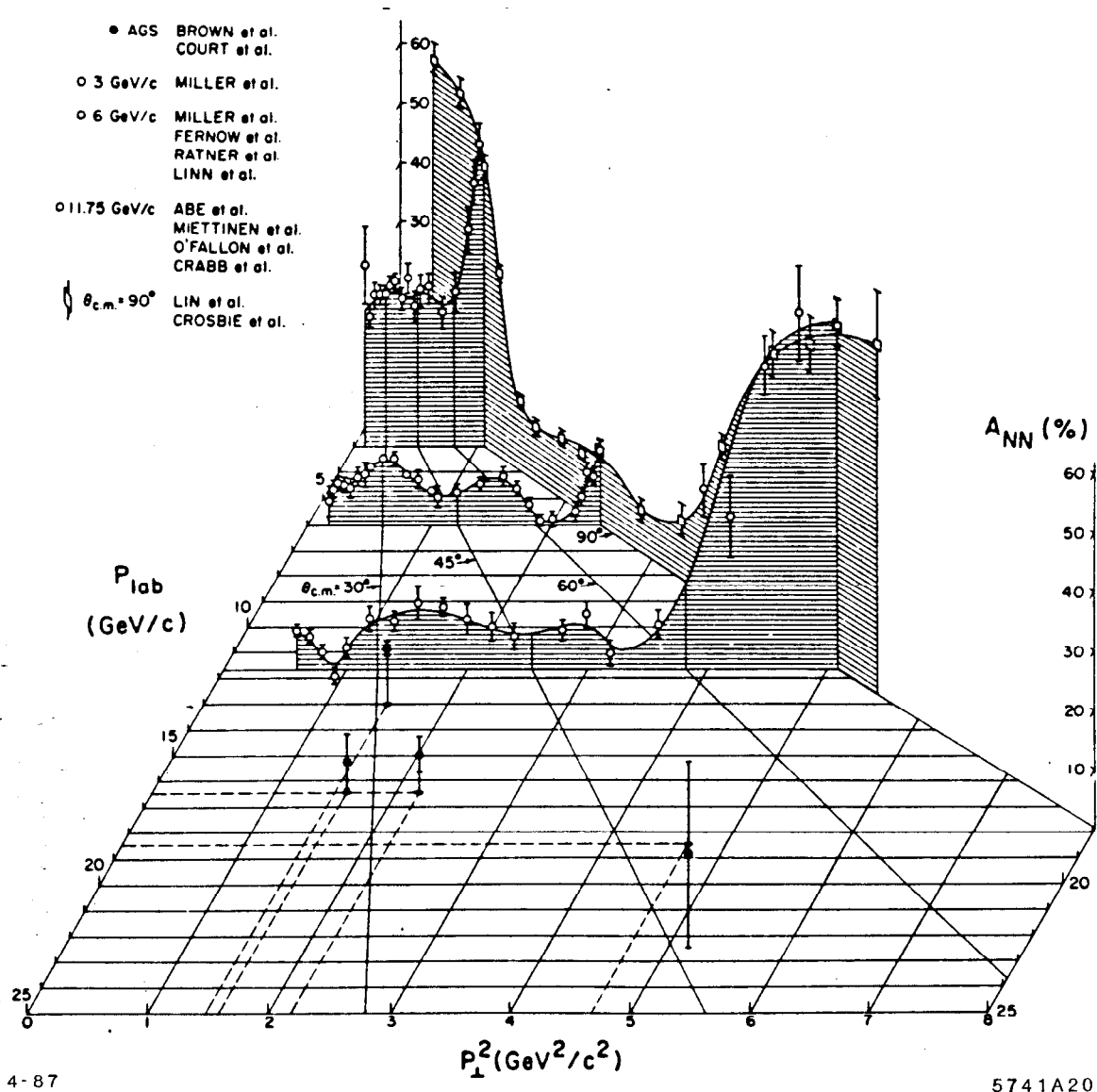


Fig. 11. Spin asymmetry for polarized  $pp$  elastic scattering. From ref. 42.

Perhaps the most dramatic application of color transparency is to the QCD analysis of the deuteron form factor at large momentum transfer.<sup>30,46</sup> A basic feature of the perturbative QCD formalism is that the six-quark wave function at small impact separation controls the deuteron form factor at large  $Q^2$ . (We discuss this further in chapter 22.) Thus even a complex six-quark state can have negligible final state interactions in a nuclear target—provided it is produced in a large momentum transfer reaction. One thus predicts that the “transparency ratio”  $\frac{d\sigma}{dt}[eA \rightarrow ed(A-1)] / \frac{d\sigma}{dt}[ed \rightarrow ed]$  will increase with momentum transfer. The normalization of the effective number of deuterons in the nucleus can be determined by single-arm quasi-elastic scattering.

Other experimental tests of the reduced amplitude formalism are discussed in section 23.

## 5. Diffractive Electroproduction Channels at Large Momentum Transfer

As a further example of the richness of the physics of exclusive electroproduction consider the “diffractive” channel  $\gamma^* p \rightarrow \rho^0 p$ . At large momentum transfer, QCD factorization for exclusive amplitudes applies, and we can write each helicity amplitude in the form:<sup>20</sup>

$$\mathcal{M}_{\gamma^* p \rightarrow \rho^0 p}(s, t, q^2) = \int \prod dx_i T_H(x_i, p_T^2, \theta_{cm}, q^2) \\ \times \phi_{\rho^0}^\dagger(x_i, p_T) \phi_p^\dagger(x_i, p_T) \phi_p(x_i, p_T) .$$

This represents the convolution of the distribution amplitudes  $\phi(x, Q)$  for the in-going and out-going hadrons with the quark-gluon hard scattering amplitude  $T_H(\gamma^* + (qqq)_p \rightarrow (q\bar{q})_{\rho^0} + (qqq)_p)$  for the scattering of the quarks from the initial to final hadron directions. Since  $T_H$  involves only large momentum transfer, it can be expanded in powers of  $\alpha_s(Q^2)$ . The distribution amplitudes  $\phi(x_i, p_T)$  only depend logarithmically on the momentum transfer scale, as determined from the meson and baryon evolution equations. As we discussed above, the functional dependence of the meson and baryon distribution amplitudes can be predicted from QCD sum rules. A surprising feature of the Chernyak and Zhitnitskii analysis<sup>6</sup> of the distribution amplitude of helicity-zero mesons is the prediction of a double-hump shape of  $\phi_M(x, Q)$  with a minimum at equal partition of the light-cone momentum fractions. (See fig. 12.) This result has now been confirmed in a lattice gauge theory calculation of the pion distribution amplitude moments by

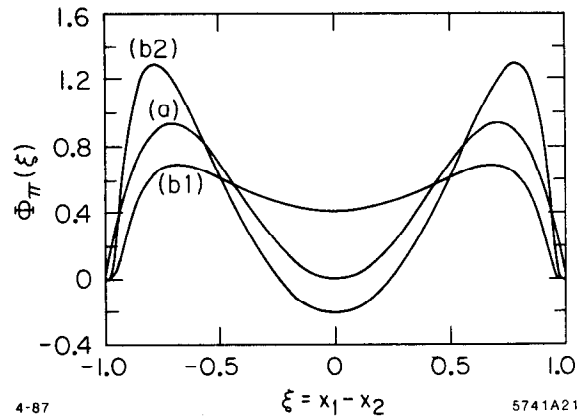


Fig. 12. Theoretical predictions for the pion distribution amplitude.

4-87

5741A21

Martinelli and Sachrajda.<sup>8</sup> Similar conclusions also emerge from the wave function ansatz of Dziembowski and Mankiewicz.<sup>28</sup>

The main dynamical dependence of the electroproduction amplitude is determined by  $T_H$ . To leading order in  $\alpha_s(p_T^2)$ ,  $T_H$  can be calculated from minimally-connected tree graphs; power counting predicts

$$T_H = \frac{e\alpha_s^3(p_T^2)}{(p_T^5)} f\left(\theta_{cm}, \frac{Q^2}{p_T^2}\right)$$

and thus

$$\frac{d\sigma}{dt}(\gamma^* p \rightarrow \rho p) \sim \frac{\alpha\alpha_s^6(p_T^2)}{(p_T^2)^7} F\left(\theta_{cm}, \frac{Q^2}{p_T^2}\right)$$

to leading order in  $1/p_T^2$  and  $\alpha_s(p_T^2)$ . This prediction is consistent with the dimensional counting rule  $d\sigma/dt \sim s^{2-n} f(\theta_{cm})$  where  $n = 9$  is the total number of initial and final fields. The scaling laws hold for both real and virtual photons. As shown in fig. 13, the data<sup>47</sup> for  $\gamma p \rightarrow \pi^+ n$  are consistent with the QCD scaling law prediction.

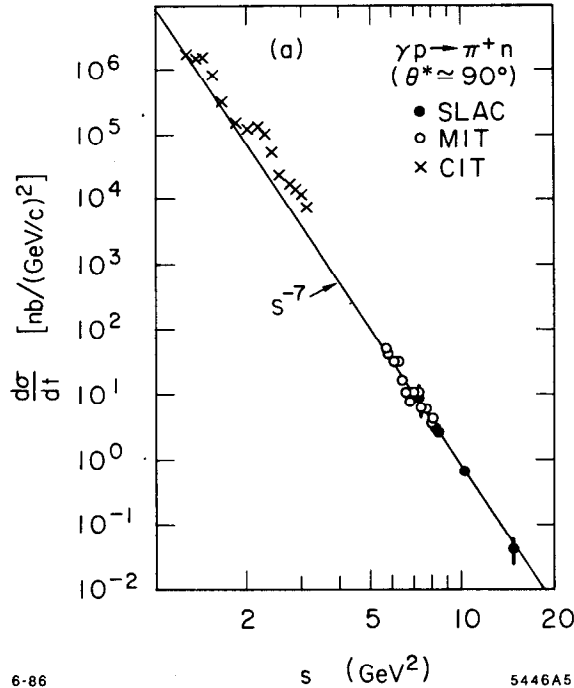


Fig. 13. Comparison of pion photoproduction data<sup>47</sup> at  $\theta_{cm} = \pi/2$  with the quark counting rule prediction.

The leading contributions at large momentum transfer in QCD satisfy hadron helicity conservation<sup>26</sup>

$$\lambda_p = \lambda_{p'} + \lambda_\rho.$$

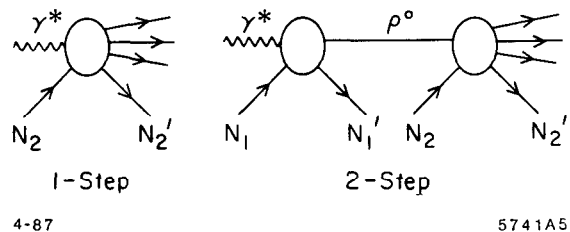
This selection rule is an important test of the vector coupling of the gluon in QCD. The result is independent of the photon helicity! Furthermore, the leading behavior comes from the “point-like” Fock component of the photon. The vector-meson-dominance contribution corresponds to the  $q\bar{q}$  state where the constituent momenta are restricted to be collinear to the photon. This region gives a power-law suppressed  $(1/p_T^2)^8$  contribution to the cross section at fixed  $\theta_{cm}$ .

The dependence on the photon mass in exclusive electroproduction amplitudes in QCD occurs through the scaling variable  $Q^2/p_T^2$ . Thus for  $Q^2 \ll p_T^2$ , the transverse photon electroproduction amplitudes are predicted to be insensitive to  $Q^2$ . This is in striking consequence to the vector meson dominance picture, which predicts a universal  $1/(1 + Q^2/m_\rho^2)$  dependence in the amplitude. Furthermore, since only the point-like component of the photon is important at large  $p_T$ , one expects no absorption of the initial state photon as it penetrates a nuclear target. The reaction  $\gamma^* n \rightarrow \pi^- p$  is a particularly interesting test of color transparency since the dependence on photon mass and momentum transfer can be probed.

The conventional theory<sup>48</sup> of shadowing of photon interactions is illustrated in fig. 14. At large  $Q^2$  the two-step amplitude is suppressed and the shadowing effect becomes negligible. This is the basis for a general expectation that shadowing of nuclear structure functions is actually a higher-twist phenomena, vanishing with increasing  $Q^2$  at fixed  $x$ . [A recent analysis on shadowing in electroproduction by Qiu and Mueller<sup>49</sup> based on higher-twist internucleon interactions in the gluon evolution equation in a nucleus suggests that shadowing decreases slowly as  $Q^2$  increases.] Thus we predict simple additivity for exclusive electroproduction in nuclei

$$\overline{\frac{d\sigma}{dt}} (\gamma^* A \rightarrow \rho^0 N(A-1)) = A \frac{d\sigma}{dt} (\gamma^* N \rightarrow \rho^0 N)$$

Fig. 14. Conventional description of nuclear shadowing of low- $Q^2$  virtual photon nuclear interactions. The 2-step amplitude is opposite in phase to the direct contribution on nucleon  $N_2$  because of the diffractive vector meson production on upstream nucleon  $N_1$ .



4-87

5741A5

to leading order in  $1/p_T^2$ . (The bar indicates that the cross sections are integrated over the nucleon Fermi motion.) This is another application of color transparency. What is perhaps surprising is that the prediction holds for small  $Q^2$ , even  $Q^2 = 0$ ! Note that the leading contribution in  $1/p_T^2$  (all orders in  $\alpha_s(p_T^2)$ ) comes from the  $\gamma \rightarrow q\bar{q}$  point-like photon coupling in  $T_H$  where the relative transverse momentum of the  $q\bar{q}$  are of order  $p_T$ . Thus the "impact" or transverse size of the  $q\bar{q}$  is  $1/p_T$ , and such a "small" color dipole has negligible strong interactions in a nucleus. The final state proton and  $\rho^0$  also couple in leading order to Fock components which are small in impact space, again having minimal initial or final state interactions. If this additivity and absence of shadowing is verified, it will also be important to explore the onset of conventional shadowing and absorption as  $p_T^2$  and  $Q^2$  decrease.

## 6. Electroproduction of Diffractive Channels and the QCD Pomeron

Exclusive processes such as virtual Compton scattering,  $\gamma^*p \rightarrow \gamma p$  and  $\rho^0$  electroproduction  $\gamma^*p \rightarrow \rho^0 p$  play a special role in QCD as key probes of "pomeron" exchange and its possible basis in terms of multiple-gluon exchange.<sup>17</sup> At large photon energy, the diffractive amplitudes are dominated by  $J = 1$  Regge singularities.

Recent measurements of  $\gamma^*p \rightarrow \rho^0 p$  by the EMC group<sup>50</sup> using the high energy muon beam at the SPS show three unexpected features: (1) The  $\rho^0$  is produced with zero helicity at  $Q^2 \geq 1$  GeV<sup>2</sup>; (2) the falloff in momentum transfer becomes remarkably flat for  $Q^2 \geq 5$  GeV<sup>2</sup>; and (3) the integrated cross section falls off approximately as  $1/Q^4$ .

The most surprising feature of the EMC data is the very slow fall-off in  $t$  for the highest  $Q^2$  data. (See fig. 15.) Using the parameterization  $e^{bt'}$ ,  $t' = |t - t_{min}|$ , the slope for  $7 \leq Q^2 \leq 25$  GeV<sup>2</sup>,  $E_L = 200$  GeV data is  $b \sim 2$  GeV<sup>-2</sup>. If one assumes Pomeron factorization, then the fall-off in momentum transfer to the proton should be at least as fast as the square of the proton form factor,<sup>51</sup> representing the probability to keep the scattered proton intact. (See fig. 16(b).) The predicted slope for  $|t| < 1.5$  GeV<sup>2</sup> is  $b \sim 3.4$  GeV<sup>-2</sup>, much steeper than the EMC data. The background due to inelastic effects is estimated by the EMC group to be less than 20% in this kinematic domain.

In the vector meson dominance picture one expects: (1) dominantly transverse  $-\rho$  polarization (s-channel helicity conservation); (2) fall-off in  $t$  similar to the square of the proton form factor (Pomeron factorization); and (3) a  $1/Q^2$  asymptotic fall-off when longitudinal photons dominate.

The physics of electroproduction is quite different in QCD. At large  $Q^2 \gg p_T^2$  diffractive channels take on a novel character.<sup>17</sup> (See fig. 16(c).) The transverse

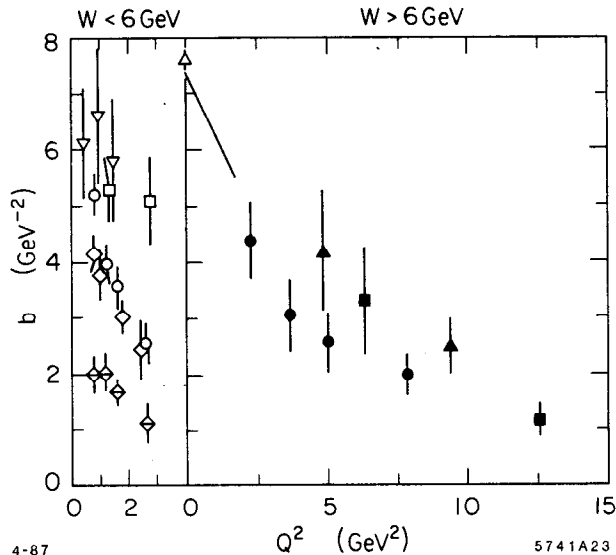


Fig. 15. The slope parameter  $b$  for the form  $d\sigma/dt = Ae^{bt'}$  fit to the EMC data (ref. 50) for  $\mu p \rightarrow \mu\rho^0 p$  for  $|t'| \leq 1.5 \text{ GeV}^2$ .

momentum  $k_T$  in the upper loop connecting the photon and  $\rho^0$  is of order the photon mass scale,  $k_T \sim Q$ . (Other regions of phase space are suppressed by Sudakov form factors). Thus just as in deep inelastic inclusive scattering, the diffractive amplitude involves the proton matrix element of the product of operators near the light-cone. In the case of virtual Compton scattering  $\gamma^* p \rightarrow \gamma p'$ , one measures product of two electromagnetic currents. Thus one can test an operator product expansion similar to that which appears in deep inelastic lepton-nucleon scattering, but for non-forward matrix elements. In such a case the upper loop in fig. 16(c) can be calculated using perturbative methods. The  $\rho$  enters through the same distribution amplitude that appears in large momentum transfer exclusive reactions. Since the gauge interactions conserve helicity, this implies  $\lambda_\rho = 0$ ,  $\lambda_p = \lambda'_p$  independent of the photon helicity. The predicted canonical  $Q^2$  dependence is  $1/Q^4$ , which is not inconsistent with the EMC data.

Since the EMC data is at high energy ( $E_\gamma = 200 \text{ GeV}$ ,  $s \gg p_T^2$ ) one expects that the vector gluon exchange diagrams dominate quark-exchange contributions. One can show that the virtuality of the gluons directly coupled to the  $\gamma \rightarrow \rho$  transition is effectively of order  $Q^2$ , allowing a perturbative expansion. The effect is a known feature of the higher Born, multi-photon exchange contributions to massive Bethe Heitler processes in QED.<sup>15</sup>

The dominant exchange in the t-channel should thus be the two-gluon ladder shown in fig. 16(c). This is analogous to the diagrams contributing to the evolution of the gluon structure function. If each gluon carries roughly half of the momentum

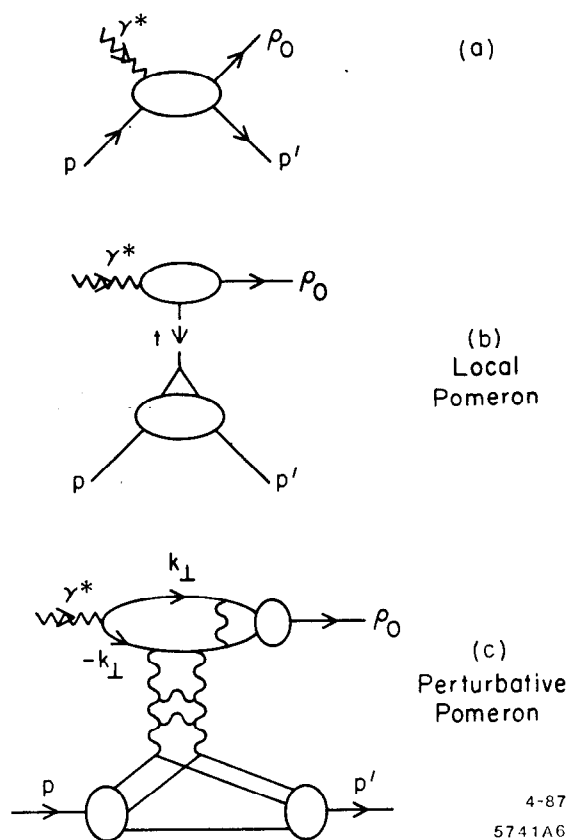


Fig. 16. (a) Diffractive electroproduction of vector mesons. (b) Local pomeron contribution coupling to one quark. (c) Perturbative pomeron contribution. For large transverse loop momentum  $k_t^2 \approx Q^2$  two-gluon exchange contributions are dominant.

transfer to different quarks in the nucleon, then the fall-off in  $t$  can be significantly slower than that of the proton form factor, since in the latter case the momentum transfer to the nucleon is due to the coupling to one quark. This result assumes that the natural fall-off of the nucleon wave function in transverse momentum is Gaussian rather than power-law at low momentum transfer.

In the case of quasi-elastic diffractive electroproduction in a nuclear target, we expect neither shadowing of the incident photon nor final state interactions of the outgoing vector meson at large  $Q^2$  (color transparency).

Thus  $\rho^0$  electroproduction and virtual Compton scattering can give essential information on the nature of diffractive (pomeron exchange) processes. Data at all energies and kinematic regions are clearly essential.



## 7. Exclusive Nuclear Processes in QCD

One of the most elegant areas of application of QCD to nuclear physics is the domain of large momentum transfer exclusive nuclear processes. Rigorous results have been given by Lepage, Ji and myself<sup>46</sup> for the asymptotic properties of the deuteron form factor at large momentum transfer. The basic factorization is shown in fig. 17. In the asymptotic  $Q^2 \rightarrow \infty$  limit the deuteron distribution amplitude, which controls large momentum transfer deuteron reactions, becomes fully symmetric among the five possible color-singlet combinations of the six quarks. One can also study the evolution of the "hidden color" components (orthogonal to the  $np$  and  $\Delta\Delta$  degrees of freedom) from intermediate to large momentum transfer scales; the results also give constraints on the nature of the nuclear force at short distances in QCD. The existence of hidden color degrees of freedom further illustrates the complexity of nuclear systems in QCD. It is conceivable that six-quark  $d^*$  resonances corresponding to these new degrees of freedom may be found by careful searches of the  $\gamma^*d \rightarrow \gamma d$  and  $\gamma^*d \rightarrow \pi d$  channels.

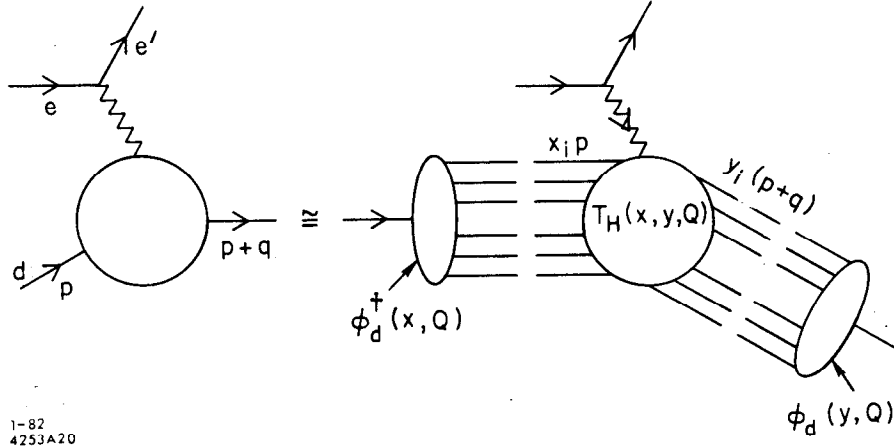


Fig. 17. Factorization of the deuteron form factor at large  $Q^2$ .

The QCD analyses suggests a consistent way to eliminate the effects of nucleon compositeness in exclusive nuclear reactions.<sup>30,52</sup> The basic observation is that for vanishing nuclear binding energy  $\epsilon_d \rightarrow 0$ , the deuteron can be regarded as two nucleons sharing the deuteron four-momentum. The  $\gamma^*d \rightarrow np$  amplitude then contains two factors representing the probability amplitude for the proton and neutron to remain intact after absorbing momentum transfers

$$\hat{t} = (p_p - \frac{1}{2} p_d)^2 \quad \text{and} \quad \hat{u} = (p_n - \frac{1}{2} p_d)^2 .$$

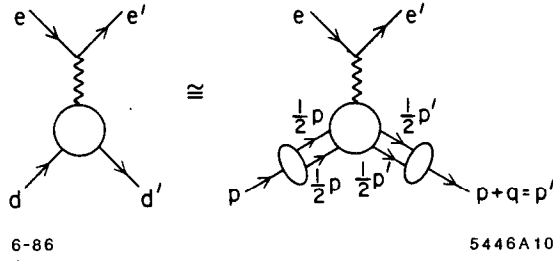


Fig. 18. Application of the reduced amplitude formalism to the deuteron form factor at large momentum transfer.

The "reduced" amplitude

$$m_r(\gamma^* d \rightarrow np) = \frac{M(\gamma^* d \rightarrow np)}{F_{1N}(\hat{t})F_{1N}(\hat{u})}$$

is predicted to have the same fixed angle scaling behavior as  $\gamma^* M \rightarrow q\bar{q}$ ; i.e., the nucleons are reduced to point particles. We thus predict

$$\frac{d\sigma}{d\Omega_{cm}}(\gamma^* d \rightarrow np) \sim \frac{f(\Omega_{cm})}{(p_T^2)^2}$$

to leading order in  $1/p_T^2$ .

The analogous analysis (see fig. 18) of the deuteron form factor as defined in

$$\frac{d\sigma}{dt}(\ell d \rightarrow \ell d) = \frac{d\sigma}{dt}\Big|_{point} |F_d(Q^2)|^2$$

yields a scaling law for the reduced form factor

$$f_d(Q^2) \equiv \frac{F_d(Q^2)}{F_{1N}\left(\frac{Q^2}{4}\right)F_{1N}\left(\frac{Q^2}{4}\right)} \sim \frac{1}{Q^2}$$

i.e., the same scaling law as a meson form factor. As shown in fig. 19, this scaling is consistent with experiment for  $Q^2 = p_T^2 \gtrsim 1 \text{ GeV}^2$ . There is also evidence for reduced amplitude scaling for  $\gamma d \rightarrow pn$  at large angles and  $p_T^2 \gtrsim 1 \text{ GeV}^2$ . We thus expect similar precocious scaling behavior to hold for  $\bar{p}d \rightarrow \pi^- p$  and other  $\bar{p}d$  exclusive reduced amplitudes. In each case the incident and outgoing hadron and nuclear states are predicted to display color transparency, i.e. the absence of initial and final state interactions if they participate in a large momentum transfer exclusive reaction.

We give more detailed discussions of the application of QCD to the deuteron and the reduced amplitude formalism in sections 22 and 23.

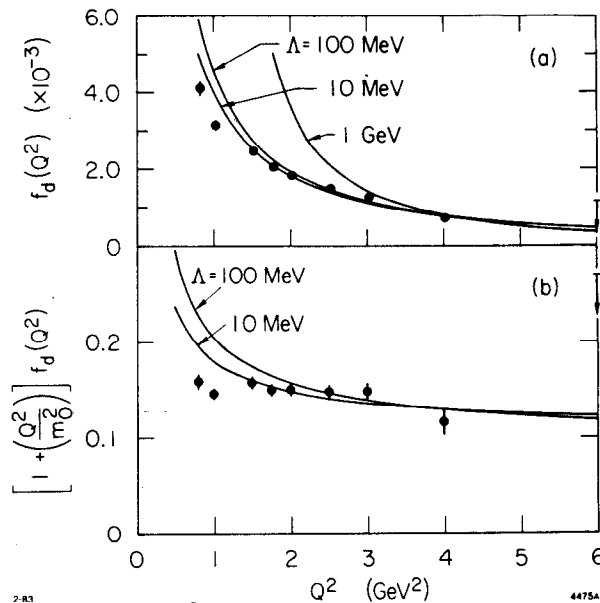


Fig. 19. (a) Comparison of the asymptotic QCD predictions with experiment using  $F_N(Q^2) = [1 + (Q^2/0.71 \text{ GeV}^2)]^{-2}$ . The normalization is fit at  $Q^2 = 4 \text{ GeV}^2$ . (b) Comparison of the prediction  $[1 + (Q^2/m_0^2)]f_d(Q^2) \propto (\ln Q^2)^{-1-(2/5)(C_F/\beta)}$  with data. The value  $m_0^2 = 0.28 \text{ GeV}^2$  is used.

## 8. Electroproduction: A General View

The factorization formula<sup>53</sup>

$$\begin{aligned} \frac{d\sigma(AB \rightarrow CX)}{d^3p_c/E_c} &\cong \sum_{ab,cd} \int_0^1 dx_a \int_0^1 dx_b \int_0^1 \frac{dx_c}{x_c^2} \\ &\times G_{a/A}(x_a, Q) G_{b/B}(x_b, Q) \tilde{G}_{C/c}(x_c, Q) \\ &\times \delta(s' + t' + u') \frac{s'}{\pi} \frac{d\sigma}{dt'}(ab \rightarrow cd) \end{aligned}$$

for the inclusive production processes  $AB \rightarrow CX$  has general validity in gauge theory. The systems  $A, B, C$  can be leptons, photons, hadrons, or nuclei. The primary subprocess in electroproduction is  $eq \rightarrow eq$ . The electron structure function  $G_{e/e}(x, Q)$  automatically provides the (leading logarithmic) QED radiative corrections. The energy distribution of the beam itself plays the role of the non-perturbative or initial structure function. (See fig. 20(b).) The subprocess  $\gamma^*q \rightarrow gq$  corresponds to photon-induced two-jet production. (See fig. 20(a).) This

subprocess dominates reactions in which the large transverse momentum trigger is a hadron rather than the scattered lepton. Thus one sees that conventional deep inelastic  $eq \rightarrow eq$  scattering subprocess is just one of the several modes of electroproduction.

The dominant contribution to the meson semi-inclusive cross section is predicted by QCD factorization to be due to jet fragmentation from the recoil quark and spectator di-quark jets. When the momentum transfer is in the intermediate range  $1 \lesssim Q^2 \lesssim 10 \text{ GeV}^2$ , several other contributions for meson production are expected to become important in  $eN \rightarrow e'MX$ . These include:

- (1) Higher twist contributions to jet fragmentation:

$$\frac{dN_\pi}{dz} = D_{\pi/q}(z, Q^2) \cong A(1-z)^2 + \frac{C}{Q^2} \quad (z \rightarrow 1).$$

The scaling term reflects the behavior of the pion fragmentation function at large fractional momentum ( $z \rightarrow 1$ ) as predicted by perturbative QCD (one-gluon exchange). (See fig. 21(a).) The  $C/Q^2$  term<sup>54</sup> is computed from the same perturbative diagrams. For large  $z$  where this term dominates, we predict that the deep inelastic cross section will be dominantly longitudinal rather than transverse  $R = \sigma_L/\sigma_T > 1$ .

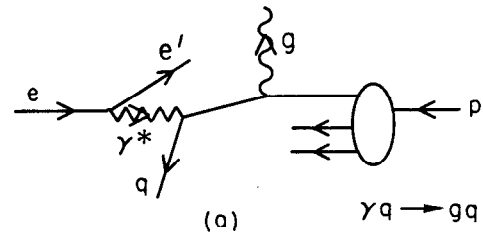
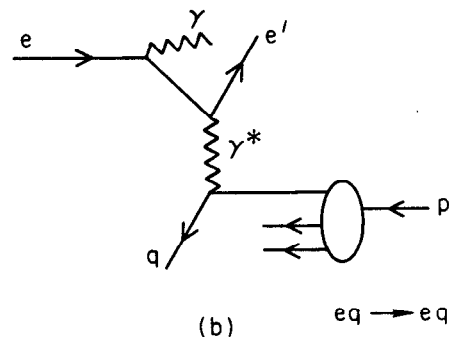


Fig. 20. Application of gauge theory factorization to electroproduction. (a) The  $\gamma q \rightarrow gq$  subprocess produces hadron jets at high  $p_T$ . (b) The  $eq \rightarrow eq$  produces one quark jet and one recoil electron jet at high  $p_T$ . The QED radiative corrections are incorporated into the electron and photon QED structure functions.



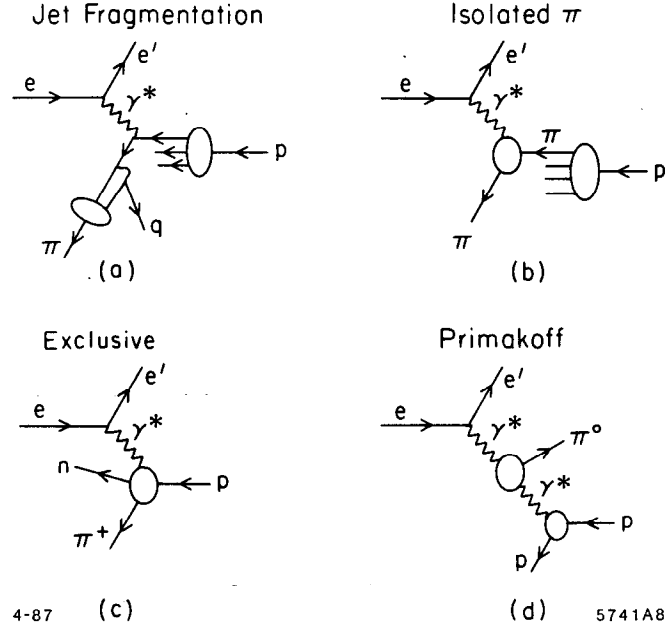


Fig. 21. QCD contributions to pion electroproduction. (a) Jet fragmentation, including leading and  $1/Q^2$  higher twist contributions. (b) Isolated pion contributions at order  $1/Q^4$ . (c) Exclusive production. (d) Primakoff contribution.

(2) "Direct" meson production. Isolated pions may also be created by elastic scattering off of an effective pion current: (See fig. 21(b).)

$$\frac{d\sigma}{dQ^2 dx_\pi} = G_{\pi/p}(x_\pi) \left. \frac{d\sigma}{dQ^2} \right|_{e\pi \rightarrow e\pi}$$

$$\left. \frac{d\sigma}{dy dQ^2} \right|_{e\pi \rightarrow e\pi} = \frac{4\pi\alpha^2}{(Q^2)^2} |F_\pi(Q^2)|^2 (1-y).$$

Here  $y = q \cdot p / p_e \cdot p$ . In the case of a nuclear target, one can test for non-additivity of virtual pions due to nuclear effects, as predicted in models<sup>55</sup> for the EMC effect<sup>50</sup> at small  $x_{Bj}$ . Jaffe and Hoodbhoy<sup>9</sup> have shown that the existence of quark exchange diagrams involving quarks of different nucleons in the nucleus invalidates general applicability of the simplest convolution formulae conventionally used in such analyses. The  $G_{\pi/p}(x, Q)$  structure function is predicted to behave roughly as  $(1-x)^5$  at large  $x$ , as predicted from spectator quark counting rules.<sup>24,53</sup> Applications of these rules to other off-shell nucleon processes are discussed in refs. 30 and 56.

(3) Exclusive Channels. (See fig. 21(c).) The mesons can of course be produced in exclusive channels; e.g.  $\gamma^* p \rightarrow \pi^+ n$ ,  $\gamma^* p \rightarrow \rho^0 p$ . Pion electroproduction

extrapolated to  $t = m_\pi^2$  provides our basic knowledge of the pion form factor at spacelike  $Q^2$ . With the advent of the perturbative QCD analyses of large momentum transfer exclusive reactions, predictions can be given over the whole range of large  $t$  and  $Q^2$ . We discussed some of the features of  $\rho^0$  electroproduction above.

(4) Another possible meson production channel is Primakoff production  $\gamma^* \gamma \rightarrow \pi^0$ , etc., identifiable from very low target recoil events. (See fig. 21(d).) Such measurements would allow the determination of the  $\gamma \rightarrow \pi^0$  transition form factor. This quantity, combined with the QCD analysis of the pion form factor leads to a method to determine the QCD running coupling constant  $\alpha_s(Q^2)$  solely from exclusive measurements.<sup>37</sup>

The above examples make it clear that complete final state measurements are necessary for separating the various production channels; detailed study of meson electroproduction can yield valuable information concerning basic issues in QCD.

## 9. Higher Twist Contributions to Deep Inelastic Scattering

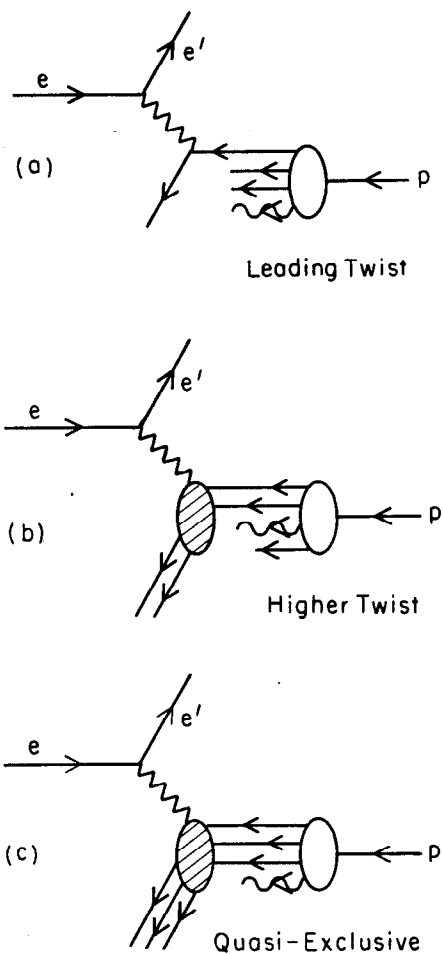
One of the most difficult aspects of electroproduction phenomenology is the separation of logarithmic scaling violations predicted by QCD evolution from the scale violations induced by power law corrections. The lack of a full understanding of these higher twist terms has prevented the extraction of reliable values of the QCD scale  $\Lambda_{QCD}$  from the data. As we have noted above, shadowing behavior in nuclei is likely associated with higher twist contributions. In addition, it is not clear whether ordinary Regge behavior of the inelastic lepton scattering cross section, which is a valid parameterization at fixed  $Q^2$ , persists into the scaling region or whether it is associated with higher twist dynamical effects. The fact that the non-singlet structure functions obey additive sum rules suggests that Regge behavior is absent in leading twist.

In some cases the higher twist effect corresponds to coherent many-particle processes which potentially could be identified by study of the final state. As an example, consider the processes illustrated in fig. 22. At intermediate  $Q^2$  and  $x = x_{Bj} \sim 1$  the cross section has the simplified form

$$\frac{d\sigma}{dQ^2 dx} = \frac{4\pi\alpha^2}{Q^4} \left[ A(1-x)^3 + B(1-x) \left( \frac{1}{Q^2} \right)^2 + C(1-x)^{-1} \left( \frac{1}{Q^2} \right)^4 \right].$$

The three terms correspond to lepton scattering off of one, two, or three quarks, respectively. The power in  $1/Q^2$  increases with the number of active quarks:  $(Q^2)^{2(n_A-1)}$ . The power in  $(1-x)$  counts the number of spectators<sup>53</sup> required to stop as  $x \rightarrow 1$ :  $(1-x)^{2n_s-1}$ . The "diquark" term gives a large  $\sigma_L$  contribution.<sup>54</sup> The analogous structure in the pion structure function has been confirmed in the

Drell-Yan reaction  $\pi N \rightarrow \mu^+ \mu^- X$  at large  $x$ .<sup>54</sup> The relative normalization of the power-law suppressed terms is uncertain, although the model calculations based on tree-graph gluon exchange diagrams performed by Blankenbecler, Gunion, and Nason<sup>57</sup> suggests very large coefficients  $B$  and  $C$ . If this is true for the physical situation, then the existence of such terms would make it very difficult to isolate the logarithmic corrections to scaling, except at very high momentum transfers—where unfortunately the sensitivity to the numerical value of  $\Lambda_{QCD}$  is small. Internal target experiments may be able to confirm the different contributions by studies of the recoil and spectator systems as functions of  $Q^2$  and  $x$  together with separation of  $\sigma_L$  and  $\sigma_T$ .



4-87

5741A7

Fig. 22. Leading and higher twist contributions to deep inelastic lepton scattering due to multi-particle hard scattering subprocesses.

## 10. Formation Zone Phenomena in Deep Inelastic Scattering

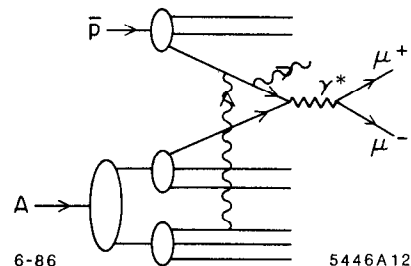
One of the remarkable consequences of QCD factorization for inclusive reactions at large  $p_T$  is the absence of inelastic initial or final state interactions of the high energy particles in a nuclear target. Since structure functions measured in deep inelastic lepton scattering are essentially additive (up to the EMC deviations), factorization implies that the  $q\bar{q} \rightarrow \mu^+\mu^-$  subprocesses in Drell-Yan reactions occurs with equal effect on each nucleon throughout the nucleus. At first sight this seems surprising since one expects energy loss from inelastic initial state interactions.

In fact, potential inelastic reactions such as quark or gluon bremsstrahlung induced in the nucleus which could potentially decrease the incident parton energy (illustrated in fig. 23) are suppressed by coherence if the quark or gluon energy (in the laboratory frame) is large compared to the target length:

$$E_q > \mu^2 L_A$$

Here  $\mu^2$  is the difference of mass squared that occurs in the initial or final state collision. This phenomenon has its origin in studies of QED processes by Landau and Pomeranchuk. The QCD analysis is given by Bodwin, Lepage and myself.<sup>11</sup> Elastic collisions, however, are still allowed, so one expects collision broadening of the initial parton transverse momentum. Recent measurements of the Drell-Yan process  $\pi A \rightarrow \mu^+\mu^- X$  by the NA-10 group<sup>58</sup> at the CERN-SPS confirm that the cross section for muon pairs at large transverse momentum is increased in a tungsten target relative to a deuteron target. (See fig. 24). Since the total cross section for lepton-pair production scales linearly with  $A$  (aside from relatively small EMC-effect corrections), there must be a corresponding decrease of the ratio of the differential cross section at low values of the di-lepton transverse momentum. This is also apparent in the data.

Fig. 23. Induced radiation from the propagation of an antiquark through a nuclear target in massive lepton production. Such inelastic interactions are coherently suppressed at parton energies large compared to a scale proportional to the length of the target.



These results have striking implications for the interaction of the recoil quark jet in deep inelastic electron-nucleus scattering. For the quark (and gluons) satisfying the length condition, there should be no extra radiation induced as the parton



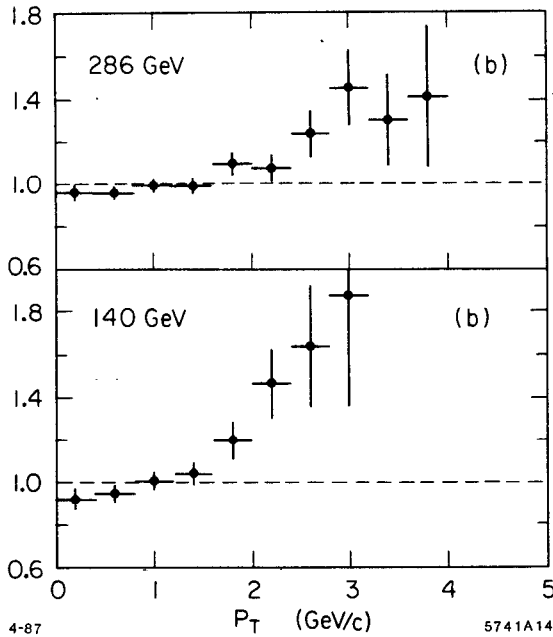
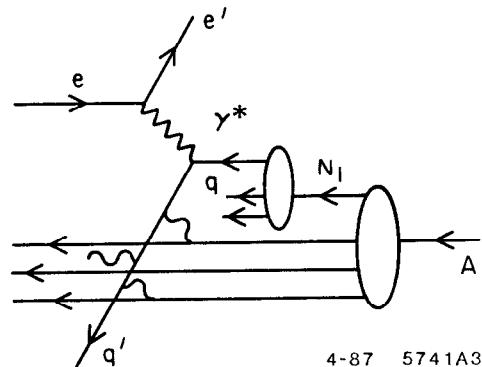


Fig. 24. The ratio  $\sigma(\pi^- W \rightarrow \mu^+ \mu^- X) / \sigma(\pi^- D \rightarrow \mu^+ \mu^- X)$  as a function of the pair transverse momentum. From ref. 58.

traverses the nucleus. Thus gluon radiation of the type illustrated in fig. 25 should be suppressed. However, low energy gluons, emitted in the deep inelastic electron-quark collision, can suffer radiative losses, leading to cascading of soft particles in the nucleus. It is clearly very important to study this phenomena as a function of recoil quark energy and nuclear size.

Fig. 25. Propagation of the struck quark through a nuclear target. Induced gluon radiation (inelastic final state interactions) is suppressed at high quark energies. Elastic scattering in the final state however is not suppressed.



4-87 5741A3

It should be emphasized that the absence of inelastic initial or final state collisions for high energy partons does not preclude collision broadening due to elastic initial or final state interactions. The elastic corrections are unitary to leading order in  $1/Q$  and do not effect the normalization of the deep inelastic

cross section. Thus we predict that the mean square transverse momentum of the recoil quark and its leading particles will increase as  $A^{1/3}$ .

The transverse momentum of the recoil quark reflects the intrinsic transverse momentum of the nucleon wave function. The EMC effect<sup>50</sup> implies that quarks in a nucleus have smaller average longitudinal momentum than in a nucleon. (See fig. 26.) Independent of the specific physical mechanism underlying the EMC effect, the quarks in a nucleus would also be expected to have smaller transverse momentum. This effect can counteract to a certain extent the collision broadening of the outgoing jet.

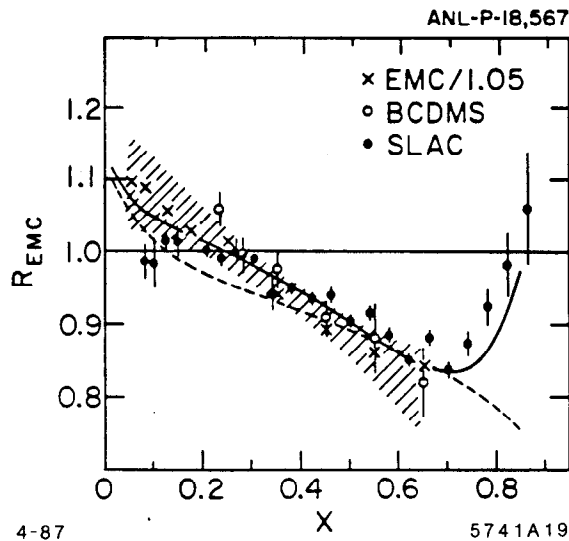


Fig. 26. Ratio of nuclear and nucleon structure functions. The theoretical curves are from the pion current calculation of Berger and Coester, ref. 55.

Unlike the struck quark the remnant of the target system does not evolve with the probe momentum  $Q$ . However, since the quantum numbers of the spectator system is  $\bar{3}$  in color, nonperturbative hadronization must occur. Since the transverse momentum of the leading particles in the spectator jet is not affected by the QCD radiative corrections, it more closely reflects the intrinsic transverse momentum of the hadron state.

It is also interesting to study the behavior of the transverse momentum of the quark and spectator jets as a function of  $x_{Bj}$ . For  $x_{Bj} \sim 1$ , the 3-quark Fock state dominates the reaction. If the valence state has a smaller transverse size<sup>20</sup> than that of the nucleon, averaged over all of its Fock components, then we expect an increase of  $\langle k_{\perp}^2 \rangle$  in that regime. Evidence for a significant increase of  $\langle k_{\perp}^2 \rangle$  in

the projectile fragmentation region at large quark momentum fractions has been reported by the SFM group<sup>59</sup> at the ISR for  $pp \rightarrow \text{di-jet} + X$  reactions.

## 11. Diffraction Channels and Nuclear Structure Function Non-Additivity

One unusual source of non-additivity in nuclear structure functions (EMC effect) are electroproduction events at large  $Q^2$  and low  $x$  which nevertheless leave the nucleus completely intact  $x < (1/ML_A)$ . In the case of QED, analogous processes such as  $\gamma^* A \rightarrow \mu^+ \mu^- X$  yield nuclear-coherent contributions which scales as  $A_{eff} = Z^2/A$ . (See fig. 27(a).) Such processes contribute to the Bjorken-scaling, leading-twist cross section.<sup>60</sup> In QCD we expect<sup>61</sup> the nuclear dependence to be less than additive for the analogous gluon exchange contributions (see fig. 27(b)) because of their diffractive coupling to the nucleus. One can identify nuclear-coherent events contributions by observing a rapidity gap between the produced particles and the recoiling target. An interesting question is how the gluon momentum fraction sum rule is modified by the diffractive contributions.

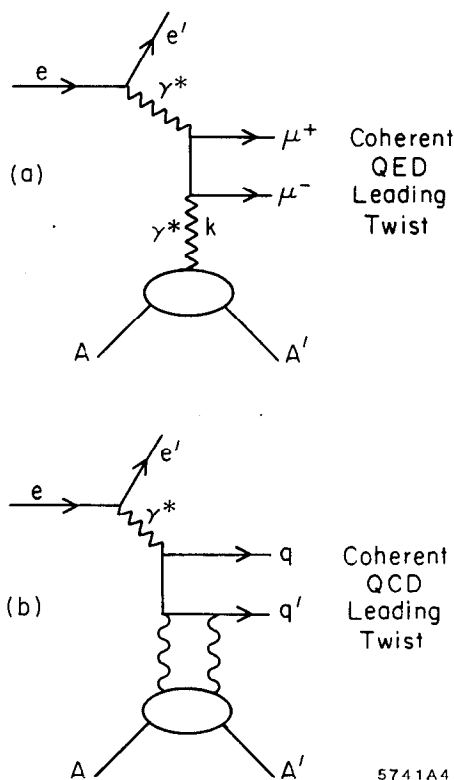


Fig. 27. Leading twist contributions to deep inelastic-lepton-nucleus scattering that leave the target intact. (a) QED example. (b) QCD example.

## 12. Studying “Jet-Coalescence” in Electroproduction

What happens if two jets overlap in phase-space? Certainly independent fragmentation of the jets will fail because of coherent effects. For example, in QED there are strong final state interactions when two charged particles are produced at low relative velocity. In the case of particles of opposite charge  $Z_1e, -Z_2e$ , the QED Born cross sections are corrected by the factor<sup>14</sup> :

$$\sigma = \sigma_0 \frac{2\pi Z_1 Z_2 \alpha / v}{1 - \exp(2\pi Z_1 Z_2 \alpha / v)}$$

which increases the cross section dramatically at low relative velocity  $v$ . We expect similar effects in QCD when two jets can coalesce to attractive color channels ( $Z_1 Z_2 \alpha \rightarrow C_F \alpha_s$  for  $q\bar{q}$  color singlets). In the case of electroproduction, the low relative velocity enhancements provide a simple estimate of the increase of the  $ep \rightarrow eX$  cross section at low values of  $W^2 = (q+p)^2$ , beyond that given by simple duality arguments.

Gunion, Soper and I<sup>15</sup> have recently proposed this jet coalescence mechanism as an explanation of the observed leading particle correlations seen in charm hadroproduction experiments and the anomalously large cross section<sup>62</sup> observed at the SPS for  $\Sigma^- N \rightarrow A^+(csu)X$  at large  $x_L$ . [The hyperon momentum was 135 GeV/c.] In the case of heavy quark electroproduction e.g.  $\gamma^* g \rightarrow s\bar{s}, c\bar{c}$ , one predicts an enhancement of the cross section when the produced quark is at low rapidity relative to the target fragmentation region. The correction to the rate, integrated over relative rapidity, is found to vanish only as a single inverse power of the heavy quark mass, and thus may give significant corrections to charm production rates and distributions.

The Sommerfeld factor also can be used to estimate the behavior of exclusive amplitudes near threshold. For example, the production of meson pairs in two photon annihilation can be modeled<sup>16</sup> by calculating the differential cross section in QCD tree graph approximation (as in fig. 7), and then multiplying by the QCD version of the Sommerfeld factor appropriate to the relative velocity and color correlation of each quark pair. Further discussion may be found in ref. 16.

### 13. Summary on Electroproduction

Electroproduction at intermediate energies on an internal target in a storage ring such as PEP could allow the study of many fundamental phenomena in QCD:

(a) A primary goal is the channel-by-channel reconstruction of the final state in electroproduction in order to understand in detail the final state hadronization of both the quark and nucleon spectator jets in a regime where Bjorken scaling is manifest. Such studies can also provide checks on the effect of the higher-twist coherent contributions to electroproduction cross sections. The hadronization of the target jet is a still largely unexplored phenomenon.

(b) The dynamics of individual exclusive electroproduction amplitudes can be probed as a function of all kinematic energy and angle variables including the virtual photon's mass and polarization. As we have discussed, such processes can often be analyzed systematically in perturbative QCD, providing detailed checks on both QCD dynamics and hadron wave functions. The diffractive reactions also allow the study of the non-forward matrix elements of the same operator product entering the near the light-cone analysis of deep inelastic structure functions.

(c) A nuclear target provides a unique probe of short-distance QCD dynamics. The basic subprocesses can be studied in a background nuclear field. In particular, one wants to study the sources of nonadditivity in the nuclear target channel by channel. This includes tests of various shadowing mechanisms, effects of modification of mesonic degrees of freedom, the predicted "color transparency" of quasi-exclusive amplitudes at large momentum transfer inside a nucleus, and the propagation of quark jets through the nuclear medium. Further, as discussed in ref. 30, one can use large  $x$  measurements to probe nuclear matter in the far off-shell domain. We also note that exclusive channels which involve the scattering of light nuclei at high momentum transfer probe the  $NN$  interaction at short distances.

(d) Given sufficient luminosity, internal target experiments could allow the study of strange and charm particle electroproduction near threshold. By comparing electron and positron beam experiments, one can probe<sup>10</sup> virtual Compton scattering; the sum of the quark charges cubed can be obtained from the ratio of the  $e^\pm p \rightarrow e^\pm \gamma + X$  cross sections. Polarized proton and nuclear targets allow the study of detailed effects of spin via correlations with final state properties. The combination of polarized target and polarized electron beams allow measurements of the spin dependent structure functions and their sum rules,<sup>63</sup> checks of helicity selection rules, and the separation of different electroproduction channels.

Although there have been extensive tests of many aspects of electroproduction over the past decade, there are still many phenomena still not fully explored. The distinction between logarithmic and power-law scale breaking effects is still

in a confused state. Shadowing, diffraction, the interrelation with vector meson dominance, the structure of the (non-evolved) spectator jet system, Regge behavior in non-singlet structure functions, and other phenomena at the boundary between perturbative and non-perturbative effects; all are central topics in hadron and nuclear dynamics, ideally studied in electroproduction.

## 14. QCD ON THE LIGHT-CONE

A key problem in the application of QCD to hadron and nuclear physics is how to determine the wave function of a relativistic multi-particle composite system. It is not possible to represent a relativistic field-theoretic bound system limited to a fixed number of constituents at a given time since the interactions create new quanta from the vacuum. Although relativistic wave functions can be represented formally in terms of the covariant Bethe-Salpeter formalism, calculations beyond ladder approximation appear intractable. Unfortunately, the Bethe-Salpeter ladder approximation is often inadequate. For example, in order to derive the Dirac equation for the electron in a static Coulomb field from the Bethe-Salpeter equation for muonium with  $m_\mu/m_e \rightarrow \infty$  one requires an infinite number of irreducible kernel contributions to the QED potential. Matrix elements of currents and the wave function normalization also require, at least formally, the consideration of an infinite sum of irreducible kernels. The relative-time dependence of the Bethe Salpeter amplitudes for states with three or more constituent fields adds severe complexities.

A different and more intuitive procedure would be to extend the Schrödinger wave function description of bound states to the relativistic domain by developing a relativistic many-body Fock expansion for the hadronic state. Formally this can be done by quantizing QCD at equal time, and calculating matrix elements from the time-ordered expansion of the  $S$ -matrix. However, the calculation of each covariant Feynman diagram with  $n$ -vertices requires the calculation of  $n!$  frame-dependent time-ordered amplitudes. Even worse, the calculation of the normalization of a bound state wave function (or the matrix element of a charge or current operator) requires the computation of contributions from all amplitudes involving particle production from the vacuum. (Note that even after normal-ordering, the interaction Hamiltonian density for QED,  $H_I = e : \bar{\psi} \gamma_\mu \psi A^\mu :$ , contains contributions  $b^\dagger d^\dagger a^\dagger$  which create particles from the perturbative vacuum.)

Fortunately, there is a natural and consistent covariant framework, originally due to Dirac,<sup>64</sup> (quantization on the "light front") for describing bound states in gauge theory analogous to the Fock state in non-relativistic physics. This frame-

work is the light-cone quantization formalism in which

$$\begin{aligned}
 |\pi\rangle &= |q\bar{q}\rangle \psi_{q\bar{q}}^\pi + |q\bar{q}g\rangle \psi_{q\bar{q}g}^\pi + \dots \\
 |p\rangle &= |qqq\rangle \psi_{qqq}^p + |qqqg\rangle \psi_{qqqg}^p + \dots
 \end{aligned}
 \tag{4}$$

Each wave function component  $\psi_n$ , etc. describes a state of fixed number of quark and gluon quanta evaluated in the interaction picture at equal light-cone "time"  $\tau = t + z/c$ . Given the  $\{\psi_n\}$ , virtually any hadronic property can be computed, including anomalous moments, form factors, structure functions for inclusive processes, distribution amplitudes for exclusive processes, etc.

The use of light-cone quantization and equal  $\tau$  wave functions, rather than equal  $t$  wave functions, is necessary for a sensible Fock state expansion. It is also convenient to use  $\tau$ -ordered light-cone perturbation theory (LCPTh) in place of covariant perturbation theory for much of the analysis of light-cone dominated processes such as deep inelastic scattering, or large- $p_\perp$  exclusive reactions. Light-cone quantization and perturbation theory are developed in detail in the following sections.

## 15. Quantization of Gauge Theory on the Light-Cone <sup>65</sup>

One of the most important advantages of quantizing a gauge theory on the light-cone (or light-front, as originally termed by Dirac) is the existence of a consistent Fock state basis with only positive metric quanta: in  $A^+ = 0$  gauge there are no ghosts either of the Gupta-Bleuler or Faddeev-Popov kind. In QCD, hadronic matrix elements, including structure functions and electroweak transition amplitude have a straightforward representation in terms of a physical Fock basis of positive metric quarks and gluons. The light-cone quantization procedure of field theory is given in detail in Ref. 20. Here we only review the essential points.

The gauge field  $A^\mu$  is a traceless  $3 \times 3$  color matrix ( $A^\mu \equiv \sum_a A^{a\mu} T^a$ ,  $\text{Tr}(T^a T^b) = 1/2 \delta^{ab}$ ,  $[T^a, T^b] = ic^{abc} T^c, \dots$ ), and the quark field  $\psi$  is a color triplet spinor (for simplicity, we include only one flavor). At a given light-cone time, say  $\tau = 0$ , the independent dynamical fields are  $\psi_+ \equiv \Lambda_+ \psi$  and  $A_\perp^i$  with conjugate fields  $i\psi_+^\dagger$  and  $\partial^+ A_\perp^i$ , where  $\Lambda_\pm = \gamma^0 \gamma^\pm / 2$  are projection operators ( $\Lambda_+ \Lambda_- = 0$ ,  $\Lambda_\pm^2 = \Lambda_\pm$ ,  $\Lambda_+ + \Lambda_- = 1$ ) and  $\partial^\pm = \partial^0 \pm \partial^3$ . Using the equations of motion, the remaining fields in  $\mathcal{L}$  can be expressed in terms of  $\psi_+$ ,  $A_\perp^i$ :

$$\begin{aligned}
\psi_- &\equiv \Lambda_- \psi = \frac{1}{i\partial^+} \left[ i\vec{D}_\perp \cdot \vec{\alpha}_\perp + \beta m \right] \psi_+ \\
&= \tilde{\psi}_- - \frac{1}{i\partial^+} g \vec{A}_\perp \cdot \vec{\alpha}_\perp \psi_+ , \\
A^+ &= 0 , \\
A^- &= \frac{2}{i\partial^+} i\vec{\partial}_\perp \cdot \vec{A}_\perp + \frac{2g}{(i\partial^+)^2} \left\{ \left[ i\partial^+ A_\perp^i, A_\perp^i \right] + 2\psi_+^\dagger T^a \psi_+ T^a \right\} \\
&\equiv \tilde{A}^- + \frac{2g}{(i\partial^+)^2} \left\{ \left[ i\partial^+ A_\perp^i, A_\perp^i \right] + 2\psi_+^\dagger T^a \psi_+ T^a \right\} ,
\end{aligned} \tag{5}$$

with  $\beta = \gamma^0$  and  $\vec{\alpha}_\perp = \gamma^0 \vec{\gamma}$ . This result is a special feature of light-cone gauge: field operators do not appear in the denominator. Furthermore  $A^+ = 0$  is consistent with the equation of methods and does not need to be enforced as a special constraint on the Hilbert space.

To quantize QCD, we expand the fields at  $\tau = 0$  in terms of creation and annihilation operators,

$$\begin{aligned}
\psi_+(x) = \int_{k^+ > 0} \frac{dk^+ d^2 k_\perp}{k^+ 16\pi^3} \sum_\lambda \left\{ b(\underline{k}, \lambda) u_+(\underline{k}, \lambda) e^{-ik \cdot x} \right. \\
\left. + d^\dagger(\underline{k}, \lambda) v_+(\underline{k}, \lambda) e^{ik \cdot x} \right\} , \quad \tau = x^+ = 0
\end{aligned} \tag{6}$$

$$A_\perp^i(x) = \int_{k^+ > 0} \frac{dk^+ d^2 k_\perp}{k^+ 16\pi^3} \sum_\lambda \left\{ a(\underline{k}, \lambda) \epsilon_\perp^i(\lambda) e^{-ik \cdot x} + c \cdot c \right\} , \quad \tau = x^+ = 0 ,$$

with commutation relations ( $\underline{k} = (k^+, \vec{k}_\perp)$ ):

$$\begin{aligned}
\{b(\underline{k}, \lambda), b^\dagger(\underline{p}, \lambda')\} &= \{d(\underline{k}, \lambda), d^\dagger(\underline{p}, \lambda')\} \\
&= [a(\underline{k}, \lambda), a^\dagger(\underline{p}, \lambda')] \\
&= 16\pi^3 k^+ \delta^3(\underline{k} - \underline{p}) \delta_{\lambda\lambda'} ,
\end{aligned} \tag{7}$$

$$\{b, b\} = \{d, d\} = \dots = 0 ,$$

where  $\lambda$  is the quark or gluon helicity. These definitions imply canonical commutation relations for the fields with their conjugates ( $\tau = x^+ = y^+ = 0, \underline{x} =$



$(x^-, \underline{x}_\perp), \dots$ :

$$\begin{aligned} \left\{ \psi_+(\underline{x}), \psi_+^\dagger(\underline{y}) \right\} &= \Lambda_+ \delta^3(\underline{x} - \underline{y}) , \\ \left[ A^i(\underline{x}), \partial^+ A_\perp^j(\underline{y}) \right] &= i\delta^{ij} \delta^3(\underline{x} - \underline{y}) . \end{aligned} \quad (8)$$

The creation and annihilation operators define the Fock state basis for the theory at  $\tau = 0$ , with a vacuum  $|0\rangle$  defined such that  $b|0\rangle = d|0\rangle = a|0\rangle = 0$ . One can construct the energy momentum tensor  $T^{\mu\nu}$  and the conserved four momenta:

$$P^\nu = \frac{1}{2} \int dx^- T^{+\nu}(x^-, \tau = 0) ,$$

The evaluation of states with  $\tau$  is governed by the light-cone Hamiltonian,  $H_{LC} = P^-$ , conjugate to  $\tau$ . The Hamiltonian can be readily expressed in terms of  $\psi_+$  and  $A_\perp^i$ :

$$H_{LC} = H_0 + V , \quad (9)$$

where

$$\begin{aligned} H_0 &= \int d^3x \left\{ \text{Tr} \left( \partial_\perp^i A_\perp^j \partial_\perp^i A_\perp^j \right) + \psi_+^\dagger (i\partial_\perp \cdot \alpha_\perp + \beta m) \frac{1}{i\partial^+} (i\partial_\perp \cdot \alpha_\perp + \beta m) \psi_+ \right\} \\ &= \sum_{\substack{\lambda \\ \text{colors}}} \int \frac{dk^+ d^2k_\perp}{16\pi^3 k^+} \left\{ a^\dagger(\underline{k}, \lambda) a(\underline{k}, \lambda) \frac{k_\perp^2}{k^+} + b^\dagger(\underline{k}, \lambda) b(\underline{k}, \lambda) \right. \\ &\quad \left. \times \frac{k_\perp^2 + m^2}{k^+} + d^\dagger(\underline{k}, \lambda) b(\underline{k}, \lambda) \frac{k_\perp^2 + m^2}{k^+} \right\} + \text{constant} \end{aligned} \quad (10)$$

is the free Hamiltonian and  $V$  the interaction:

$$\begin{aligned} V &= \int d^3x \left\{ 2g \text{Tr} \left( i\partial^\mu \tilde{A}^\nu \left[ \tilde{A}_\mu, \tilde{A}_\nu \right] \right) - \frac{g^2}{2} \text{Tr} \left( \left[ \tilde{A}^\mu, \tilde{A}^\nu \right] \left[ \tilde{A}_\mu, \tilde{A}_\nu \right] \right) \right. \\ &\quad \left. + g \bar{\psi} \tilde{A} \psi + g^2 \text{Tr} \left( \left[ i\partial^+ \tilde{A}^\mu, \tilde{A}_\mu \right] \frac{1}{(i\partial^+)^2} \left[ i\partial^+ \tilde{A}^\nu, \tilde{A}_\nu \right] \right) \right. \\ &\quad \left. + g^2 \bar{\psi} \tilde{A} \frac{\gamma^+}{2i\partial^+} \tilde{A} \psi - g^2 \bar{\psi} \gamma^+ \left( \frac{1}{(i\partial^+)^2} \left[ i\partial^+ \tilde{A}^\nu, \tilde{A}_\nu \right] \right) \bar{\psi} \right. \\ &\quad \left. + \frac{g^2}{2} \bar{\psi} \gamma^+ T^a \psi \frac{1}{(i\partial^+)^2} \bar{\psi} \gamma^+ T^a \psi \right\} , \end{aligned} \quad (11)$$

with  $\bar{\psi} = \bar{\psi}_- + \psi_+$  ( $\rightarrow \psi$  as  $g \rightarrow 0$ ) and  $\tilde{A}^\mu = (0, \tilde{A}^-, A_\perp^i)$  ( $\rightarrow A^\mu$  as  $g \rightarrow 0$ ). The

Fock states are obviously eigenstates of  $H_0$  with

$$H_0 |n : k_i^+, k_{\perp i}\rangle = \sum_i \left( \frac{k_{\perp i}^2 + m^2}{k^+} \right) |n : k_i^+, k_{\perp i}\rangle . \quad (12)$$

It is equally obvious that they are not eigenstates of  $V$ , though any matrix element of  $V$  between Fock states is trivially evaluated. The first three terms in  $V$  correspond to the familiar three and four gluon vertices, and the gluon-quark vertex [fig. 28(a)]. The remaining terms result from the substitutions (5), and represent new four-quanta interactions containing instantaneous fermion and gluon propagators [fig. 28(b)]. The instantaneous gluon exchange contribution is analogous to the Coulomb interactions. The instantaneous fermion exchange contribution is analogous to the "seagull" term in scalar electrodynamics.

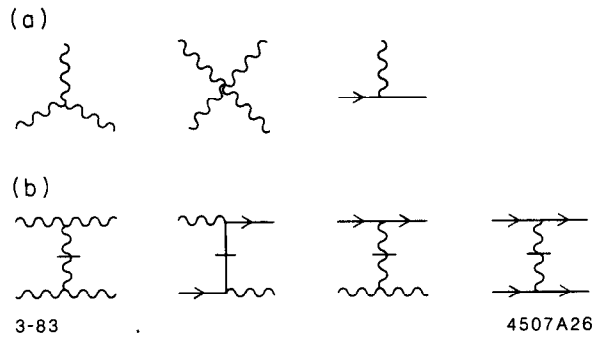


Fig. 28. (a) Basic interaction vertices in QCD.  
(b) "Instantaneous" contributions.

All terms conserve total three-momentum  $\underline{k} = (k^+, \vec{k}_{\perp})$ , because of the integral over  $\underline{x}$  in  $V$ . Furthermore, all Fock states other than the vacuum have total  $k^+ > 0$ , since each individual bare quantum has  $k^+ > 0$ . Consequently the Fock state vacuum must be an eigenstate of  $V$  and therefore an eigenstate of the full light-cone Hamiltonian.

### Light-Cone Perturbation Theory

We define light-cone Green's functions to be the probability amplitudes that a state starting in Fock state  $|i\rangle$  ends up in Fock state  $|f\rangle$  a (light-cone) time  $\tau$  later

$$\begin{aligned} \langle f|i\rangle G(f,i;\tau) &\equiv \langle f|e^{-iH_{LC}\tau/2}|i\rangle \\ &= i \int \frac{d\epsilon}{2\pi} e^{-i\epsilon\tau/2} G(f,i;\epsilon) \langle f|i\rangle , \end{aligned} \quad (13)$$

where Fourier transform  $G(f, i; \epsilon)$  can be written

$$\begin{aligned}
\langle f|i \rangle G(f, i; \epsilon) &= \left\langle f \left| \frac{1}{\epsilon - H_{LC} + i0_+} \right| i \right\rangle \\
&= \left\langle f \left| \frac{1}{\epsilon - H_{LC} + i0_+} + \frac{1}{\epsilon - H_0 + i0_+} V \frac{1}{\epsilon - H_0 + i0_+} \right. \right. \\
&\quad \left. \left. + \frac{1}{\epsilon - H_0 + i0_+} V \frac{1}{\epsilon - H_0 + i0_+} V \frac{1}{\epsilon - H_0 + i0_+} + \dots \right| i \right\rangle.
\end{aligned} \tag{14}$$

The rules for  $\tau$ -ordered perturbation theory follow immediately from this expansion when  $(\epsilon - H_0)^{-1}$  is replaced by its spectral decomposition in terms of Fock states:

$$\frac{1}{\epsilon - H_0 + i0_+} = \sum_{n, \lambda_i} \int \tilde{\Pi} \frac{dk_i^+ d^2 k_{\perp i}}{16\pi^3 k_i^+} \frac{|n : \underline{k}_i, \lambda_i\rangle \langle n : \underline{k}_i, \lambda_i|}{\epsilon - \sum_i (k^2 + m^2)_i / k_i^+ + i0_+} \tag{15}$$

where the sum is over all states  $n$  intermediate between two interactions. To calculate  $G(f, i; \epsilon)$  perturbatively then, all  $\tau$ -ordered diagrams must be considered, the contribution from each graph computed according to the following rules:

1. Assign a momentum  $k^\mu$  to each line such that the total  $k^+, k_\perp$  are conserved at each vertex, and such that  $k^2 = m^2$ , i.e.,  $k^- = (k^2 + m^2)/k^+$ . With fermions associate an on-shell spinor

$$u(\underline{k}, \lambda) = \frac{1}{\sqrt{k^+}} \left( k^+ + \beta m + \vec{\alpha}_\perp \cdot \vec{k}_\perp \right) \begin{cases} \chi(\uparrow) & \lambda = \uparrow \\ \chi(\downarrow) & \lambda = \downarrow \end{cases}$$

or

$$v(\underline{k}, \lambda) = \frac{1}{\sqrt{k^+}} \left( k^+ - \beta m + \vec{\alpha}_\perp \cdot \vec{k}_\perp \right) \begin{cases} \chi(\downarrow) & \lambda = \uparrow \\ \chi(\uparrow) & \lambda = \downarrow \end{cases}$$

where  $\chi(\uparrow) = 1/\sqrt{2}(1, 0, 1, 0)$  and  $\chi(\downarrow) = 1/\sqrt{2}(0, 1, 0, -1)^T$ . For gluon lines, assign a polarization vector  $\epsilon^\mu = (0, 2\vec{\epsilon}_\perp \cdot \vec{k}_\perp / k^+, \vec{\epsilon}_\perp)$  where  $\vec{\epsilon}_\perp(\uparrow) = -1/\sqrt{2}(1, i)$  and  $\vec{\epsilon}_\perp(\downarrow) = 1/\sqrt{2}(1, -i)$ .

2. Include a factor  $\theta(k^+)/k^+$  for each internal line.
3. For each vertex include factors as illustrated in fig. 29. To convert incoming into outgoing lines or vice versa replace

$$u \leftrightarrow v, \quad \bar{u} \leftrightarrow -\bar{v}, \quad \epsilon \leftrightarrow \epsilon^*$$

in any of these vertices.

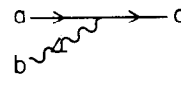
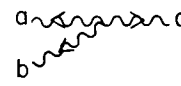
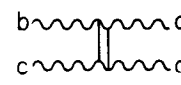
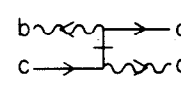
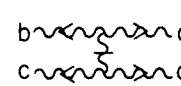
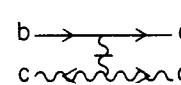
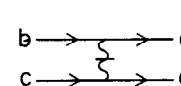
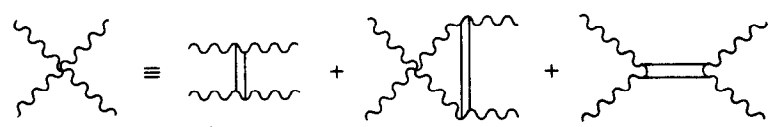
	<u>Vertex Factor</u>	<u>Color Factor</u>
	$g \bar{u}(c) \not{\epsilon}_b u(a)$	$T^b$
	$g \{ (p_a - p_b) \cdot \epsilon_c^* \epsilon_a \cdot \epsilon_b$ + cyclic permutations $\}$	$iC^{abc}$
	$g^2 \{ \epsilon_b \cdot \epsilon_c \epsilon_a^* \cdot \epsilon_d^* + \epsilon_a^* \cdot \epsilon_c \epsilon_b \cdot \epsilon_d^* \}$	$iC^{abe} iC^{cde}$
	$g^2 \bar{u}(a) \not{\epsilon}_b \frac{\gamma^+}{2(p_c^+ - p_d^+)} \not{\epsilon}_c^* u(d)$	$T^b T^d$
	$g^2 \epsilon_a^* \cdot \epsilon_b \frac{(p_a^+ - p_b^+)(p_c^+ - p_d^+)}{(p_c^+ + p_b^+)} \epsilon_d^* \cdot \epsilon_c$	$iC^{abe} iC^{cde}$
	$g^2 \bar{u}(a) \gamma^+ u(b) \frac{(p_c^+ - p_d^+)}{(p_c^+ + p_d^+)^2} \epsilon_d^* \cdot \epsilon_c$	$iC^{cde} T^e$
	$g^2 \frac{\bar{u}(a) \gamma^+ u(b) \bar{u}(d) \gamma^+ u(c)}{(p_c^+ - p_d^+)^2}$	$T^e T^e$
		
3-83		4507A25

Fig. 29. Graphical rules for QCD in light-cone perturbation theory.

4. For each intermediate state there is a factor

$$\frac{1}{\epsilon - \sum_{\text{interm}} k^- + i0_+}$$

where  $\epsilon$  is the incident  $P^-$ , and the sum is over all particles in the intermediate state.

5. Integrate  $\int dk^+ d^2 k_\perp / 16\pi^3$  over each independent  $k$ , and sum over internal helicities and colors.
6. Include a factor  $-1$  for each closed fermion loop, for each fermion line that both begins and ends in the initial state (i.e.  $\bar{v} \dots u$ ), and for each diagram in which fermion lines are interchanged in either of the initial or final states.

As an illustration, we give a representative contribution

$$\frac{1}{\epsilon - \sum_{i=b,d} \left( \frac{k_{\perp}^2 + m^2}{k^+} \right)_i} \cdot \frac{\theta(k_a^+ - k_b^+)}{k_a^+ - k_b^+}$$

$$\times \frac{g^2 \sum_{\lambda} \bar{u}(b) \epsilon^*(\underline{k}_a - \underline{k}_b, \lambda) u(a) \bar{u}(d) \not{\epsilon}(\underline{k}_a - \underline{k}_b, \lambda) u(c)}{\epsilon - \sum_{i=b,c} \left( \frac{k_{\perp}^2 + m^2}{k^+} \right)_i - \frac{(k_{\perp a} - k_{\perp b})^2}{k_a^+ - k_b^+}} \cdot \frac{1}{\epsilon - \sum_{i=a,c} \left( \frac{k_{\perp}^2 + m^2}{k^+} \right)_i}$$

(times a color factor) to the  $q\bar{q} \rightarrow q\bar{q}$  Green's function. (The vertices for quarks and gluons of definite helicity have very simple expressions in terms of the momenta of the particles.) These same rules apply for scattering amplitudes, but with propagators omitted for external lines, and with  $\epsilon = P^-$  of the initial (and final) states.

Finally, notice that this quantization procedure and perturbation theory (graph by graph) are manifestly invariant under a large class of Lorentz transformations:

1. boosts along the 3-direction — i.e.  $p^+ \rightarrow K p^+$ ,  $p^- \rightarrow K^{-1} p^-$ ,  $p_{\perp} \rightarrow p_{\perp}$  for each momentum;
2. transverse boosts — i.e.  $p^+ \rightarrow p^+$ ,  $p^- \rightarrow p^- + 2p_{\perp} \cdot Q_{\perp} + p^+ Q_{\perp}^2$ ,  $p_{\perp} \rightarrow p_{\perp} + p^+ Q_{\perp}$  for each momentum ( $Q_{\perp}$ , like  $K$ , is dimensionless);
3. rotations about the 3-direction.

It is these invariances which lead to the frame independence of the Fock state wave functions. A comparison between  $\tau$ -ordered and time-ordered perturbation theory is given in Table I.

## 16. Discretized Light-Cone Quantization

Is it possible to solve the light-cone equation of motion  $H_{LC}\Psi = M^2\Psi$  for QCD, at least in an approximate form? Recently H. C. Pauli and I have taken a direct approach of attempting to diagonalize the light-cone Hamiltonian on a free particle discretized momentum Fock state basis. Since  $H_{LC}$ ,  $P^+$ ,  $\vec{P}_{\perp}$ , and the conserved charges all commute,  $H_{LC}$  is block diagonal. By choosing periodic (or anti-periodic) boundary conditions for the basis states along the negative light-cone

$$\psi(z^- + L) = \pm \psi(z^- - L),$$

the Fock basis becomes restricted to finite dimensional representations. The eigenvalue problem thus reduces to the diagonalization of a finite Hermitian matrix. To

Table I. Comparison Between Time-Ordered and  $\tau$ -Ordered Perturbation Theory

Equal $t$	Equal $\tau = t + z$
$k^0 = \sqrt{\vec{k}^2 + m^2}$ (particle mass shell)	$k^- = \frac{k_\perp^2 + m^2}{k^+}$ (particle mass shell)
$\sum \vec{k}$ conserved	$\sum \vec{k}_\perp, k^+$ conserved
$\mathcal{M}_{ab} = V_{ab} + \sum_c V_{ac} \frac{1}{\sum_a k^0 - \sum_c k^0 + i\epsilon} V_{cb}$	$\mathcal{M}_{ab} = V_{ab} + \sum_c V_{ac} \frac{1}{\sum_a k^- - \sum_c k^- + i\epsilon} V_{cb}$
$n!$ time-ordered contributions	$k^+ > 0$ only
Fock states $\psi_n(\vec{k}_i)$	Fock states $\psi_n(\vec{k}_{\perp i}, x_i)$
$\sum_{i=1}^n \vec{k}_i = \vec{P} = 0$	$x = \frac{k^+}{P^+}, \sum_{i=1}^n x_i = 1, \sum_{i=1}^n \vec{k}_{\perp i} = 0$ ( $0 < x_i < 1$ )
$\mathcal{E} = P^0 - \sum_{i=1}^n k_i^0$	$\mathcal{E} = P^+ \left( P^- - \sum_{i=1}^n k_i^- \right)$
$= M - \sum_{i=1}^n \sqrt{k_i^2 + m_i^2}$	$= M^2 - \sum_{i=1}^n \left( \frac{k_\perp^2 + m^2}{x} \right)_i$

see this, note that periodicity in  $z^-$  requires

$$P^+ = \frac{2\pi}{L} K, \quad k_i^+ = \frac{2\pi}{L} n_i, \quad \sum_{i=1}^n n_i = K.$$

The dimension of the representation corresponds to the number of partitions of the integer  $k$  as a sum of positive integers  $n$ . One can easily show that  $P^-$  scales as  $L$ : we define  $P^- \equiv \frac{L}{2\pi} H$ . The eigenstates with  $P^2 = M^2$  at fixed  $P^+$  and  $\vec{P}_\perp = 0$  thus satisfy

$$KH |\Psi\rangle = M^2 |\Psi\rangle,$$

independent of  $L$  (which corresponds to a Lorentz boost factor). Unlike conventional space-time lattices,  $L$  in DLCQ does not impose a physical scale on the theory.

For a finite resolution  $K$ , the wave function is sampled at the discrete points

$$x_i = \frac{k_i^+}{P^+} = \frac{n_i}{K} = \left\{ \frac{1}{K}, \frac{2}{K}, \dots, \frac{K-1}{K} \right\}$$

The continuum limit is clearly  $K \rightarrow \infty$ .

The commuting operators  $K$ ,  $Q$  and  $H = H_0 + V$  are given by

$$K = \sum_{n=1} n(b_n^\dagger b_n + d_n^\dagger d_n) + n(a_n^\dagger a_n)$$

$$Q = \sum_{n=0} (b_n^\dagger b_n - d_n^\dagger d_n)$$

$$H_0 = \sum_{n=1} \frac{m_\perp^2}{n} (b_n^\dagger b_n + d_n^\dagger d_n) + \frac{k_\perp^2}{n} a_n^\dagger a_n$$

$$V = \frac{g^2}{\pi} \sum_{n,m,k,\ell=0} b_k^\dagger b_\ell d_n^\dagger d_m \frac{\delta_{n-m,n-\ell}}{(n-m)^2} + \dots$$

I have only displayed one fermion anti-fermion (abelian) interaction, corresponding to instantaneous gluon exchange. The  $Q = 0$  Fock state basis states are of the form

$$b_n^\dagger d_m^\dagger a_\ell^\dagger |0\rangle = |n; m; \ell\rangle$$

( $n + m + \ell = K$ ) where  $|0\rangle$  is the perturbative vacuum. (Spin, color and transverse momentum for any number of dimensions are represented as extra internal variables.) We then solve

$$HK |\Psi\rangle = M^2 |\Psi\rangle$$

on the free particle basis

$$|\Psi\rangle = \sum_i C_i |i\rangle .$$

We also take the  $k_\perp$  as discrete variables on a finite cartesian basis consistent with the ultraviolet cutoff.

The eigenvalues of  $H$  projected on the discrete light cone basis give not only the bound state spectrum, but also all of the multi-particle scattering states with the same quantum numbers.

The simplest application of DLCQ to local gauge theory is QED in one-space and one-time dimensions. Since  $A^+ = 0$  is a physical gauge there are no photon degrees of freedom. The fermion anti-fermion interaction is simply

$$V = \frac{g^2}{\pi} \left[ \frac{1}{(n-\ell)^2} - \frac{1}{(k-m)^2} \right]$$

There are also induced mass terms from pairwise contractions of the normal-ordered Hamiltonian. Explicit forms for the matrix representation of  $H_{QED}$  are given in ref. 38.

Schwinger has shown that massless  $(QED)_{1+1}$  is equivalent to a free boson theory. In the light-cone formalism we can demonstrate the solution explicitly. One defines<sup>66</sup> bilinear operators in the fermion fields  $a_n$  and  $a_n^\dagger$  which have normal boson commutation rules. Then for  $Q = 0$

$$H = m^2 \sum_{n=1}^{\infty} \frac{1}{n} (b_n^\dagger b_n + d_n^\dagger d_n) + \frac{g^2}{\pi} \sum_{n=1}^{\infty} \frac{1}{n} a_n^\dagger a_n .$$

Thus for  $m^2 = 0$  (or  $g^2/\pi \gg m^2$ ),  $H_{QED}$  is equivalent to free boson theory with  $m_b^2 = g^2/\pi$ .

For the general case  $m^2 \neq 0$ ,  $(QED)_{1+1}$  can be solved by numerical diagonalization. The complete spectrum (normalized to the ground state mass) for  $K = 16$  is shown as a function of coupling constant in fig. 30. Since the physics can only depend on the ratio  $m/g$ , it is convenient to introduce the parametrization

$$\lambda = \sqrt{\frac{1}{1 + \pi(m/g)^2}}$$

which maps the entire range of  $m$  and  $g$  onto the finite interval  $0 \leq \lambda \leq 1$ .

Figure 10 shows the structure function for the ground state of  $(QED)_{1+1}$  as a function of  $\lambda$ . In the weak binding limit  $g \rightarrow 0$  or  $(m \rightarrow \infty)$ , the structure function becomes a delta function at equal partition of the constituent momentum, as expected.

In the strong coupling limit  $g \rightarrow \infty$  ( $m \rightarrow 0$ ) the structure function becomes flat. This is consistent with the interpretation of the Schwinger boson as a point-like composite of a fermion and anti-fermion. The contribution to higher Fock states to the lowest mass structure function is strikingly small; the probability of non-valence states is less than 1% for any value of  $\lambda$ .

The basis of the discretized light cone quantization method (DLCQ) for solving field theories is thus conceptually simple: In general, one quantizes the independent



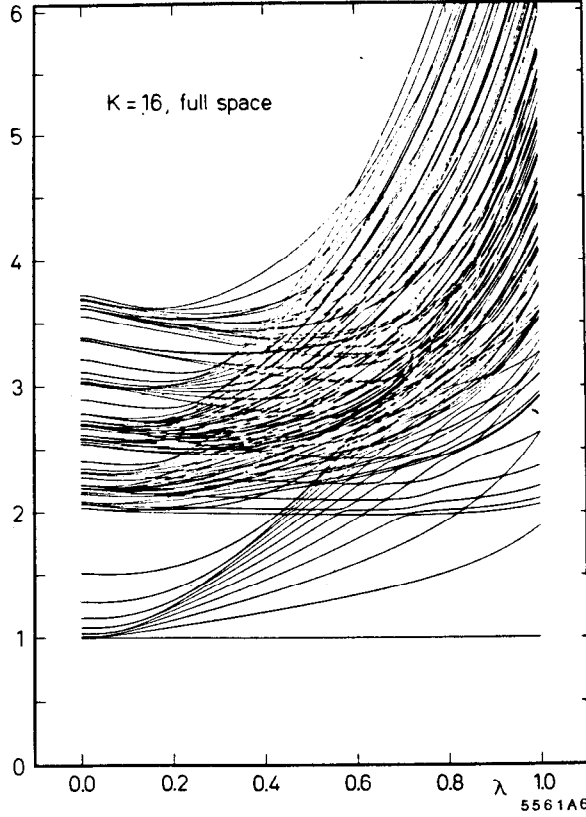


Fig. 30. Spectrum of QED in one-space and one-time dimension for harmonic resolution  $K = 16$ . The ratios  $M_i/M_1$  are plotted as a function of the scaled coupling constant  $\lambda = 1$ . The Schwinger limit is  $\lambda = 1$ . (From ref. 38.)

fields at equal light cone time  $\tau$  and requires them to be periodic in light cone space with period  $2L$ . The commuting operators, the light cone momentum  $P^+ = \frac{2\pi}{L}K$  and the light cone energy  $P^- = \frac{L}{2\pi}H$  are constructed explicitly in a Fock space representation and diagonalized simultaneously. The eigenvalues give the physical spectrum: the invariant mass squared  $M^2 = P^\nu P_\nu$ . The eigenfunctions give the wave functions at equal  $\tau$  and allow one to compute the current matrix elements, structure functions, and distribution amplitudes required for physical processes. All of these quantities are manifestly independent of  $L$ , since  $M^2 = P^+P^- = HK$ . Lorentz-invariance is violated by periodicity, but reestablished at the end of the calculation by going to the continuum limit:  $L \rightarrow \infty$ ,  $K \rightarrow \infty$  with  $P^+$  finite. In the case of gauge theory, the use of the light cone gauge  $A^+ = 0$  eliminates negative metric states in both abelian and non-abelian theories.

As we have discussed above, the application of DLCQ to a gauge invariant abelian field theory like QED<sub>2</sub> is straightforward. For any given resolution  $K$

the number of contributing Fock states is finite because of the positivity of the light cone momenta and the Pauli principle (in the case of massless fermions). No unexpected problems appear in the calculations. QED<sub>2</sub> in  $A^+ = 0$  gauge is much simpler than the scalar Yukawa field theory, since the transverse degrees of freedom and therefore the photons are absent in 1+1 dimensions. One can see immediately in the DLCQ approach that QED<sub>2</sub> has an arbitrary mass scale. This scale can be adjusted by (re)normalizing the lowest mass to an arbitrary but fixed value.

We have also established precise agreement between the DLCQ results and the exact solutions of the Schwinger model proper at any resolution  $K$ , as well as in the continuum limit. This result gives further evidence that quantizing a system at equal light cone time is equivalent to quantizing it at equal usual time.

In the case of the massive Schwinger model (QED<sub>2</sub>), we established the existence of the continuum limit numerically; for sufficiently large resolution  $K$  the results become independent of  $K$ . The essential criteria for convergence is that the intrinsic dynamical structure of the wave functions is sufficiently resolved at the rational values  $x = n/K$ ,  $n = 1, 2, \dots, K - 1$  accessible at a given  $K$ . Unlike the case in the usual space-time methods, the size of the discretization or lattice length scale  $L$ , is irrelevant.

In the large  $K$  limit, the eigenvalues agree quantitatively with the results of Bergknoff<sup>66</sup> and with those of a lattice gauge calculation by Crewther and Hamer.<sup>67</sup> This result is important in establishing the equivalence of different complementary nonperturbative methods.

We also verified numerically that different Fock space representations yield the same physical results. In particular we solved the QED<sub>2</sub> spectrum in the space corresponding to the solutions of the free, massive Dirac equation  $(i\gamma^\mu \partial_\mu + m_F)\psi = 0$  as well as of the massless equation  $i\gamma^\mu \partial_\mu \psi = 0$ . We only found convergence problems for the very large coupling regime  $\lambda$  near 1.

Even for moderately large values of the resolution, DLCQ provides one with a qualitatively correct picture of the whole spectrum of eigenfunctions. This aspect becomes important for the development of scattering theory within the DLCQ approach. For example we have found the rather surprising result that the lowest eigenfunction has virtually no components of  $|2f; 2\bar{f}\rangle$  and higher particle Fock states (*i.e.* no 'sea quarks').

There are a number of important advantages of the DLCQ method which have emerged from this study of two-dimensional field theories.

(1) The Fock space is denumerable and finite in particle number for any fixed resolution  $K$ . In the case of gauge theory in 3+1 dimensions, we expect that photon or gluon quanta with zero 4-momentum decouple from neutral or color-singlet bound states, and thus need not be included in the Fock basis. The transverse

momenta are additive and can be introduced on a cartesian grid. Hornbostel<sup>68</sup> has developed methods to implement the color degrees of freedom for the non-Abelian theories.

(2) Unlike lattice gauge theory, there are no special difficulties with fermions: e.g., no fermion doubling, fermion determinants, or necessity for a quenched approximation. Furthermore, the discretized theory has basically the same ultraviolet structure as the continuum theory. We emphasize that unlike lattice calculations, there is no constraint or relationship between the physical size of the bound state and the length scale  $L$ .

(3) The DLCQ method has the remarkable feature of generating the complete spectrum of the theory; bound states and continuum states alike. These can be separated by tracing their minimum Fock state content down to small coupling constant since the continuum states have higher particle number content. In lattice gauge theory it appears intractable to obtain information on excited or scattering states or their correlations. The wave functions generated at equal light cone time have the immediate form required for relativistic scattering problems.

(4) DLCQ is basically relativistic many body theory, including particle number creation and destruction, and is thus a basis for relativistic nuclear and atomic problems. In the non-relativistic limit the theory is equivalent to many-body Schrödinger theory.

The immediate goal is gauge theory in 3+1 dimensions. Even in the Abelian case it will be interesting to analyze QED and the positronium spectrum in the large  $\alpha$  limit. Whether the non-Abelian theory can be solved using DLCQ – considering its greater number of degrees of freedom and its complex vacuum and symmetry properties is an open question. The studies for Abelian gauge theory in 1+1 dimensions do give some grounds for optimism.

## 17. Exclusive Reactions as Tests of QCD and Hadron Wave Functions

Even if we do not have as yet complete information on the hadronic wave functions in QCD, it is still possible to make predictions at large momentum transfer directly from the theory. Many of the results (such as meson form factors and  $\gamma\gamma$  annihilation into meson pairs) can be proved rigorously, in the sense that they can be demonstrated to arbitrary order in perturbation theory. Other results require an all-orders resummation.

The processes which are most easily analyzed are those in which all final particles are measured at large invariant masses compared to each other, i.e. large momentum transfer exclusive reactions. This includes form factors of hadrons and nuclei at large momentum transfer  $Q$  and large angle scattering reactions such

as photoproduction  $\gamma p \rightarrow \pi^+ n$ , nucleon-nucleon scattering, photo-disintegration  $\gamma d \rightarrow np$  at large angles and energies, etc. A key result is that such amplitudes factorize at large momentum transfer in the form of a convolution of a hard scattering amplitude  $T_H$  which can be computed perturbatively from quark-gluon subprocesses multiplied by process-independent “distribution amplitudes”  $\phi(x, Q)$  which contain all of the bound-state non-perturbative dynamics of each of the interacting hadrons. To leading order in  $1/Q$  the scattering amplitude has the form<sup>69</sup>

$$\mathcal{M} = \int_0^1 T_H(x_j, Q) \prod_{H_i} \phi_{H_i}(x_j, Q) [dx] . \quad (16)$$

Here  $T_H$  is the probability amplitude to scatter quarks with fractional momentum  $0 < x_j < 1$  from the incident to final hadron directions, and  $\phi_{H_i}$  is the probability amplitude to find quarks in the wave function of hadron  $H_i$  collinear up to the scale  $Q$ , and

$$[dx] = \prod_{j=1}^{n_i} dx_j \delta\left(1 - \sum_k^{n_i} x_k\right) \quad (17)$$

The key to the derivation of this factorization of perturbative and non-perturbative dynamics is the use of the Fock basis  $\{\psi_n(x_i, \vec{k}_{\perp i}, \lambda_i)\}$  defined at equal  $\tau = t + z/c$  on the light-cone to represent relativistic color singlet bound states. Here  $\lambda_i$  are the helicities;  $x_i \equiv (k_i^0 + k_i^z)/(p^0 + p^z)$ ,  $(\sum_{i=1}^n x_i = 1)$ , and  $\vec{k}_{\perp i}$ ,  $(\sum_{i=1}^n \vec{k}_{\perp i} = 0)$ , are the relative momentum coordinates. Thus the proton is represented as a column vector of states  $\psi_{qqq}, \psi_{qqqg}, \psi_{qqq\bar{q}q} \dots$ . In the light-cone gauge,  $A^+ = A^0 + A^3 = 0$ , only the minimal “valence” Fock state needs to be considered at large momentum transfer since any additional quark or gluon forced to absorb large momentum transfer yields a power-law suppressed contribution to the hadronic amplitude.

The factorization of large momentum transfer exclusive amplitudes can be understood as follows: the  $T_H$  amplitude in leading order is the minimally-connected quark-gluon matrix element taking the valence quarks from the initial to final directions. It arises by iterating the gluon-exchange kernel in each wave function wherever large relative momentum occurs. The distribution amplitude is the coefficient in the wave function remaining after the iteration of the kernel, analogous to the wave function at the origin in non-relativistic quantum mechanics. All intermediate states in  $T_H$  have constituents with relative transverse momentum larger than the momentum transfer  $\tilde{Q}$ . All the integrations up to  $\tilde{Q}$  are contained in  $\phi(x, \tilde{Q})$ .

The hard scattering amplitude  $T_H(x_i, Q, \theta_{cm})$  has dimensions  $[L]^{n-4}$  where  $n$  is the total number of incoming and outgoing field lines. At large momentum

transfer  $Q$  is the only relevant scale:

$$T_H \sim \left[ \frac{1}{Q} \right]^{n-4} f(x_i, \theta_{cm}) .$$

This gives the main source of power-law behavior of the amplitude. One can check the power fall-off explicitly in  $A^+ = 0$  gauge for tree graphs: each intermediate fermion line gives  $1/Q^2$ , each gluon propagator gives  $Q^0$  since its numerator couplings cancel its denominator. The result is the same for instantaneous gluon exchange. Since all intermediate states have  $k_{\perp}^2 > \tilde{Q}^2$ , one can calculate  $T_H$  perturbatively in powers of the running coupling constant; the leading power of  $\alpha_s(Q^2)$  is given by the number of exchanged gluons. The minimum number (valence) Fock state dominates the amplitude in  $A^+ = 0$  gauge. (This is not true in covariant gauges.)

The scale  $\tilde{Q}^2$  is set by the minimum virtuality of the propagators in  $T_H$ ; e.g. for form factors  $\tilde{Q}^2 = \min_{ij} \{x_i, y_j\} Q^2$  where  $\left\{ \begin{smallmatrix} x_i \\ y_j \end{smallmatrix} \right\}$  and the light-cone fractions for the initial and final state. The endpoint region where  $x_i \sim 0$  is thus potentially dangerous. In some processes, such as meson form factors or  $\gamma\gamma \rightarrow M\bar{M}$ , the meson distribution amplitude falls sufficiently fast such that such regions give power-law suppressed contributions. In other processes such as hadron-hadron scattering one must deal with Landshoff pinch singularities. Mueller<sup>21</sup> has shown that the Sudakov vertex form factors which appear when a quark or a gluon leg is close to the mass shell suppress near-on-shell contributions so that the leading power analysis is modified by a small residual fractional power law correction. The Sudakov form factor also eliminates possible anomalous contributions from endpoint regions of integration in the calculation of baryon form factors. In the case of the  $F_M(Q^2)$  and  $\gamma\gamma \rightarrow M\bar{M}$  processes, formal proofs of QCD factorization can also be given using operator product expansions and the renormalization group.

The momentum dependent of  $\phi(x, Q)$  comes from the sensitivity to the upper limit of interaction of the transverse momentum integrals. This arises from the gluon exchange kernels which give integral of the form

$$\int_{\mu^2}^{Q^2} \frac{dk_{\perp}^2}{k_{\perp}^2} \alpha_s(k_{\perp}^2) \sim \ln \frac{\ln Q^2/\Lambda^2}{\ln \mu^2 Q^2} .$$

One can use the iterative structure of the wave function equation in  $A^+ = 0$  gauge to sum the logarithmic dependence in the form of a sum of terms with anomalous dimension factors  $(\ln Q^2/\Lambda^2)^{-\gamma_n}$  where the  $\gamma_n$  are determined by perturbative QCD.

## 18. Helicity Selection Rule in QCD

Since  $\phi(x, Q)$  involves axially-symmetric  $k_{\perp}$  integrations,  $L_z = 0$  to leading order in  $1/Q^2$ , and the sum of the valence quark helicities equals that of the hadron. Furthermore, since QCD is a vector theory, quark helicity is conserved between initial and final states in the hard-scattering amplitude. Thus QCD predicts hadron helicity conservation:

$$\sum_{\text{initial}} \lambda_i^H = \sum_{\text{final}} \lambda_i^H$$

at large momentum transfer. Notice that this result is independent of photon or lepton helicity in photoproduction or electroproduction amplitudes and holds to all orders in  $\alpha_s(Q^2)$ . Thus an essential feature of the perturbative QCD is the prediction of hadron helicity conservation up to kinematical and dynamical corrections of order  $m/Q$  and  $\langle \psi\bar{\psi} \rangle^{1/3}/Q$  where  $Q$  is the momentum transfer or heavy mass scale,  $m$  is the light quark mass. Here  $\langle \psi\bar{\psi} \rangle$  is a measure of non-perturbative effects ascribed to chiral symmetry breaking of the QCD vacuum. Applying this prediction to  $p\bar{p}$  annihilation, one predicts  $\lambda_p + \lambda_{\bar{p}} = 0$ , i.e.,  $S_z = J_z = \pm 1$  is the leading amplitude for heavy resonance production. Thus the  $\psi$  is expected to be produced with  $J_z = \pm 1$ , whereas the  $\chi$  and  $\eta_c$  cross sections should be suppressed, at least to leading power in the heavy quark mass.

## 19. Helicity Selection Rule and Exclusive Charmonium Decays

The helicity selection rule may be relevant to an interesting puzzle concerning the exclusive decays of  $J/\psi$  and  $\psi' \rightarrow \rho\pi, K^*\bar{K}$  and possibly other Vector-Pseudoscalar (VP) combinations. One expects  $J/\psi(\psi')$  to decay to hadrons via three gluons or, occasionally, via a single direct photon. In either case the decay proceeds via  $|\Psi(0)|^2$ , where  $\Psi(0)$  is the wave function at the origin in the non-relativistic quark model for  $c\bar{c}$ . Thus it is reasonable to expect on the basis of perturbative QCD, that for any final hadronic state  $h$ , we have:

$$Q_h \equiv \frac{B(\psi' \rightarrow h)}{B(J/\psi \rightarrow h)} \simeq \frac{B(\psi' \rightarrow e^+e^-)}{B(J/\psi \rightarrow e^+e^-)} = 0.135 \pm 0.023 .$$

Usually this is true, as is well documented in ref. 70 for  $p\bar{p}\pi^0, 2\pi^+2\pi^-\pi^0, \pi^+\pi^-\omega$ , and  $3\pi^+3\pi^-\pi^0$ , hadronic channels. The startling exceptions occur for  $\rho\pi$  and  $K^*\bar{K}$  where the present experimental limits<sup>70</sup> are

$$Q_{\rho\pi} < 0.0063 \quad \text{and} \quad Q_{K^*\bar{K}} < 0.0027 .$$

Recently San Fu Tuan, Peter Lepage, and I<sup>71</sup> have proposed an explanation of the puzzle by assuming (a) the general validity of the perturbative QCD theorem<sup>72</sup>

that total hadron helicity is conserved in high momentum transfer exclusive processes, but supplemented by (b) violation of the QCD theorem when the  $J/\psi$  decay to hadrons via three hard gluons is modulated by the gluons forming an intermediate gluonium state  $\mathcal{O}$  before transition to hadrons. In essence the model of Hou and Soni<sup>73</sup> takes over in this latter stage.

Since the vector state  $V$  has to be produced with helicity  $\lambda = \pm 1$ , the  $VP$  decays should be suppressed by a factor  $1/s$  in the rate. The  $\psi'$  seems to respect this rule. The  $J/\psi$  does *not* and that is the mystery. Put in more quantitative terms, we expect on the basis of perturbative QCD<sup>72</sup>

$$Q_{\rho\pi} \equiv \frac{B(\psi' \rightarrow \rho\pi)}{B(J/\psi \rightarrow \rho\pi)} \sim [M_{J/\psi}/M_{\psi'}]^6$$

assuming quark helicity is conserved in strong interactions. This includes a form factor suppression proportional to  $[M_{J/\psi}/M_{\psi'}]^4$ . The suppression (3) is not large enough, though, to account for the data— the exponent would have to be greater than 23 to explain it.

One can question the validity of the QCD helicity conservation theorem at the charmonium mass scale. Helicity conservation has received important confirmation in  $J/\psi \rightarrow p\bar{p}$  where the angular distribution is known experimentally to follow  $[1 + \cos^2 \theta]$  rather than  $\sin^2 \theta$  for helicity flip. The helicity theorem also works<sup>74</sup> for  $J/\psi \rightarrow \pi^0\omega^0$  where the three gluons exchange is replaced by a highly virtual photon exchange  $[\gamma(q^2), q^2 \gg 0]$  in this isospin violating process. The  $\psi'$  decays clearly respect hadron helicity conservation. It is difficult to understand how the  $J/\psi$  could violate this rule since the  $J/\psi$  and  $\psi'$  masses are so close. Corrections from quark mass terms, soft gluon corrections and finite energy corrections would not be expected to lead to large  $J/\psi$  differences. It is hard to imagine anything other than a resonant or interference effect that could account for such dramatic energy dependence.

A relevant violation of the QCD theorem which does have significance to this problem, is the recognition that the theorem is built on the underlying assumption of short-range “point-like” interactions amongst the constituents throughout. For instance  $J/\psi(c\bar{c}) \rightarrow 3g$  has a short range  $\cong 1/m_c$  associated with the short time scale of interaction. If, however, subsequently the three gluons were to resonate forming a gluonium state  $\mathcal{O}$  which has large transverse size  $\cong 1/M_H$  covering an extended (long) time period, then the theorem is invalid. Note that even if the gluonium state  $\mathcal{O}$  has large mass, close to  $M_{J/\psi}$ , its size could still be the standard hadronic scale of  $1 fm$ , just as the case for the  $D$ -meson and  $B$ -mesons.

We have thus proposed, following Hou and Soni, that the enhancement of  $J/\psi \rightarrow K^*\bar{K}$  and  $J/\psi \rightarrow \rho\pi$  decay modes is caused by a quantum mechanical mixing of the  $J/\psi$  with a  $J^{PC} = 1^{--}$  vector gluonium state  $\mathcal{O}$  which causes the

breakdown of the QCD helicity theorem. The decay width for  $J/\psi \rightarrow \rho\pi(K^*\bar{K})$  via the sequence  $J/\psi \rightarrow O \rightarrow \rho\pi(K^*\bar{K})$  must be substantially larger than the decay width for the (non-pole) continuum process  $J/\psi \rightarrow 3 \text{ gluons} \rightarrow \rho\pi(K^*\bar{K})$ . In the other channels (such as  $p\bar{p}, p\bar{p}\pi^0, 2\pi^+2\pi^-\pi^0$ , etc.), the branching ratios of the  $O$  must be so small that the continuum contribution governed by the QCD theorem dominates over that of the  $O$  pole. For the case of the  $\psi'$  the contribution of the  $O$  pole must always be inappreciable in comparison with the continuum process where the QCD theorem holds. The experimental limits on  $Q_{\rho\pi}$  and  $Q_{K^*\bar{K}}$  are now substantially more stringent than when Hou and Soni made their estimates of  $M_O, \Gamma_{O \rightarrow \rho\pi}$  and  $\Gamma_{O \rightarrow K^*\bar{K}}$  in 1982.

It is interesting, indeed, that the existence of such a gluonium state  $O$  was first postulated by Freund and Nambu<sup>75</sup> based on  $OZI$  dynamics soon after the discovery of the  $J/\psi$  and  $\psi'$  mesons. In fact Freund and Nambu predicted that the  $O$  would decay copiously precisely into  $\rho\pi$  and  $K^*\bar{K}$  with severe suppression of decays into other modes like  $e^+e^-$  as required for the solution of the puzzle.

Final states  $h$  which can proceed only through the intermediate gluonium state satisfy the ratio:

$$Q_h = \frac{B(\psi' \rightarrow e^+e^-)}{B(J/\psi \rightarrow e^+e^-)} \frac{(M_{J/\psi} - M_O)^2 + \frac{1}{4} \Gamma_O^2}{(M_{\psi'} - M_O)^2 + \frac{1}{4} \Gamma_O^2}.$$

We have assumed that the coupling of the  $J/\psi$  and  $\psi'$  to the gluonium state scales as the  $e^+e^-$  coupling. The value of  $Q_h$  is small if the  $O$  is close in mass to the  $J/\psi$ . Thus we require

$$(M_{J/\psi} - M_O)^2 + \frac{1}{4} \Gamma_O^2 \lesssim 2.6 Q_h \text{ GeV}^2.$$

The experimental limit for  $Q_{K^*\bar{K}}$  then implies

$$\left[ (M_{J/\psi} - M_O)^2 + \frac{1}{4} \Gamma_O^2 \right]^{1/2} \lesssim 80 \text{ MeV}$$

This implies  $|M_{J/\psi} - M_O| < 80 \text{ MeV}$  and  $\Gamma_O < 160 \text{ MeV}$ . Typical allowed values are

$$M_O = 3.0 \text{ GeV}, \quad \Gamma_O = 140 \text{ MeV}$$

or

$$M_O = 3.15 \text{ GeV}, \quad \Gamma_O = 140 \text{ MeV}.$$

Notice that the gluonium state could be either lighter or heavier than the  $J/\psi$ . The branching ratio of the  $O$  into a given channel must exceed that of the  $J/\psi$ .



It is not necessarily obvious that a  $J^{PC} = 1^{--}$  gluonium state with these parameters would necessarily have been found in experiments to date. One must remember that though  $O \rightarrow \rho\pi$  and  $O \rightarrow K^*\bar{K}$  are important modes of decay, at a mass of order 3.1 GeV many other modes (all be it less important) are available. Hence, a total width  $\Gamma_O \cong 100$  to 150 MeV is quite conceivable. Because of the proximity of  $M_O$  to  $M_{J/\psi}$ , the most important signatures for an  $O$  search via exclusive modes  $J/\psi \rightarrow K^*\bar{K}h$ ,  $J/\psi \rightarrow \rho\pi h$ ;  $h = \pi\pi, \eta, \eta'$ , are no longer available by phase-space considerations. However, the search could still be carried out using  $\psi' \rightarrow K^*\bar{K}h$ ,  $\psi' \rightarrow \rho\pi h$ ; with  $h = \pi\pi$ , and  $\eta$ . Another way to search for  $O$  in particular, and the three-gluon bound states in general, is via the inclusive reaction  $\psi' \rightarrow (\pi\pi) + X$ , where the  $\pi\pi$  pair is an iso-singlet. The three-gluon bound states such as  $O$  should show up as peaks in the missing mass (i.e., mass of  $X$ ) distribution.

Perhaps the most direct way to search for the  $O$  is to scan  $\bar{p}p$  or  $e^+e^-$  annihilation at  $\sqrt{s}$  within  $\sim 100$  MeV of the  $J/\psi$ , triggering on vector/pseudoscalar decays such as  $\pi\rho$  or  $\bar{K}K^*$ .

The fact that the  $\rho\pi$  and  $K^*\bar{K}$  channels are strongly suppressed in  $\psi'$  decays but not in  $J/\psi$  decays clearly implies dynamics beyond the standard charmonium analysis. As we have shown, the hypothesis of a three-gluon state  $O$  with mass within  $\cong 100$  MeV of the  $J/\psi$  mass provides a natural, perhaps even compelling, explanation of this anomaly. If this description is correct, then the  $\psi'$  and  $J/\psi$  hadronic decays are not only confirming hadron helicity conservation (at the  $\psi'$  momentum scale) but are also providing a signal for bound gluonic matter in QCD.

## 20. Further Remarks on Nucleon Form Factors

Let us now consider the implications of the perturbative QCD helicity selection rule specifically for the nucleon form factor. At large  $Q^2$ , the baryon form factor can be systematically computed by iterating the valence Fock state wave function equation of motion wherever large relative momentum occurs. To leading order the kernel is effectively one-gluon exchange. The sum of the hard gluon exchange contributions is the gauge invariant amplitude  $T_H$ . The residual factor from the wave function is the distribution amplitude  $\phi_B$  which plays the role of the wave function at the origin in the analogous non-relativistic calculation. Thus we obtain the form: [See fig. 2(a)]

$$F_B(Q^2) = \int_0^1 [dy] \int_0^1 [dx] \phi_B^\dagger(y_j, Q) T_H(x_i, y_j, Q) \phi_B(x_i, Q) \quad , \quad (18)$$

where to leading order in  $\alpha_s(Q^2)$ ,  $T_H$  is computed from  $3q + \gamma^* \rightarrow 3q$  tree graph

amplitudes: [fig. 2(b)]

$$T_H = \left[ \frac{\alpha_s(Q^2)}{Q^2} \right]^2 f(x_i, y_j) \quad (19)$$

and

$$\phi_B(x_i, Q) = \int [d^2 k_\perp] \psi_V(x_i, \vec{k}_{\perp i}) \theta(k_{\perp i}^2 < Q^2) \quad (20)$$

is the valence three-quark wave function [fig. 2(c)] evaluated at quark impact separation  $b_\perp \sim \mathcal{O}(Q^{-1})$ . Since  $\phi_B$  only depends logarithmically on  $Q^2$  in QCD, the main dynamical dependence of  $F_B(Q^2)$  is the power behavior  $(Q^2)^{-2}$  derived from scaling of the elementary propagators in  $T_H$ . Thus, modulo logarithmic factors, one obtains a dimensional counting rule<sup>76</sup> for any hadronic or nuclear form factor at large  $Q^2$  ( $\lambda = \lambda' = 0$  or  $1/2$ )

$$F(Q^2) \sim \left( \frac{1}{Q^2} \right)^{n-1}, \quad (21)$$

$$F_1^N \sim \frac{1}{Q^4}, \quad F_\pi \sim \frac{1}{Q^2}, \quad F_d \sim \frac{1}{Q^{10}}, \quad (22)$$

where  $n$  is the minimum number of fields in the hadron. As explained above, total hadronic helicity is conserved at large momentum transfer for any QCD exclusive reaction.<sup>77</sup> The dominant nucleon form factor thus corresponds to  $F_1(Q^2)$  or  $G_M(Q^2)$ ; the Pauli form factor  $F_2(Q^2)$  is suppressed by an extra power of  $Q^2$ . In the case of the deuteron, the dominant form factor has helicity  $\lambda = \lambda' = 0$ , corresponding to  $\sqrt{A(Q^2)}$ . The general form of the logarithmic dependence of  $F(Q^2)$  can be derived from the operator product expansion at short distance or by solving an evolution equation for the distribution amplitude computed from gluon exchange [fig. 2(c)], the only QCD contribution which falls sufficiently small at large transverse momentum to effect the large  $Q^2$  dependence.

The distribution amplitude for a baryon is determined by an evolution equation which can be derived from the Bethe-Salpeter equation at large transverse momentum projected on the light-cone:<sup>69</sup>

$$\left( Q^2 \frac{\partial}{\partial Q^2} + \frac{3C_F}{2\beta} \right) \phi(x_i, Q) = \frac{C_B}{\beta} \int [dy] V(x_i, y_i) \phi(y_i, Q), \quad (23)$$

where  $C_F = (n_c^2 - 1)/2n_c = 4/3$ ,  $C_B = (n_c + 1)/2n_c = 2/3$ ,  $\beta = 11 - (2/3)n_f$ , and  $V(x_i, y_i)$  is computed to leading order in  $\alpha_s$  from the single-gluon-exchange kernel. The evolution equation automatically sums to leading order in  $\alpha_s(Q^2)$  all of the contributions from multiple gluon exchange which determine the tail of the

valence wave function and thus the  $Q^2$ -dependence of the distribution amplitude. The general solution of this equation is

$$\phi(x_i, Q) = x_1 x_2 x_3 \sum_{n=0}^{\infty} a_n \left( \ell n \frac{Q^2}{\Lambda^2} \right)^{-\gamma_n} \tilde{\phi}_n(x_i) \quad , \quad (24)$$

where the anomalous dimensions  $\gamma_n$  and the eigenfunctions  $\tilde{\phi}_n(x_i)$  satisfy the characteristic equation:

$$x_1 x_2 x_3 \left( -\gamma_n + \frac{3C_F}{2\beta} \right) \tilde{\phi}_n(x_i) = \frac{C_B}{\beta} \int_0^1 [dy] V(x_i, y_i) \tilde{\phi}_n(y_i) \quad . \quad (25)$$

In the large  $Q^2$  limit, only the leading anomalous dimension  $\gamma_0$  contributes to the form factor.

A useful technique for solving the evolution equations is to construct completely anti-symmetric representations as a polynomial orthonormal basis for the distribution amplitude of multi-quark bound states.<sup>45</sup> In this way one obtains a distinctive classification of nucleon ( $N$ ) and delta ( $\Delta$ ) wave functions and the corresponding  $Q^2$  dependence which discriminates  $N$  and  $\Delta$  form factors. The anti-symmetrization technique is presented in detail in ref. 45 for nuclear systems.

The result for the large  $Q^2$  behavior of the baryon form factor in QCD is then<sup>6,69,78</sup>

$$F_B(Q^2) = \frac{\alpha_s^2(Q^2)}{Q^4} \sum_{n,m} d_{nm} \left( \ell n \frac{Q^2}{\Lambda^2} \right)^{-\gamma_m - \gamma_n} \quad (26)$$

where the  $\gamma_n$  are computable anomalous dimensions of the baryon three-quark wave function at short distance and the  $d_{nm}$  are determined from the value of the distribution amplitude  $\phi_B(x, Q_0^2)$  at a given point  $Q_0^2$  and the normalization of  $T_H$ . Asymptotically, the dominant term has the minimum anomalous dimension. The dominant part of the form factor comes from the region of the  $x$  integration where each quark has a finite fraction of the light cone momentum; the end point region where the struck quark has  $x \simeq 1$  and spectator quarks have  $x \sim 0$  is asymptotically suppressed by quark (Sudakov) form factor gluon radiative corrections.

In Table II we give a summary of the main scaling laws and properties of large momentum transfer exclusive and inclusive cross sections which are derivable starting from the light-cone Fock space basis and the perturbative expansion for QCD.

As shown in fig. 31, the power laws predicted by perturbative QCD are consistent with experiment.<sup>79</sup> The behavior  $Q^4 G_M(Q^2) \sim \text{const}$  at large  $Q^2$  provides a direct check that the minimal Fock state in the nucleon contains three

Table II. Comparison of Exclusive and Inclusive Cross Sections

Exclusive Amplitudes	Inclusive Cross Sections
$M \sim \Pi \phi(x_i, Q) \otimes T_H(x_i, Q)$	$d\sigma \sim \Pi G(x_a, Q) \otimes d\hat{\sigma}(x_a, Q)$
$\phi(x, Q) = \int [d^2 k_\perp] \psi_{\text{val}}^Q(x, k_\perp)$	$G(x, Q) = \sum_n \int [d^2 k_\perp] [dx]'  \psi_n^Q(x, k_\perp) ^2$
Measure $\phi$ in $\gamma\gamma \rightarrow M\bar{M}$	Measure $G$ in $\ell p \rightarrow \ell X$
$\sum_{i \in H} \lambda_i = \lambda_H$	$\sum_{i \in H} \lambda_i \neq \lambda_H$
<b>Evolution</b>	
$\frac{\partial \phi(x, Q)}{\partial \log Q^2} = \alpha_s \int [dy] V(x, y) \phi(y)$	$\frac{\partial G(x, Q)}{\partial \log Q^2} = \alpha_s \int dy P(x/y) G(y)$
$\lim_{Q \rightarrow \infty} \phi(x, Q) = \prod_i x_i \cdot C_{\text{flavor}}$	$\lim_{Q \rightarrow \infty} G(x, Q) = \delta(x) C$
<b>Power Law Behavior</b>	
$\frac{d\sigma}{dx} (A+B \rightarrow C+D) \cong \frac{1}{s^{n-2}} f(\theta_{c.m.})$	$\frac{d\sigma}{d^2 p/E} (AB \rightarrow CX) \cong \sum \frac{(1-x_T)^{2n_s-1}}{(Q^2)^{n_{act}-2}} f(\theta_{c.m.})$
$n = n_A + n_B + n_C + n_D$	$n_{act} = n_a + n_b + n_c + n_d$
$T_H$ : expansion in $\alpha_s(Q^2)$	$d\hat{\sigma}$ : expansion in $\alpha_s(Q^2)$
<b>Complications</b>	
End point singularities	Multiple scales
Pinch singularities	Phase-space limits on evolution
High Fock states	Heavy quark thresholds
	Higher twist multi-particle processes
	Initial and final state interactions

quarks and that the quark propagator and the  $qq \rightarrow qq$  scattering amplitudes are approximately scale-free. More generally, the nominal power law predicted for large momentum transfer exclusive reactions is given by the dimensional counting rule  $M \sim Q^{4-n_{TOT}} F(\theta_{cm})$  where  $n_{TOT}$  is the total number of elementary fields which scatter in the reaction. The predictions are apparently compatible with experiment.<sup>80</sup> As discussed above, for some scattering reactions there are contributions from multiple scattering diagrams (Landshoff contributions) which together with Sudakov effects can lead to small power-law corrections, as well as a complicated spin, and amplitude phase phenomenology.<sup>81</sup> As shown in fig. 8, recent measurements of  $\gamma\gamma \rightarrow \pi^+\pi^-, K^+K^-$  at large invariant pair mass are consistent with the QCD predictions.<sup>82</sup> In principle it should be possible to use measurements of the scaling and angular dependence of the  $\gamma\gamma \rightarrow M\bar{M}$  reactions to measure the shape of the distribution amplitude  $\phi_M(x, Q)$ . In addition, it has been recently shown that the  $Q^2$  dependence of virtual processes such as  $\gamma^*\gamma \rightarrow \pi^+\pi^-$  (measured in tagged  $ee \rightarrow ee\pi\pi$  collisions) depends in detail on the  $x$ -dependence of the pion distribution amplitude.

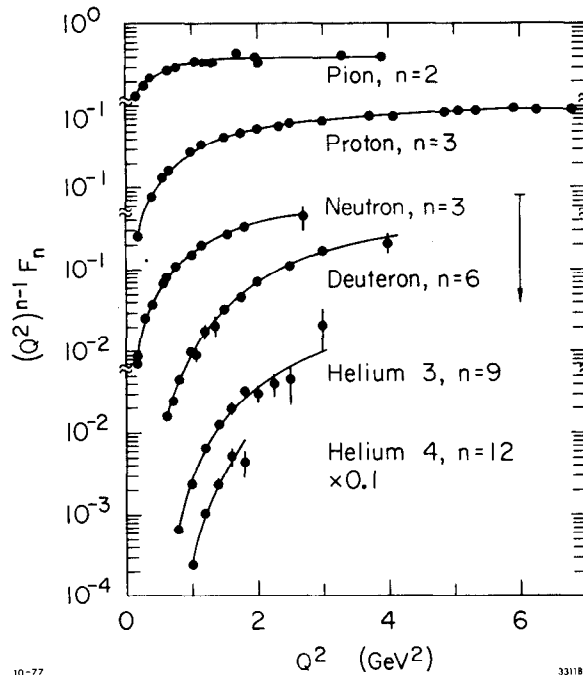


Fig. 31. Comparison of experiment with the QCD dimensional counting rule  $(Q^2)^{n-1} F(Q^2) \sim \text{const}$  for form factors. The proton data extends beyond  $30 \text{ GeV}^2$ .

A serious challenge to QCD is not only to get the correct power law scaling for the proton form factor correct ( $F_1 \sim 1/Q^4$ ,  $F_2 \sim 1/Q^6$ ) but also to obtain

the correct sign and magnitude of the  $1/Q^4$  coefficient. This is highly non-trivial: a non-relativistic 3 quark wave function invariably gives a negative sign for this coefficient (i.e., it predicts a zero at finite space-like  $q^2$  for  $F_1(Q^2)$  and  $G_M(Q^2)$ ) and too small magnitude. This challenge appears to be successfully met by the QCD sum rule analysis of the proton distribution amplitude.

The requirement that the nucleon is the  $I = 1/2$ ,  $S = 1/2$  color singlet representation of three quark fields in QCD uniquely specifies the  $x_i$  permutation symmetry of the proton distribution amplitude:<sup>83</sup>

$$\begin{aligned} \phi_p^p(x_i, \mu) \propto & \frac{1}{\sqrt{6}} [d_\uparrow u_\downarrow u_\uparrow + u_\uparrow u_\downarrow d_\uparrow - 2u_\uparrow d_\downarrow u_\uparrow] \cdot \frac{1}{8} f_N [\phi_N(x_1 x_2 x_3) + \phi_N(x_3 x_2 x_1)] \\ & + \frac{1}{\sqrt{2}} [d_\uparrow u_\downarrow u_\uparrow - u_\uparrow u_\downarrow d_\uparrow] \cdot \frac{1}{8\sqrt{3}} f_N [\phi_N(x_3 x_2 x_1) - \phi_N(x_1 x_2 x_3)] \end{aligned}$$

The neutron distribution amplitude is determined by the substitution  $\phi_n = -\phi_p(u \rightarrow d)$ . Moments of the nucleon distribution amplitude can be computed from the correlation function of the appropriate local quark field operators that carry the nucleon quantum numbers.

The model wave function proposed in Ref. 83, consistent with the derived moments, is

$$\phi_N(x_1 x_2 x_3) = \phi_{asympt} \cdot [11.35(x_1^2 + x_2^2) + 8.82x_3^2 - 1.68x_3 - 2.94 - 6.72(x_2^2 - x_1^2)]$$

where  $\phi_{asympt} = 120 x_1 x_2 x_3$ . The renormalization scale is  $\mu \cong 1$  GeV. The normalization of the nucleon valence wave function is also determined:

$$f_N(\mu = 1 \text{ GeV}) = (5.2 \pm 0.3) \times 10^{-3} \text{ GeV} .$$

A striking feature of the QCD sum rule prediction is the strong asymmetry implied by the first moment: 65% of the proton momentum (at  $P_z \Rightarrow \infty$ ) is carried by the  $u$  quark with helicity parallel to that of the proton. [See fig. 3.] The two remaining quarks each carry  $\sim 15$  to 20% of the total momentum.

The distribution amplitudes based on QCD sum rules are strikingly different from the symmetric forms derived in the  $Q^2 \rightarrow \infty$  limit. This is in analogy to the case of deep inelastic structure functions which only approach the formal limit of a  $\delta$ -function at  $x = 0$  at a momentum transfer scale very remote from the experimentally accessible range. The implication that the nucleon and pion valence wave functions are broad in longitudinal momentum also suggests a broad transverse momentum distribution (small radius) and indicates that quarks bound in light hadrons are highly relativistic.

The striking shape of the CZ wave function is due to the fact that only the first few eigensolutions to the nucleon evolution equation are used as a basis. Since one is so far from full evolution, there is no compelling reason why this should be correct. The essential feature of the sum rule predictions is the strong asymmetry, together with the value of  $f_N$  which give perturbative predictions for the proton and neutron form factors consistent both in *sign* and *magnitude* with experiment. (See fig. 5.) These main features of the QCD sum rule calculation for the nucleon distribution amplitude have recently been confirmed by King and Sachrajda.<sup>7</sup>

It has also been suggested that the relatively large normalization of  $Q^4 G_M^p(Q^2)$  at large  $Q^2$  can be understood if the valence three-quark state has small transverse size, i.e., is large at the origin.<sup>84</sup> The physical radius of the proton measured from  $F_1(Q^2)$  at low momentum transfer then reflects the contributions of the higher Fock states  $qqqq$ ,  $qqq\bar{q}q$  (or meson cloud), etc. A small size for the proton valence wave function (e.g.,  $R_{qqq}^p \sim 0.2$  to  $0.3$  fm) can also explain the large magnitude of  $\langle k_{\perp}^2 \rangle$  of the intrinsic quark momentum distribution needed to understand hard-scattering inclusive reactions. The necessity for small valence state Fock components can be demonstrated explicitly for the pion wave function, since  $\psi_{q\bar{q}}/\pi$  is constrained by sum rules derived from  $\pi^+ \rightarrow \ell^+ \nu$ , and  $\pi^0 \rightarrow \gamma\gamma$ . One finds a valence state radius  $R_{q\bar{q}}^\pi \sim 0.4$  fm, corresponding to a probability  $P_{q\bar{q}}^\pi \sim 1/4$ .

As shown by Carlson, Gari, and Stefanis<sup>90</sup>, the proton and neutron form factors, the axial-vector nucleon form factor, and the leading  $N - \Delta$  transition form factor can all be related to the shape of the nucleon distribution amplitude. Measurements of these form factors will provide severe tests on the applicability of the QCD sum rule predictions.

We have emphasized that dimensional counting rules give a direct connection between the degree of hadron compositeness and the power-law fall of exclusive scattering amplitudes at fixed center of mass angle:  $M \sim Q^{4-n} F(\theta_{cm})$  where  $n$  is the minimum number of initial and final state quanta. This rule gives the QCD prediction for the nominal power law scaling, modulo corrections from the logarithmic behavior of  $\alpha_s$ , the distribution amplitude, and small power-law corrections from Sudakov-suppressed Landshoff multiple scattering contributions. For  $\bar{p}p$  one predicts:

$$\frac{d\sigma}{d\Omega} (\bar{p}p \rightarrow \gamma\gamma) \simeq \frac{\alpha^2}{(p_T^2)^5} f^{\gamma\gamma}(\cos\theta, \ln p_T)$$

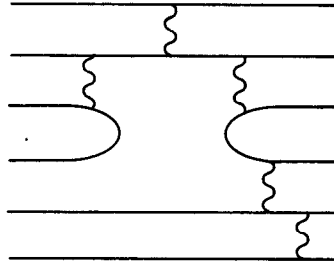
$$\frac{d\sigma}{d\Omega} (\bar{p}p \rightarrow \gamma M) \simeq \frac{\alpha^2}{(p_T^2)^6} f^{\gamma M}(\cos\theta, \ln p_T)$$

$$\frac{d\sigma}{d\Omega} (p\bar{p} \rightarrow M\bar{M}) \simeq \frac{1}{(p_T^2)^7} f^{M\bar{M}}(\cos\theta, \ln p_T)$$

$$\frac{d\sigma}{d\Omega} (p\bar{p} \rightarrow B\bar{B}) \simeq \frac{1}{(p_T^2)^9} f^{B\bar{B}}(\cos\theta, \ln p_T)$$

The angular dependence reflects the structure of the hard scattering perturbative  $T_H$  amplitude, which in turn follows from the flavor pattern of the contributing duality diagrams. For example, a minimally connected diagram such as that illustrated in fig. 32 is approximately characterized as

$$T_H \sim \frac{1}{t^2} \frac{1}{s} \frac{1}{u}.$$



6-86

5446A7

Fig. 32. A perturbative contribution to the hard scattering amplitude in nucleon-nucleon collisions.

Comparisons between channels related by crossing of the Mandelstam variables places a severe constraint on the angular dependence and analytic form of the underlying QCD exclusive amplitude. For example, it is possible to measure and compare

$$\bar{p}p \rightarrow \gamma\gamma : \gamma p \rightarrow \gamma p : \gamma\gamma \rightarrow \bar{p}p$$

$$\bar{p}p \rightarrow \gamma\pi^0 : \gamma p \rightarrow \pi^0 p : \pi^0 p \rightarrow \gamma p.$$

SLAC measurements<sup>47</sup> of the  $\gamma p \rightarrow \pi^+ n$  cross section at  $\theta_{CM} = \pi/2$  are consistent



with the normalization and scaling (see fig. 13.)

$$\frac{d\sigma}{dt} (\gamma p \rightarrow \pi^+ n) \simeq \frac{1 \text{ nb}}{(s/10 \text{ GeV})^7} f(t/s) .$$

We thus expect similar normalization and scaling for  $\frac{d\sigma}{dt} (\bar{p}p \rightarrow \gamma\pi^0)$ ; all angle measurements up to  $s \lesssim 15 \text{ GeV}^2$  appear possible given a high luminosity  $\bar{p}$  beam.

The dimensional counting rules give the leading power behavior of exclusive amplitudes and are essential features of the theory. They appear to be reasonably well verified by experiment including the recent series of measurements of meson-nucleon reactions done at BNL.<sup>41</sup> By comparing the magnitude and angular dependence of various meson-nucleon cross sections in the power-law scaling regime, one can establish that quark interchange amplitudes rather than flavor-independent gluon exchange diagrams appear to dominate at large momentum transfer.

In the case of  $pp$  elastic scattering, the fixed angle data on a log-log plot (see fig. 33) appears consistent with the nominal  $s^{-10} f(\theta_{CM})$  dimensional counting production. However, as emphasized by Hendry,<sup>43</sup> the  $s^{10} d\sigma/dt$  cross section exhibits oscillatory behavior with  $p_T$ . Even more serious is the fact that polarization measurements (see fig. 11) show significant spin-spin correlations ( $A_{NN}$ ), and the single spin asymmetry ( $A_N$ ) is not consistent with predictions based on hadron helicity conservation rule discussed above. Such predictions are expected to be valid for the leading power behavior. Recent analyses of these effects have been given by Farrar<sup>91</sup> and Lipkin.<sup>92</sup> It is likely that there are significant non-leading power law contributions in the accessible energy range. Clearly,  $\bar{p}p \rightarrow \bar{p}p$  data in the large-angle large-energy regime will be very helpful in clarifying these fundamental issues.

The simplest exclusive channels accessible to a  $\bar{p}p$  facility are  $\bar{p}p \rightarrow e^+e^-$ ,  $\mu^+\mu^-$ ,  $\tau^+\tau^-$  which to leading order in  $\alpha$  provides a direct measurement of the Dirac and Pauli time-like proton form factor. The  $\theta_{CM}$  angular dependence can be used to separate  $F_2$  and  $F_1$  and check the basic prediction,

$$F_2(s)/F_1(s) \sim M^2/s .$$

Perturbative QCD predicts asymptotic scaling of the form

$$s^2 F_1(s) \sim f(\ln s) .$$

A high luminosity  $\bar{p}$  facility could push time-like measurements of both form factors well beyond those available from  $e^+e^-$  storage rings. Since the normalization is similar to that of  $p\bar{p} \rightarrow \gamma\gamma$ , one should be able to measure the proton form factors out to center of mass energy squared as large as  $s \sim 10 \text{ GeV}^2$ .

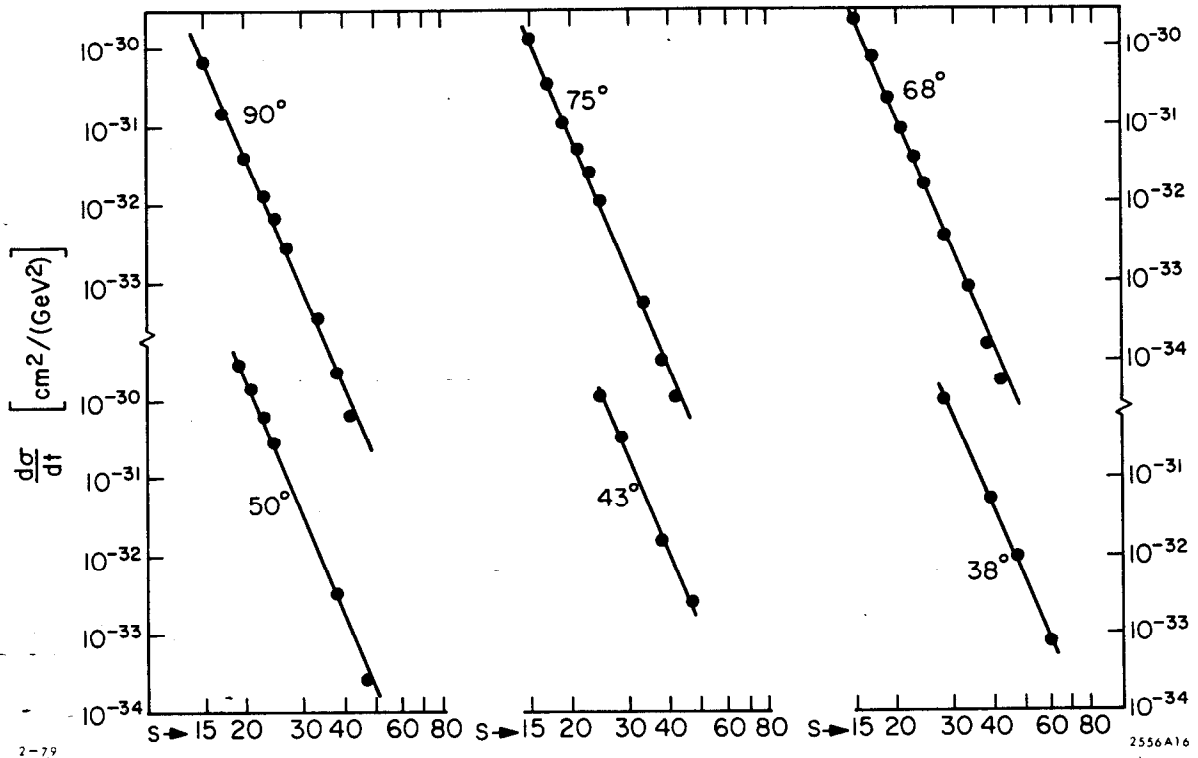
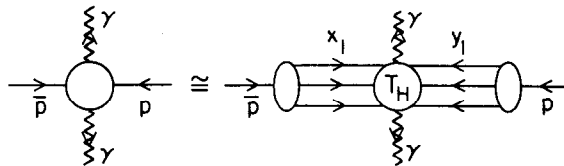


Fig. 33. Comparison of proton-proton scattering at fixed  $\theta_{cm}$  with the dimensional counting prediction. The best fit is  $s^{-9.7}$ .

## 21. Studying the Compton Amplitude in $p\bar{p}$ and $\gamma\gamma$ Annihilation

Another important example of an exclusive process in QCD is the process  $p\bar{p} \rightarrow \gamma\gamma$  or  $\gamma\gamma \rightarrow p\bar{p}$  as illustrated in fig. 34. We can write to leading order in  $1/p_T^2$ ,

$$M_{p\bar{p} \rightarrow \gamma\gamma}(p_T^2, \theta_{CM}) = \int_0^1 [dx] \int_0^1 [dy] \phi_{\bar{p}}(x, p_T) T_H(qq + \bar{q}\bar{q} \rightarrow \gamma\gamma) \phi_p(y, p_T)$$



6-86

5446A2

Fig. 34. Application of QCD factorization to  $\bar{p}p$  annihilation into photons.

where  $\phi_p(x, p_T)$  is the anti-proton distribution amplitude and  $T_H \sim \alpha_s^2(p_T^2)/(p_T^2)$  gives the scaling behavior of the minimally connected tree graph amplitude for the two-photon annihilation of three quarks and three antiquarks collinear with the initial hadron directions. (See figs. 35 and 36.) QCD thus predicts

$$\frac{d\sigma}{d\Omega_{CM}}(p\bar{p} \rightarrow \gamma\gamma) \simeq \frac{\alpha_s^4(p_T^2)}{(p_T^2)^5} f(p_T, \theta_{CM}, \ln p_T^2).$$

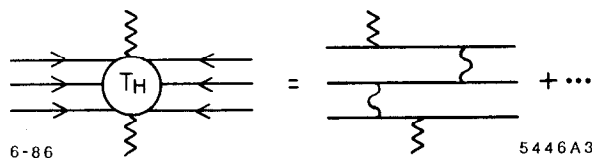


Fig. 35. Example of a lowest order perturbative contribution to  $T_H$  for the process  $p\bar{p} \rightarrow \gamma\gamma$ .

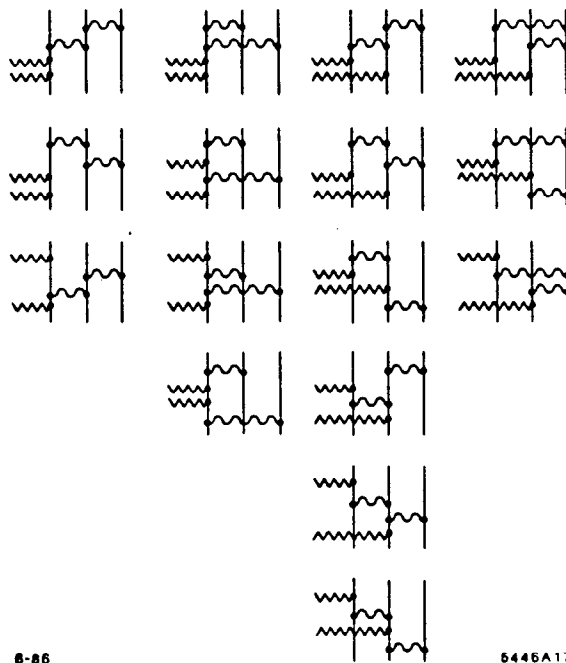


Fig. 36. Leading diagrams for  $\gamma + \gamma \rightarrow \bar{p} + p$  calculated in refs. 24 and 25.

The complete calculations of the tree graph structure of both  $\gamma\gamma \rightarrow M\bar{M}$  and  $\gamma\gamma \rightarrow B\bar{B}$  amplitudes has now been completed. One can use crossing to compute  $T_H$  for  $p\bar{p} \rightarrow \gamma\gamma$  to leading order in  $\alpha_s(p_T^2)$  from the calculations reported by

Farrar, Maina, and Neri<sup>93</sup> and Gunion and Millers.<sup>94</sup> Examples of the predicted angular distributions are shown in figs. 37 and 38. The region of applicability of the leading power-law results is presumed to be set by the scale where  $Q^4 G_M(Q^2)$  is roughly constant, i.e.  $Q^2 > 4 \text{ GeV}^2$ . (See fig. 6.) The available data are too close to threshold for a meaningful test.

As discussed above, the model for the proton distribution amplitude proposed by Chernyak and Zhitnitskii based on QCD sum rules leads to normalization and sign consistent with the measured proton form factor. (See fig. 5.) The CZ proton distribution amplitude yields predictions for  $\gamma\gamma \rightarrow p\bar{p}$  in rough agreement with the experimental normalization, although the production energy is too low for a clear test. It should be noted that unlike meson pair production the QCD predictions for baryons are highly sensitive to the form of the running coupling constant and the endpoint behavior of the wave functions.

Fig. 37. QCD prediction for the scaling and angular distribution for  $\gamma+\gamma \rightarrow \bar{p}+p$  calculated by Farrar et al.<sup>93</sup> The dashed-dot curve corresponds to  $\frac{4\Lambda^2}{s} = 0.0016$  and a maximum running coupling constant  $\alpha_s^{max} = 0.8$  The solid curve corresponds to  $\frac{4\Lambda^2}{s} = 0.016$  and a maximum running coupling constant  $\alpha_s^{max} = 0.5$  The dashed curve corresponds to a fixed  $\alpha_s = 0.3$ . The results are very sensitive to the endpoint behavior of the proton distribution amplitude. The CZ form is assumed.

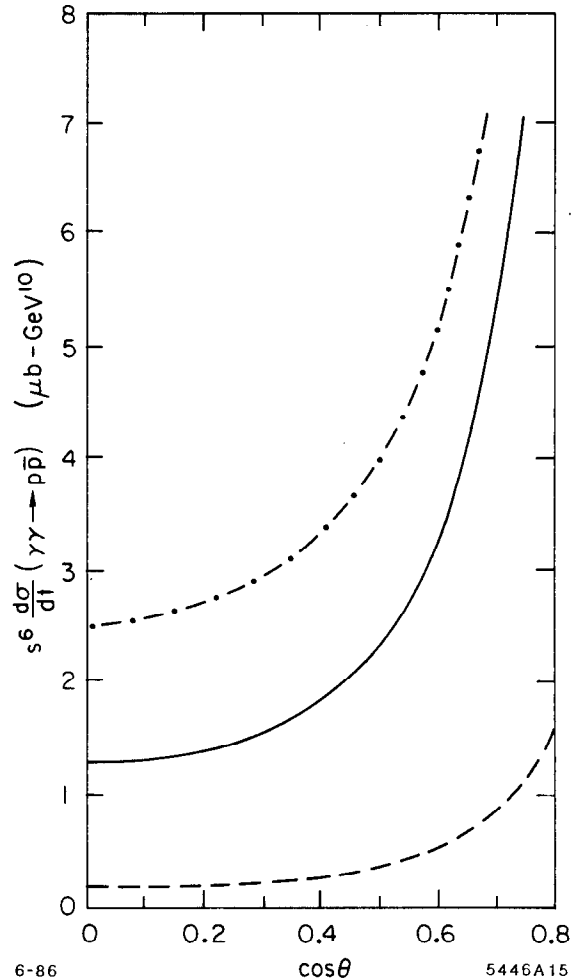
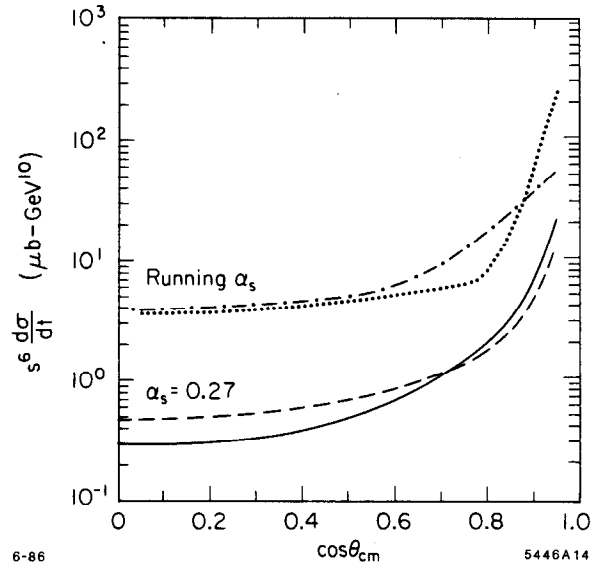


Fig. 38. QCD prediction for the scaling and angular distribution for  $\gamma + \gamma \rightarrow \bar{p} + p$  calculated by Gunion, Sparks, and Millers.<sup>94</sup> CZ distribution amplitudes are assumed. The solid and running curves are for real photon annihilation. The dashed and dot-dashed curves correspond to one photon space-like, with  $\frac{Q_b^2}{s} = 0.1$ .



The  $\gamma^* \gamma^* \rightarrow \bar{B}B$  and  $M\bar{M}$  amplitudes for off-shell photons have now been calculated by Millers and Gunion.<sup>94</sup> The results show important sensitivity to the form of the respective baryon and meson distribution amplitudes. The consequences of  $|gg\rangle$  mixing in singlet mesons in  $\gamma\gamma$  processes is discussed in ref. 95.

It is possible that data from  $p\bar{p}$  collisions at energies up to 9 GeV could greatly clarify the question of whether the perturbative QCD predictions are reliable at moderate momentum transfer. An important check of the QCD predictions can be obtained by combining data from  $p\bar{p} \rightarrow \gamma\gamma$ ,  $\gamma\gamma \rightarrow p\bar{p}$  with large angle Compton scattering  $\gamma p \rightarrow \gamma p$ . This comparison checks in detail the angular dependence and crossing behavior expected from the theory. Furthermore in  $p\bar{p}$  collisions one can even study time-like photon production into  $e^+e^-$  and examine the virtual photon mass dependence of the Compton amplitude. Predictions for the  $q^2$  dependence of the  $p\bar{p} \rightarrow \gamma\gamma^*$  amplitude can be obtained by crossing the results of ref. 94.

## 22. The Deuteron in QCD

Of the five color-singlet representations of six quarks, only one corresponds to the usual system of two color singlet baryonic clusters.<sup>85</sup> The exchange of a virtual gluon in the deuteron at short distance inevitably produces Fock state components where the three-quark clusters correspond to color octet nucleons or isobars. Thus, in general, the deuteron wave function will have a complete spectrum of "hidden-color" wave function components, although it is likely that these states are important only at small inter-nucleon separation.

Despite the complexity of the multi-color representations of nuclear wave functions, the analysis<sup>46</sup> of the deuteron form factor at large momentum transfer can be carried out in parallel with the nucleon case. Only the minimal six-quark Fock state needs to be considered to leading order in  $1/Q^2$ . The deuteron form factor can then be written as a convolution [see fig. 17],

$$F_d(Q^2) = \int_0^1 [dx] [dy] \phi_d^\dagger(y, Q) T_H^{6q+\gamma^* \rightarrow 6q}(x, y, Q) \phi_d(x, Q), \quad (27)$$

where the hard scattering amplitude scales as

$$T_H^{6q+\gamma^* \rightarrow 6q} = \left[ \frac{\alpha_s(Q^2)}{Q^2} \right]^5 t(x, y) [1 + O(\alpha_s(Q^2))] \quad (28)$$

The anomalous dimensions  $\gamma_n^d$  are calculated from the evolution equations for  $\phi_d(x_i, Q)$  derived to leading order in QED from pairwise gluon-exchange interactions: ( $C_F = 4/3$ ,  $C_d = -C_F/5$ )

$$\prod_{k=1}^6 x_k \left[ \frac{\partial}{\partial \xi} + \frac{3C_F}{\beta} \right] \tilde{\Phi}(x_i, Q) = -\frac{C_d}{\beta} \int_0^1 [dy] V(x_i, y_i) \tilde{\Phi}(y_i, Q). \quad (29)$$

Here we have defined

$$\Phi(x_i, Q) = \prod_{k=1}^6 x_k \tilde{\Phi}(x_i, Q), \quad (30)$$

and the evolution is in the variable

$$\xi(Q^2) = \frac{\beta}{4\pi} \int_{Q_0^2}^{Q^2} \frac{dk^2}{k^2} \alpha_s(k^2) \sim \ln \left( \frac{\ln \frac{Q^2}{\Lambda^2}}{\ln \frac{Q_0^2}{\Lambda^2}} \right). \quad (31)$$

The kernel  $V$  is computed to leading order in  $\alpha_s(Q^2)$  from the sum of gluon interactions between quark pairs. The general matrix representations of  $\gamma_n$  with

bases  $\left| \prod_{i=1}^5 x_i^{m_i} \right\rangle$  is given in ref. 45. The effective leading anomalous dimension  $\gamma_0$ , corresponding to the eigenfunction  $\tilde{\Phi}(x_i) = 1$ , is  $\gamma_0 = (6/5)(C_F/\beta)$ . the next section).

In order to make more detailed and experimentally accessible predictions, we will define the “reduced” nuclear form factor in order to remove the effects of nucleon compositeness:<sup>86</sup>

$$f_d(Q^2) \equiv \frac{F_d(Q^2)}{F_N^2(Q^2/4)} \quad (32)$$

The arguments for each of the nucleon form factors ( $F_N$ ) is  $Q^2/4$  since in the limit of zero binding energy each nucleon must change its momentum from  $\sim p/2$  to  $(p+q)/2$ . Since the leading anomalous dimensions of the nucleon distribution amplitude is  $C_F/2\beta$ , the QCD prediction for the asymptotic  $Q^2$ -behavior of  $f_d(Q^2)$  is

$$f_d(Q^2) \sim \frac{\alpha_s(Q^2)}{Q^2} \left( \ln \frac{Q^2}{\Lambda^2} \right)^{-\frac{2}{5} \frac{C_F}{\beta}}, \quad (33)$$

where  $-(2/5)(C_F/\beta) = -8/145$  for  $n_f = 2$ .

Although this QCD prediction is for asymptotic momentum transfer, it is interesting to compare it directly with the available high  $Q^2$  data<sup>79</sup> (see fig. 19). In general one would expect corrections from higher twist effects (e.g., mass and  $k_\perp$  smearing), higher particle number Fock states, higher order contributions in  $\alpha_s(Q^2)$ , as well as non-leading anomalous dimensions. However, the agreement of the data with simple  $Q^2 f_d(Q^2) \sim \text{const}$  behavior for  $Q^2 > 1/2 \text{ GeV}^2$  implies that, unless there is a fortuitous cancellation, all of the scale-breaking effects are small, and the present QCD perturbative calculations are viable and applicable even in the nuclear physics domain. The lack of deviation from the QCD parameterization also suggests that the parameter  $\Lambda$  is small. A comparison with a standard definition such as  $\Lambda_{\overline{MS}}$  would require a calculation of next to leading effects. A more definitive check of QCD can be made by calculating the normalization of  $f_d(Q^2)$  from  $T_H$  and the evolution of the deuteron wave function to short distances. It is also important to confirm experimentally that the helicity  $\lambda = \lambda' = 0$  form factor is indeed dominant.

Because of hidden color, the deuteron cannot be described solely in terms of standard nuclear physics degrees of freedom, and in principle, any physical or dynamical property of the deuteron is modified by the presence of such non-Abelian components. In particular, the standard “impulse approximation” form

for the deuteron form factor

$$F_d(Q^2) = F_d^{\text{body}}(Q^2) F_N(Q^2) \quad , \quad (34)$$

where  $F_N$  is the on-shell nucleon form factor, cannot be precisely valid at any momentum transfer scale  $Q^2 = -q^2 \neq 0$  because of hidden color components. More important, even if only the nucleon-nucleon component were important, Thus the conventional factorization cannot be reliable for composite nucleons since the struck nucleon is necessarily off-shell<sup>87</sup> in the nuclear wave function:  $|k'^2 - k^2| \sim \frac{1}{2}Q^2$ . Thus in general one requires knowledge of the nucleon form factors  $F_N(q^2, k^2, k'^2)$  for the case in which one or both nucleon legs are off-shell. In QCD such amplitudes have completely different dynamical dependence compared to the on-shell form factors.

Although on-shell factorization has been used extensively in nuclear physics as a starting point for the analysis of nuclear form factors,<sup>88</sup> its range of validity has never been seriously questioned. Certainly in the non-relativistic domain where target recoil and off-shell effects can be neglected, the charge form factor of a composite system can be computed from the convolution of charge distributions. However, in the general situation, the struck nucleon must transfer a large fraction of its momentum to the spectator system, rendering the nucleon state off-shell. As shown in ref. 45, the region of validity of on-shell form factor factorization for the deuteron is very small:

$$Q^2 < 2 M_d \epsilon_d$$

*i.e.*,  $Q \lesssim 100$  MeV. However, in this region the nucleon form factor does not deviate significantly from unity, so the standard factorization is of doubtful utility. The reduced form factor result has general utility at any momentum scale. It is also important to confirm experimentally that the helicity  $\lambda = \lambda' = 0$  form factor is indeed dominant.

The calculation of the normalization  $T_H^{6q+\gamma^* \rightarrow 6q}$  to leading order in  $\alpha_s(Q^2)$  will require the evaluation of over 300,000 Feynman diagrams involving five exchanged gluons. Fortunately this appears possible using the algebraic computer methods introduced by Farrar and Neri.<sup>89</sup> The method of setting the appropriate scale  $\hat{Q}$  of  $\alpha_s^5(\hat{Q}^2)$  in  $T_H$  is given in ref. 96.

We note that the deuteron wave function which contributes to the asymptotic limit of the form factor is the totally antisymmetric wave function corresponding to the orbital Young symmetry given by [6] and isospin ( $T$ ) + spin ( $S$ ) Young symmetry given by {33}. The deuteron state with this symmetry is related to the  $NN$ ,  $\Delta\Delta$ , and hidden color ( $CC$ ) physical bases, for both the  $(TS) = (01)$  and



(10) cases, by the formula<sup>97</sup>

$$\psi_{[6]\{33\}} = \sqrt{\frac{1}{9}} \psi_{NN} + \sqrt{\frac{4}{45}} \psi_{\Delta\Delta} + \sqrt{\frac{4}{5}} \psi_{CC} . \quad (35)$$

Thus the physical deuteron state, which is mostly  $\psi_{NN}$  at large distance, must evolve to the  $\psi_{[6]\{33\}}$  state when the six quark transverse separations  $b_{\perp}^i \leq O(1/Q) \rightarrow 0$ . Since this state is 80% hidden color, the deuteron wave function cannot be described by the meson-nucleon isobar degrees of freedom in this domain. The fact that the six-quark color singlet state inevitably evolves in QCD to a dominantly hidden-color configuration at small transverse separation also has implications for the form of the nucleon-nucleon ( $S_z = 0$ ) potential, which can be considered as one interaction component in a coupled scattering channel system. As the two nucleons approach each other, the system must do work in order to change the six-quark state to a dominantly hidden color configuration; i.e., QCD requires that the nucleon-nucleon potential must be repulsive at short distances (see fig. 39).<sup>98</sup> The evolution equation for the six-quark system suggests that the distance where this change occurs is in the domain where  $\alpha_s(Q^2)$  most strongly varies. The general solutions of the evolution equation for multi-quark systems is discussed in ref. 45. Some of the solutions are orthogonal to the usual nuclear configurations which correspond to separated nucleons or isobars at large distances.

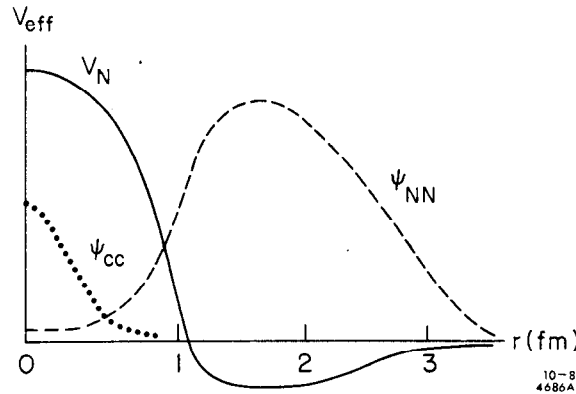


Fig. 39. Schematic representation of the deuteron wave function in QCD indicating the presence of hidden color six-quark components at short distances.

## 23. Reduced Nuclear Amplitudes

One of the basic problems in the analysis of nuclear scattering amplitudes is how to consistently account for the effects of the underlying quark/gluon component structure of nucleons. Traditional methods based on the use of an effective nucleon/meson local Lagrangian field theory are not really applicable, giving the wrong dynamical dependence in virtually every kinematic variable for composite hadrons. The inclusion of *ad hoc* vertex form factors is unsatisfactory since one must understand the off-shell dependence in each leg while retaining gauge invariance; such methods have little predictive power. On the other hand, the explicit evaluation of the multi-quark hard-scattering amplitudes needed to predict the normalization and angular dependence for a nuclear process, even at leading order in  $\alpha_s$ , requires the consideration of millions of Feynman diagrams. Beyond leading order one must include contributions of non-valence Fock states wave functions, and a rapidly expanding number of radiative corrections and loop diagrams.

The reduced amplitude method,<sup>86</sup> although not an exact replacement for a full QCD calculation, provides a simple method for identifying the dynamical effects of nuclear substructure, consistent with covariance, QCD scaling laws and gauge invariance. The basic idea has already been introduced for the reduced deuteron form factor. More generally if we neglect nuclear binding, then the light-cone nuclear wave function can be written as a cluster decomposition of collinear nucleons:  $\psi_{q/A} = \psi_{N/A} \prod_N \Psi_{q/N}$  where each nucleon has  $1/A$  of the nuclear momentum. A large momentum transfer nucleon amplitude then contains as a factor the probability amplitude for each nucleon to remain intact after absorbing  $1/A$  of the respective nuclear momentum transfer. We can identify each probability amplitude with the respective nucleon form factor  $F(\hat{t}_i = \frac{1}{A^2} t_A)$ . Thus for any exclusive nuclear scattering process, we define the reduced nuclear amplitude

$$m = \frac{\mathcal{M}}{\prod_{i=1}^A F_N(\hat{t}_i)} \quad (36)$$

The QCD scaling law for the reduced nuclear amplitude  $m$  is then identical to that of nuclei with point-like nuclear components: e.g., the reduced nuclear form factors obey

$$f_A(Q^2) \equiv \frac{F_A(Q^2)}{\left[ F_N(Q^2/A^2) \right]^A} \sim \left[ \frac{1}{Q^2} \right]^{A-1}. \quad (37)$$

Comparisons with experiment and predictions for leading logarithmic corrections to this result are given in ref. 86. In the case of photo- (or electro-) disintegration

of the deuteron one has

$$m_{\gamma d \rightarrow np} = \frac{\mathcal{M}_{\gamma d \rightarrow np}}{F_n(t_n)F_p(t_p)} \sim \frac{1}{p_T} f(\theta_{cm}) \quad (38)$$

i.e., the same elementary scaling behavior as for  $\mathcal{M}_{\gamma M \rightarrow q\bar{q}}$ . Comparison with experiment is encouraging (see fig. 40), showing that as was the case for  $Q^2 f_d(Q^2)$ , the perturbative QCD scaling regime begins at  $Q^2 \gtrsim 1 \text{ GeV}^2$ . Detailed comparisons and a model for the angular dependence and the virtual photon-mass dependence of deuteron electro-disintegration are discussed in ref. 86. Other potentially useful checks of QCD scaling of reduced amplitudes are

$$\begin{aligned} m_{pp \rightarrow d\pi^+} &\sim p_T^{-2} f(t/s) \\ m_{pd \rightarrow H^3\pi^+} &\sim p_T^{-4} f(t/s) \\ m_{\pi d \rightarrow \pi d} &\sim p_T^{-4} f(t/s) . \end{aligned} \quad (39)$$

It is also possible to use these QCD scaling laws for the reduced amplitude as a parametrization for the background for detecting possible new di-baryon resonance states.

## 24. Conclusions

The nucleus plays two complimentary roles in QCD:

1. We may utilize a nuclear target as a control medium or background field to modify or probe quark and gluon subprocesses. We have discussed in these lectures several novel examples, such as *color transparency*: the predicted diminished attenuation of hadrons participating in high momentum transfer *exclusive reactions*, and *formation zone phenomena* the absence of hard collinear target-induced radiation by quarks or gluons interacting in a high momentum transfer *inclusive reactions*. More generally, the nucleus may act to modify the properties of its constituent nucleons; a myriad of non-additive and shadowing effects have been suggested to explain the EMC/SLAC observations. Measurements of nuclear non-additivity in individual electroproduction channels are needed to unravel these effects. We have also emphasized the importance of the NA-10 observations for the Drell-Yan process in nuclei: the transverse momentum distribution of lepton pairs is broadened; nevertheless, structure function factorization is maintained. Thus as predicted by QCD, the incoming quark or anti-quark can suffer *elastic* initial state interactions even though hard collinear *inelastic* interactions do not occur. These observations are important for the general understanding of the propagation of quark and gluon jets in nuclear matter.

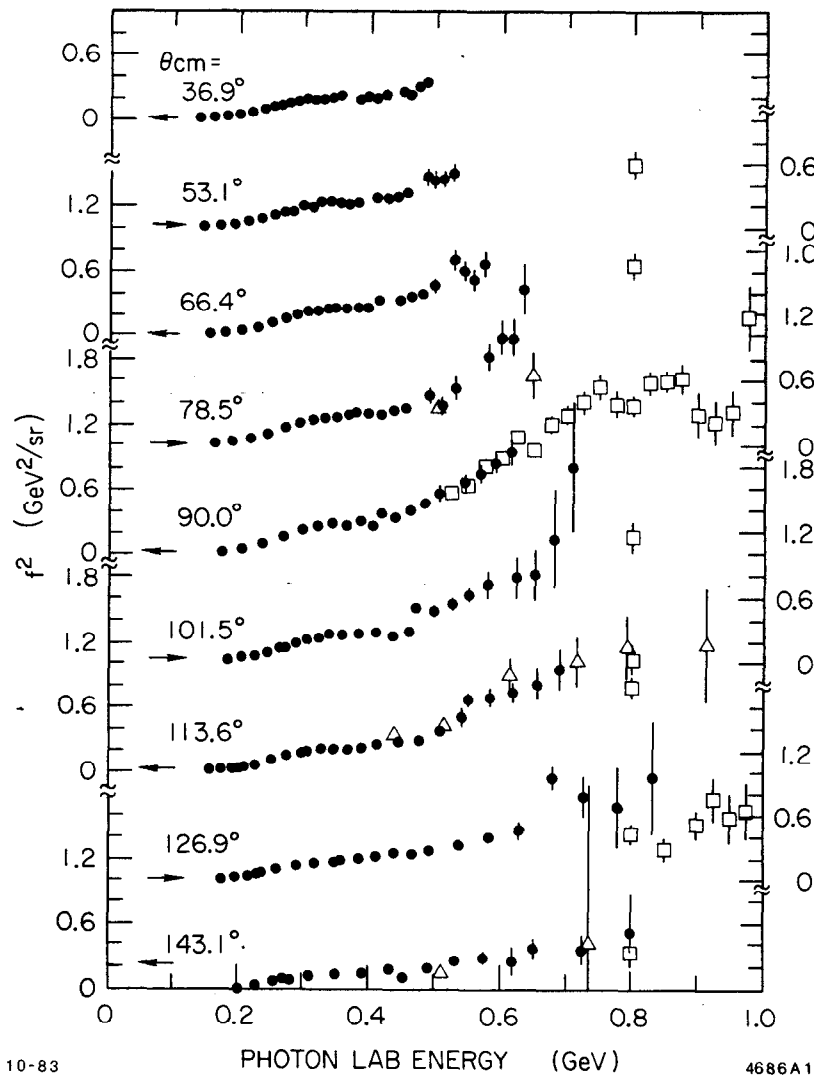


Fig. 40. Comparison of deuteron photo-disintegration data with the scaling prediction which requires  $f^2(\theta_{c.m.})$  to be independent of energy at large momentum transfer. The data are from H. Myers *et al.*, Phys. Rev. **121**, 630 (1961); R. Ching and C. Schaerf, Phys. Rev. **141**, 1320 (1966); P. Dougan *et al.*, Z. Phys. **A276**, 55 (1976).

2. The nucleus itself must be described as a QCD structure. At short distances nuclear wave functions and nuclear interactions necessarily involve *hidden color* degrees of freedom orthogonal to the channels described by the usual nucleon or isobar degrees of freedom. In the case of the deuteron, five color-singlet Fock states are required just to describe its six-quark valence wave function. At asymptotic momentum transfer, the deuteron form factor and distribution amplitude are rigorously calculable. At sub-asymptotic momenta, one can derive new types of scaling laws for exclusive nuclear

amplitudes in terms of the reduced amplitude formalism. We have also emphasized some novel features of *nuclear diffractive* amplitudes—high energy hadronic or electromagnetic reactions which leave the entire nucleus intact. In the case of deep inelastic scattering, such leading twist contributions can give unusual non-additive contributions to the nuclear structure function at low  $x_{Bj}$ . In the case of vector meson electroproduction at highly virtual photon mass, diffractive processes can give essential information on non-forward matrix elements of the same operator products which control deep inelastic lepton scattering.

The application of QCD to nuclei—*Nuclear Chromodynamics* has brought together two formerly distinct communities of physicists. Given that the natural scale of QCD is 1 fermi, nuclear physics can hardly be studied as an isolated subject. Indeed several traditional assumptions of nuclear theory are incompatible with QCD, such as (a) standard on-shell form factor factorization and (b) Dirac equation phenomenology for nucleon interactions in nuclei—since the  $NN\bar{N}$  intermediate state is severely suppressed by nucleon compositeness. Conversely, the very difficult questions for particle theorists—the structure of the hadrons in terms of their quark and gluon degrees of freedom, the gluonium and other exotic spectra, coherence effects, jet hadronization and particle formation, the nature of the pomeron, diffractive and forward processes, etc., require experimental input in the GeV regime or even lower. We have discussed a number of new experimental facilities relevant to the study of these problems.

In these lectures, I have reviewed several areas where theory has made significant progress over the past few years. This includes the extension of factorization and evolution equations to the domain of exclusive hadronic and nuclear amplitudes. Moreover, QCD sum rule techniques have made tantalizing predictions for the required hadron wave functions, results which are being confirmed by lattice gauge theory computations.

### Acknowledgements

I would like to thank Professor Robert Delbourgo and his colleagues at the University of Tasmania for their hospitality and for organizing this very interesting school.

Parts of these lectures are based on recent collaborations with others, particularly T. Eller, K. Hornbostel, C.R. Ji, G.P. Lepage, A. Mueller, H.C. Pauli, and S.F. Tuan. A shortened version of these lectures was also presented to the NPAS Workshop on Electronuclear Physics with Internal Targets, SLAC, 1987.

## References

1. For reviews see, e.g., E. Reya, Phys. Rept. **69**, 195 (1981); A.H. Mueller, Lectures on perturbative QCD given at the Theoretical Advanced Study Inst., New Haven, 1985; *Quarks and Gluons in Particle and Nuclei*, Proc. of the UCSB Institute for Theoretical Physics Workshop on Nuclear Chromodynamics, eds., S.J. Brodsky and E. Moniz (World Scientific, 1985).
2. E. Witten, Nucl. Phys. **B223**, 422,433 (1983). For a recent review of Skyrmion physics and further references see V.P. Nair, IAS Princeton preprint (1985).
3. C. Klopfenstein *et al.*, CUSB 83-07 (1983).
4. K. Varvell *et al.*, CERN/EP 87-46 (1987).
5. S.J. Brodsky, G.P. Lepage and P.B. Mackenzie, Phys. Rev. **D28**, 228 (1983). The problem of setting the scale of the argument of the running coupling constant is discussed in this paper.
6. V.L. Chernyak and A.R. Zhitnitskii, Phys. Rept. **112**, 173 (1984). See also Xiao-Duang Xiang, Wang Xin-Nian, and Huang Tao, BIHEP-TH-84, 23 and 29 (1984).
7. I.D. King and C.T. Sachrajda, SHEP-85/86-15 (1986), p. 36.
8. G. Martinelli and C.T. Sachrajda, CERN-TH-4637/87 (1987). The results are based on the method of S. Gottlieb and A.S. Kronfeld, Phys. Rev. **D33**, 227 (1986); A.S. Kronfeld and D.M. Photiadis, Phys. Rev. **D31**, 2939 (1985).
9. P. Hoodbhoy and R.L. Jaffe, Phys. Rev. **D35**, 113 (1987); R.L. Jaffe, CTP #1315 (1985).
10. S.J. Brodsky, J.F. Gunion and R.L. Jaffe Phys. Rev. **D6**, 2487 (1972).
11. S.J. Brodsky, G.T. Bodwin and G.P. Lepage, in the Proc. of the Volendam Multipart. Dyn. Conf., 1982, p. 841; Proc. of the Banff Summer Inst., 1981, p. 513. This effect is related to the formation zone principle of L. Landau and I. Pomeranchuk, Dok. Akademii Nauk SSSR **92**, 535,735 (1953).
12. G.T. Bodwin, Phys. Rev. **D31**, 2616 (1985); G.T. Bodwin, S.J. Brodsky and G.P. Lepage, ANL-HEP-CP-85-32-mc (1985), presented at 20th Rencontre de Moriond, Les Arcs, France, March 10-17, 1985.
13. E. Berger, ANL-HEP-PR-87-45 and references therein.
14. A. Sommerfeld, *Atombau and Spektallinen* (Vieweg, Braunschweig, 1939).
15. S.J. Brodsky, J.F. Gunion and D. Soper, SLAC-PUB-4193 (1987).
16. S. J. Brodsky, G. Kopp, and P. Zerwas Phys. Rev. Lett. **58**, 443 (1987).

17. S.J. Brodsky and A.H. Mueller, in preparation.
18. A.H. Mueller, Proc. of the Moriond Conf., 1982.
19. S.J. Brodsky, XIII Int. Symp. on Multiparticle Dynamics, 1982.
20. G.P. Lepage and S.J. Brodsky, Phys. Rev. **D22**, 2157 (1980); G.P. Lepage, S.J. Brodsky, T. Huang and P.B. Mackenzie, CLNS-82/522, published in the Proc. of the Banff Summer Institute, 1981.
21. A.H. Mueller, Phys. Rept. **73**, 237 (1981). See also S. S. Kanwal, Phys. Lett. **294**, 1984).
22. A.V. Efremov and A.V. Radyushkin, Phys. Lett. **94B**, 245 (1980).
23. S.J. Brodsky, Y. Frishman, G.P. Lepage and C. Sachrajda, Phys. Lett. **91B**, 239 (1980).
24. S.J. Brodsky and G.R. Farrar, Phys. Rev. Lett. **31**, 1153 (1973); Phys. Rev. **D11**, 1309 (1975).
25. S.J. Brodsky and G.P. Lepage, Phys. Rev. **D23**, 1152 (1981); S.J. Brodsky, G.P. Lepage and S.A.A. Zaidi, Phys. Rev. **D23**, 1152 (1981).
26. S.J. Brodsky and G.P. Lepage, Phys. Rev. **D24**, 2848 (1981).
27. V. D. Burkert, CEBAF-PR-87-006.
28. Z. Dziembowski and L. Mankiewicz, Warsaw University preprint (1986).
29. J.P. Ralston and B. Pire, Phys. Rev. Lett. **57**, 2330 (1986).
30. S.J. Brodsky and B.T. Chertok, Phys. Rev. Lett. **37**, 269 (1976); Phys. Rev. **D114**, 3003 (1976).
31. O.C. Jacob and L.S. Kisslinger, Phys. Rev. Lett. **56**, 225 (1986).
32. N. Isgur and C.H. Llewellyn Smith, Phys. Rev. Lett. **52**, 1080 (1984).
33. C-R Ji, A.F. Sill and R.M. Lombard-Nelsen, SLAC-PUB-4068 (1986).
34. R.G. Arnold *et al.*, SLAC-PUB-3810 (1986).
35. M. Gari and N. Stefanis, Phys. Lett. **B175**, 462 (1986), M. Gari and N. Stefanis, preprint RUB-TPII-86-21 (1986).
36. J. Boyer *et al.*, Phys. Rev. Lett. **56**, 207 (1986).
37. S.J. Brodsky and G.P. Lepage, Phys. Rev. **D24**, 1808 (1981). The next to leading order evaluation of  $T_H$  for these processes is given by B. Nežić, Ph.D. Thesis, Cornell Univ. (1985).
38. T. Eller, H.C. Pauli and S.J. Brodsky, Phys. Rev. **D35**, 1493 (1987).
39. A. Sen, Phys. Rev. **D24**, 3281 (1981).
40. H.C. Pauli and S.J. Brodsky, Phys. Rev. **D32**, 1993 (1985); Phys. Rev. **D32**, 2001 (1985).

41. S. Heppelmann, DPF Meeting, Salt Lake City, 1987; G.C. Blazey *et al.*, Phys. Rev. Lett. **55**, 1820 (1985).
42. A.D. Krisch, UM-HE-86-39 (1987).
43. A.W. Hendry, Phys. Rev. **D10**, 2300 (1974).
44. S.J. Brodsky, C.E. Carlson and H.J. Lipkin, Phys. Rev. **D20**, 2278 (1979); H.J. Lipkin, private communication.
45. C.-R. Ji and S.J. Brodsky, Phys. Rev. **D34**, 1460; **D33**, 1951; **D33**, 1406; **D33**, 2653 (1986); Phys. Rev. Lett. **55**, 2257 (1985).
46. S.J. Brodsky, C.-R. Ji and G.P. Lepage, Phys. Rev. Lett. **51**, 83 (1983).
47. R.L. Anderson *et al.*, Phys. Rev. Lett. **30**, 627 (1973).
48. S.J. Brodsky and J. Pumplin, Phys. Rev. **182**, 1794 (1969); S.J. Brodsky, F.E. Close and J.F. Gunion, Phys. Rev. **D6**, 177 (1972).
49. A.H. Mueller and J. Qui, Nucl. Phys. **B268**, 427 (1986); J. Qui, preprint CU-TP-361.
50. J.J. Aubert *et al.*, Phys. Lett. **123B**, 275 (1983); For recent reviews see E. L. Berger, ANL-HEP-PR-87-45 and E.L. Berger and F. Coester, ANL-HEP-PR-87-13 (to be published in Ann. Rev. of Nucl. Part. Sci.).
51. A. Donnachie and P.V. Landshoff, Phys. Lett. **185B**, 403 (1987).
52. S.J. Brodsky and J.R. Hiller, Phys. Rev. **C28**, 475 (1983).
53. J.F. Gunion, S.J. Brodsky and R. Blankenbecler, Phys. Rev. **D8**, 287 (1973); Phys. Lett. **39B**, 649 (1972); D. Sivers, S.J. Brodsky and R. Blankenbecler, Phys. Reports **23C**, 1 (1976).
54. E.L. Berger and S.J. Brodsky, Phys. Rev. **D24**, 2428 (1981).
55. E.L. Berger and F. Coester, ANL-HEP-PR-87-13 (1987).
56. I.A. Schmidt and R. Blankenbecler, Phys. Rev. **D15**, 3321 (1977).
57. J.F. Gunion, P. Nason and R. Blankenbecler, Phys. Rev. **D29**, 2491 (1984); Phys. Lett. **117B**, 353 (1982).
58. P. Bordalo *et al.*, CERN EP/87-67 and 68 (1987).
59. H.G. Fischer, presented at the Leipzig Conference, 1984.
60. G. Alexander, E. Gotsman and U. Maor, Phys. Lett. **161B**, 384 (1985).
61. S.J. Brodsky and M. Soldate, unpublished.
62. S.F. Biagi *et al.*, Z. Phys. **C28**, 175 (1985).
63. R.L. Jaffe, MIT-CTP-1445 (1987).
64. P.A.M. Dirac, Rev. Mod. Phys. **21**, 392 (1949). Further references to light-cone quantization are given in ref. 38.



65. This chapter was written in collaboration with G.P. Lepage.
66. H. Bergknoff, Nucl. Phys. **B122**, 215 (1977).
67. D.P. Crewther and C.J. Hamer, Nucl. Phys. **B170**, 353 (1980).
68. K. Hornbostel, to be published.
69. G.P. Lepage and S.J. Brodsky, Phys. Rev. **D22**, 2157 (1980).
70. M.E.B. Franklin, Ph.D Thesis (1982), SLAC-254, UC-34d; M.E.B. Franklin *et al.*, Phys. Rev. Lett. **51**, 963 (1983); G. Trilling, in Proceedings of the Twenty-First International Conference on High Energy Physics, Paris, 26-31 July 1982; E. Bloom, *ibid.*
71. S.J. Brodsky, G.P. Lepage, and San Fu Tuan, SLAC-PUB-4276 (1987).
72. S.J. Brodsky and G.P. Lepage, Phys. Rev. **D24**, 2848 (1981).
73. Wei-Shou Hou and A. Soni, Phys. Rev. Lett. **50**, 569 (1983).
74. R.M. Baltrusaitis *et al.*, Phys. Rev. **D32**, 2883 (1985).
75. P.G.O. Freund and Y. Nambu, Phys. Rev. Lett. **34**, 1645 (1975).
76. S.J. Brodsky and G.R. Farrar, Phys. Rev. Lett. **31**, 1153 (1973), and Phys. Rev. **D11**, 1309 (1975).
77. S.J. Brodsky and G.P. Lepage, Phys. Rev. **D24**, 1808 (1981).
78. M. Peskin, Phys. Lett. **88B**, 128 (1979); A. Duncan and A.H. Mueller, Phys. Lett. **90B**, 159 (1980), and Phys. Rev. **D21**, 1636 (1980).
79. M.D. Mestayer, SLAC-Report 214 (1978); F. Martin *et al.*, Phys. Rev. Lett. **38**, 1320 (1977); W.P. Schultz *et al.*, Phys. Rev. Lett. **38**, 259 (1977); R.G. Arnold *et al.*, Phys. Rev. Lett. **40**, 1429 (1978) and SLAC-PUB-2373 (1979); B.T. Chertok, Phys. Lett. **41**, 1155 (1978); D. Day *et al.*, Phys. Rev. Lett. **43**, 1143 (1979). Summaries of the data for nucleon and nuclear form factors at large  $Q^2$  are given in B.T. Chertok, in Progress in Particle and Nuclear Physics, Proceeding of the International School of Nuclear Physics, 5th Course, Erice, 1978, and Proceedings of the XVI Rencontre de Moriond, Les Arcs, Savoie, France, 1981.
80. D. Sivers, S. Brodsky and R. Blankenbecler, Phys. Rept. **23C**, 1 (1976).
81. S.S. Kanwal, Phys. Lett. **142B**, 294 (1984); A. Mueller, Phys. Rept. **73**, 237 (1981).
82. S.J. Brodsky and G.P. Lepage, Phys. Rev. **D24**, 1808 (1981). The calculation of  $\gamma\gamma \rightarrow B\bar{B}$  is given by G.R. Farrar, E. Maina and F. Neri, RU-85-08 (1985).
83. V.L. Chernyak and I.R. Zhitnitskii, Nucl. Phys. **B246**, 52 (1984).

84. S.J. Brodsky, T. Huang and G.P. Lepage, in *Particles and Fields 2*, edited by A.Z. Capri and A.N. Kamal, Plenum (1983); T. Huang, SLAC-PUB-2580 (1980), published in the Proceedings of the XXth International Conference on High Energy Physics, Madison, Wisconsin, 1980.
85. See, e.g., V. Matveev and P. Sorba, *Nuovo Cimento Lett.* **20**, 435 (1977).
86. S.J. Brodsky and J.R. Hiller, *Phys. Rev.* **C28**, 4115 (1983); S.J. Brodsky and B.T. Chertok, *Phys. Rev. Lett.* **37**, 269 (1976), *Phys. Rev.* **D14**, 3003 (1976); S.J. Brodsky, in Proceedings of the International Conference on Few Body Problems in Nuclear and Particle Physics, Laval University, Quebec, 1974.
87. For a general discussion of off-shell nucleon form factors, A.M. Bincer, *Phys. Rev.* **118**, 855 (1960).
88. S.A. Gurvitz, *Phys. Rev.* **C22**, 725 (1980). Meson exchange current contributions take the form of the reduced form factor. See R. Blankenbecler and J. F. Gunion, *Phys. Rev.* **D4**, 718 (1971).
89. G.R. Farrar and F. Neri, *Phys. Lett.* **130B**, 109 (1983).
90. C. E. Carlson, M. Gari, and N. G. Stefanis, *Phys. Rev. Lett.* **58**, 1308 (1987).
91. G.R. Farrar, RU-85-46 (1986).
92. H.J. Lipkin, private communication.
93. G.R. Farrar, E. Maina and F. Neri, *Nucl. Phys.* **B259**, 702 (1985), *Err.-ibid.* **B263**, 746 (1986).
94. J.F. Gunion, D. Millers and K. Sparks, *Phys. Rev.* **D33**, 689 (1986); D. Millers and J.F. Gunion, UCD-86-04 (1986).
95. G.W. Atkinson, J. Sucher, and K. Tsokos *Phys. Lett.* **137B** 407 (1984).
96. S.J. Brodsky, G.P. Lepage and P.B. Mackenzie, *Phys. Rev.* **D28**, 228 (1983).
97. M. Harvey, *Nucl. Phys.* **A352**, 301 (1981) and **A352**, 326 (1981).
98. Similar considerations for nonrelativistic systems are given in A. Faessler *et al.*, *Nucl. Phys.* **A402**, 555 (1983); S. Furui and A. Faessler *Nucl. Phys.* **A397**, 413 (1983).